

TECHNISCHE UNIVERSITÄT MÜNCHEN

Fachgebiet Hydromechanik

Modelling dispersion on the pore scale based on the velocity distribution function

Sheema Kooshapur

Vollständiger Abdruck der von der Ingenieur fakultät Bau Geo Umwelt der Technischen Universität zur Erlangung des akademischen Grades eines

Doktor-Ingenieurs

genehmigten Dissertation.

Vorsitzender:

Prof. Dr. Ernst Rank

Prüfer der Dissertation:

1. Prof. Dr.-Ing. Michael Manhart
2. Prof. Dr. rer. nat. Insa Neuweiler

Die Dissertation wurde am 24.05.2016 bei der Technischen Universität München eingereicht und durch die Ingenieur fakultät Bau Geo Umwelt am 11.09.2016 angenommen.

Zusammenfassung

Das Ziel der vorliegenden Arbeit ist es, ein stochastisches Modell für die Dispersion in porösen Medien zu entwickeln und diskutieren. Der stochastische Prozess modelliert Geschwindigkeitsinkremente durch einen Drift- und einen Diffusionsprozess im Geschwindigkeitsraum, so dass die Geschwindigkeitsverteilung und die konditionierte Statistik der Geschwindigkeitsinkremente erhalten werden. Der dreidimensionale Porenraum wird durch eine random, dreidimensional periodische Kugelpackung repräsentiert. Das Geschwindigkeitsfeld wird durch eine direkte Lösung der Navier-Stokes-Gleichung bei voller Auflösung des Porenraumes mit Hilfe einer eingebetteten Randbedingung in einem Kartesischen Gitter erhalten. Die Strömung wird durch einen räumlichen Druckgradienten angetrieben. Eine sorgfältige Validierung liefert die Abhängigkeit der Ergebnisse von der Gitterauflösung und der Größe des betrachteten elementaren Volumens. Das stochastische Modell wird an Hand des Transports eines passiven Tracers in einem gerade Plattenkanal und der betrachteten Kugelpackung validiert.

Abstract

The aim of this work is to present and discuss in detail a model for dispersion in porous media based on a stochastic velocity process. The stochastic velocity process consists of a drift and a diffusion part. The model utilizes probability density functions and conditional statistics of the velocity increments on the pore scale. The three dimensional porous domains are represented by irregular sphere packs. The flow field on the pore scale has been obtained by direct simulation of the Navier-Stokes equations under full representation of the pore space by an Immersed Boundary condition in a Cartesian grid. Sphere packs are generated by an algorithm that randomly places spheres under the constraint of periodicity in all three space dimensions. The flow is driven by a constant pressure gradient. Careful validation is undertaken to assess the dependence of the results on grid resolution and size of elementary volume. The validity of the model is investigated for the transport of a passive tracer in a simple channel and in a sphere pack.

Acknowledgements

I would first like to express my sincere thanks and appreciation to my supervisor Prof. Michael Manhart for his guidance and support throughout my doctoral studies. I thank Prof. Insa Neuweiler for taking the time to read and evaluate this work. I express my kindest gratitude to Prof. Ernst Rank not only for being part of my Ph.D. committee but also for his guidance and support during my studies at the Technical University of Munich.

I thank the Munich Centre of Advanced Computing (MAC@IGSSE) for financially supporting a great part of this work.

I would like to thank all my friends at the Technical University of Munich especially my colleagues at the chair of Hydromechanics. In particular I thank Dr.-Ing. Iason Papaioannou and Dr. Michael Lieb for their help and the constructive discussions we have held.

I thank all my dear friends for their kindness and support during these years. I am indebted to Ms. Aida Reyhani, Mr. Ali Shadavakhsh, Mr. Farshid Bonakdar and Ms. Maryam Moshrefzadeh for their counsel and assistance. I would especially like to thank Dr. Elham Ramin, Ms. Mandana Moshrefzadeh and Ms. Talayeh Aledavood for all their help, their loyalty and their love.

My deepest gratitude goes to my parents and siblings for their love and patience and in particular to my brother Dr. Hamed Kooshapur for his continuous encouragement and support.

Contents

Zusammenfassung	I
Abstract	II
Acknowledgements	III
Contents	VI
List of Tables	VII
List of Figures	XI
Nomenclature	XIII
1 Introduction	1
1.1 Dispersion	1
1.2 Treating non-Fickian dispersion	3
1.3 Pore scale versus macro scale	4
1.4 Standard discretization and random walk methods	6
1.5 Objective and overview	7
2 DNS Data Base	9
2.1 Method	9
2.1.1 Solution of the Navier-Stokes and transport equations	9
2.1.2 Generation of sphere packs	10
2.2 Validation	12
2.2.1 Convergence study on the dense sphere pack	13
2.2.2 Dependence of global variables on the size of the REV.	16
2.2.3 Permeability	19
2.3 Velocity field from DNS	20
2.3.1 Velocity statistics	21
2.3.2 Velocity PDFs	23
2.3.3 Negative velocities	25
2.3.4 Velocity derivatives	26
2.4 Evolution of a tracer in a sphere pack	31
2.4.1 Effect of pore space on tracer evolution	32
2.4.2 Effect of the Peclet number tracer evolution	33
2.4.3 Tracer transport results	37

3	Modelling Dispersion	43
3.1	A model for dispersion in porous media	43
3.1.1	A Markovian process for velocity in porous media	43
3.1.2	Eulerian velocity increments	44
3.2	Channel	48
3.3	du and the drift and diffusion terms	49
3.3.1	du in a channel	50
3.3.2	Diffusion term, Γ_p , in a channel	55
3.3.3	Drift term, U_p , in a channel	55
3.3.4	du in a random sphere pack	61
3.3.5	Diffusion term, Γ_p , in a sphere pack	69
3.3.6	Drift term, U_p , in a sphere pack	69
3.4	Tracer transport in a channel	74
3.4.1	Characteristics of the tracer cloud	75
3.4.2	Velocity PDFs	84
3.4.3	Tracer cloud	86
3.5	Tracer transport in a Sphere Pack	90
3.5.1	Characteristics of the tracer cloud	90
3.5.2	Velocity PDFs	98
3.5.3	Tracer cloud	101
4	Conclusions and Outlook	105

List of Tables

2.1	Hydraulic properties of random sphere packs	17
2.2	Hydraulic properties of heterogeneous sphere packs	18
2.3	Velocity statistics in a random sphere pack	22
2.4	Velocity statistics in a dense sphere pack	22
2.5	Statistics of first derivatives of the streamwise velocity component, u	27
2.6	Statistics of first derivatives of the transverse velocity component, v	27
2.7	Statistics of first derivatives of the transverse velocity component, w	28
2.8	Statistics of second derivatives of streamwise velocity in a random sphere pack	30
3.1	Statistics of u and du in a channel	51
3.2	Statistics of du and its components in a sphere pack	62

List of Figures

2.1	Regular sphere pack	11
2.2	Heterogeneous sphere pack	12
2.3	Random sphere pack	13
2.4	Porosity	13
2.5	Grid study	15
2.6	Velocity PDF of various resolutions normalized by respective \bar{u}	15
2.7	Velocity PDF of various resolutions normalized by \bar{u} of finest grid	16
2.8	Coefficient of variation	17
2.9	Velocity PDFs in a random sphere pack for various domain sizes	19
2.10	Permeability plotted against porosity	20
2.11	Streamwise velocity PDFs in dense, random and heterogeneous sphere packs	24
2.12	Transverse velocity PDFs in dense, random and heterogeneous sphere packs .	25
2.13	Negative velocities in a random sphere pack	26
2.14	Streamlines in ordered and disordered sphere packs	26
2.15	PDF of the first derivative of u in a random sphere pack normalized by \bar{u}/D	28
2.16	PDFs of the first derivatives of v and w in a random sphere pack normalized by \bar{u}/D	29
2.17	PDF of first derivative of u in a random sphere pack normalized by σ	29
2.18	PDF of second derivative of u in a random sphere pack normalized by \bar{u}/D^2	31
2.19	PDF of second derivative of u in a random sphere pack normalized by σ . . .	31
2.20	Standard deviation of tracer positions for various configurations	33
2.21	Centre of mass of tracer cloud over time for various Peclet numbers	35
2.22	Standard deviation of tracer positions for different Peclet numbers	35
2.23	Shape of tracer cloud in a random sphere pack for different Peclet numbers .	36
2.24	Skewness of tracer cloud in a random sphere pack for different Peclet numbers	37
2.25	Centre of mass of tracer cloud over time in a random sphere pack	38
2.26	Standard deviation of tracer positions over time in a random sphere pack . .	39
2.27	Skewness of tracer cloud over time in a random sphere pack	39
2.28	Γ_D/Γ plotted against time in a random sphere pack	40
2.29	Velocity PDF of the tracer cloud in a random sphere pack	40
2.30	Mean velocity of the tracer normalized by \bar{u} in a random sphere pack over time	41
2.31	Shape of the tracer cloud over time in a random sphere pack	41
3.1	Set-up of the channel flow	48
3.2	Velocity PDF in a channel	51
3.3	PDF of du in a channel	52
3.4	Conditional mean of du in a channel	52
3.5	Conditional standard deviation of du in a channel	53

3.6	Conditional variance of du in a channel	53
3.7	Conditional skewness of du in a channel	54
3.8	Conditional flatness of du in a channel	54
3.9	Diffusion term in a channel	55
3.10	U_{p1} in a channel	56
3.11	U_{p2} in a channel	57
3.12	U_{p3} in a channel	58
3.13	Drift terms in a channel when LT method is used	59
3.14	Drift terms in a channel when particle method is used	60
3.15	Average and variance of du versus time step size	61
3.16	PDF of du and its components in a sphere pack	63
3.17	Most populous velocity bin versus number of bins	63
3.18	Conditional mean of du in a sphere pack for various bin sizes	64
3.19	Conditional variance of du in a sphere pack for various bin sizes	65
3.20	Conditional extrema of du and its components in a sphere pack	66
3.21	Conditional mean of du and its components in a sphere pack	66
3.22	Conditional variance of du and its components in a sphere pack	67
3.23	Conditional skewness of du and its components in a sphere pack	67
3.24	Conditional flatness of du and its components in a sphere pack	68
3.25	Diffusion term in a sphere pack	69
3.26	Drift terms in a sphere pack	70
3.27	U_{p2} in a sphere pack	72
3.28	U_{p3} in a sphere pack	73
3.29	Drift terms obtained by 128 velocity bins in a sphere pack	74
3.30	Mean position of particles in a channel - U_{p1}	75
3.31	Standard deviation of particle positions in a channel - U_{p1}	76
3.32	Skewness of particle positions in a channel - U_{p1}	77
3.33	Mean position of particles in a channel - U_{p2}	77
3.34	Standard deviation of particle positions in a channel - U_{p2}	78
3.35	Skewness of particle positions in a channel - U_{p2}	78
3.36	Mean position of particles in a channel - U_{p3}	79
3.37	Standard deviation of particle positions in a channel - U_{p3}	80
3.38	Skewness of particle positions in a channel - U_{p3}	80
3.39	Mean position of particles in a channel from the LT method	81
3.40	Mean position of particles in a channel from the particle method	81
3.41	Standard deviation of particle positions in a channel from LT method	82
3.42	Standard deviation of particle positions in a channel from particle method	82
3.43	Skewness of particle positions in a channel from LT method	83
3.44	Skewness of particle positions in a channel from particle method	83
3.45	Velocity PDF for flow in a channel at time $t = 1s$	84
3.46	Velocity PDF for flow in a channel at time $t = 10000s$	85
3.47	Velocity PDF for flow in a channel at time $t = 10000s$ zoomed at small u	85
3.48	Velocity PDF for flow in a channel at time $t = 10000s$ zoomed at large u	86
3.49	Shape of tracer cloud in a channel - benchmark	87
3.50	Shape of tracer cloud in a channel from model - $t = 1000s$	87
3.51	Shape of tracer cloud in a channel from model - $t = 10000s$	88

3.52	Shape of tracer cloud in a channel from model - $t = 40000s$	89
3.53	Mean position of tracer cloud in a sphere pack - U_{p1}	91
3.54	Mean position of tracer cloud in a sphere pack - U_{p2}	92
3.55	Mean position of tracer cloud in a sphere pack - U_{p3}	92
3.56	Mean position of tracer cloud in a sphere pack - 256 bins	93
3.57	Standard deviation of tracer positions in a sphere pack - U_{p1}	94
3.58	Standard deviation of tracer positions in a sphere pack - U_{p2}	94
3.59	Standard deviation of tracer positions in a sphere pack - U_{p3}	95
3.60	Standard deviation of tracer positions in a sphere pack - 256 bins	95
3.61	Skewness of the tracer cloud in a sphere pack - U_{p1}	96
3.62	Skewness of the tracer cloud in a sphere pack - U_{p2}	96
3.63	Skewness of the tracer cloud in a sphere pack - U_{p3}	97
3.64	Skewness of the tracer cloud in a sphere pack - 256 bins	98
3.65	Γ_D/Γ over time in a random sphere pack - model versus DNS	98
3.66	Velocity PDFs at time $t = 250s$ in a sphere pack	99
3.67	Velocity PDFs at time $t = 250s$ in a sphere pack - zoomed	100
3.68	Velocity PDFs at time $t = 40000s$ in a sphere pack - zoomed	101
3.69	Shape of tracer cloud in a sphere pack at various times	102
3.70	Shape of tracer cloud in a sphere pack at various times - U_{p3}	103

Nomenclature

Roman letters

c	concentration
CV	coefficient of variation
D	grain size/ sphere diameter
du	velocity increment
F	Flatness
h	half width of channel
L	Length scale
m	mean of a population
M_s	the s th raw moment of a population
m_s	the s th statistical central moment around the mean of a population
N	normally distributed random number
P	probability density of velocity
p	pressure
Pe	Peclet number
Re	Reynolds number
S	skewness
Sc	Schmidt number
t	time
t_{dif}	diffusive time scale
u	pore velocity component
\mathbf{u}	velocity vector
\bar{u}	mean pore velocity component
\bar{u}_t	average velocity of the tracer cloud
U_p	drift term
U_s	superficial velocity component
\bar{v}	mean pore velocity component
V_{pore}	volume of the pore space
\bar{w}	mean pore velocity component
x	position parameter

Greek letters

Γ	molecular diffusion
Γ_D	dispersion coefficient
Γ_p	diffusion term
δ	diffusion number
ϵ	porosity
κ	permeability
μ	dynamic viscosity of fluid
ν	kinematic viscosity of fluid
ρ	mass density of fluid
σ	standard deviation of a population from its mean

Symbols

var	variance
$\langle \dots \rangle$	averaging operator
∇	Nabla operator in physical space

1 Introduction

The flow of fluids in porous media is of importance in many different fields. Resolving the behaviour of fluids as they pass through porous media for example, provides an understanding of groundwater flow and the issues concerning its contamination. The design of chemical reactors, in which heat and mass transfer in porous catalysts are of importance, is also dependent on prediction of flows through porous media [13]. Another example of a field benefiting from the understanding of flows in porous media is the oil industry where a knowledge of oil flow in reservoirs is of importance for a better understanding of the oil recovery process. In medical sciences also, flows in porous media have relevance when considering fluid flow through body tissues. A very challenging issue for instance is the brain-blood barrier which prevents various drugs from reaching the brain. Models of transport in porous media can be of vital help in finding ways of introducing drugs directly into the tissue and avoiding the blood-brain barrier [35].

Here we present some background on different issues of and approaches to various aspects of dealing with flows in porous media with emphasis on the dispersion phenomena, which we aim at modelling in this work. We start by presenting an overview of the dispersion phenomena which will be followed by some background on dealing with non-Fickian dispersion. In the next section we will continue by comparing pore scale versus macro scale studies and simulations of porous media flows. This will be followed by a very brief background on standard discretization and random walk methods as they build the foundation of what is presented in this work. The chapter will be concluded with the objectives and an overview of what will be presented in this work.

1.1 Dispersion

Dispersion of tracers in porous media is one of the key processes in understanding and modelling subsurface contaminant dynamics. When a tracer in a porous medium is spread over a volume larger than what would be expected from the molecular diffusion and mean pore velocity alone, the dispersion phenomena is said to have happened. It is generally accepted that mechanical dispersion is the spreading of a tracer cloud in the porous medium due to the variability of individual flow paths of tracer particles during convection through the irregular pore space. The flow paths in a porous medium are tortuous and also the velocity varies in each pore of the media, leading to an excessive spreading of the tracer. The dispersion phenomena has been of immense interest to scientists in the study of flows in porous media for more than a century. As early as 1905 for example Slichter [46] reported encountering dispersive behaviour in his studies of ground water.

Dispersion involves two main effects that need to be modelled on the macroscopic scale. The first one deals with the spatial spreading of plumes and fronts in a macroscopic point of view. The second aspect of dispersion affects the mixing of species on a molecular level. The latter

aspect attains importance when thermodynamical, chemical or biological non-equilibrium leads to reaction or degradation processes in the pore space.

In this work we focus on the first aspect which involves the spatial averaged concentrations of the tracer on a *Representative Elementary Volume* (REV). Modeling dispersion on this level has often been done by assuming an effective diffusivity for the tracer [2, 5]. The resulting *Advection-Diffusion Equation* (ADE) can be solved by standard discretization methods (e.g. FE, FV and FD) or by stochastic (random walk) methods.

Modelling dispersion by an effective diffusion coefficient, however, can only describe Fickian dispersion, i.e. Gaussian spreading of tracer clouds. In Fickian dispersion it is assumed that the dispersive mass flux of a tracer is linearly proportional to its concentration gradient. By this definition dispersion is assumed to be independent of its history and of temporal and spacial scales of measurement [12]. After a certain amount of time has passed since the release of a tracer in a porous media, such that the successive velocities of each individual particle are no longer correlated, the total displacement of a particle becomes equivalent to the sum of all the successive displacements which are statistically independent. Then, according to the “central limit theorem” regardless of the initial probability distribution of elementary displacements the probability density of the sum of the displacements should tend to the normal distribution. At a later time, t , the probability density of the displacement of an individual particle according to the “ergodic hypothesis” is equivalent to the spatial distribution at time t of a cloud of particles originating from the same place and time and under the same conditions [2]. Therefore, one can expect the shape of the tracer cloud to become Gaussian and the dispersion to be Fickian at later times. However these assumptions do not generally hold (e.g. at early times when the successive velocities and therefore displacements of particles are still correlated). It is worth mentioning that the relation between diffusion of particles and their velocity correlation has long been established by Taylor [50].

In their dispersivity measurements of 59 different field sites, for example, Gelhar et al. [10] observed the variability of dispersion with respect to temporal and spacial scales of observation. In fact, non-Fickian dispersion is in general considered a result of heterogeneities in the porous medium. Silliman and Simpson [45] investigated the effect of heterogeneity on dispersion through a number of different sand packing arrangements. They reported non-Fickian behaviour due to even small-scale heterogeneities. In 2002 Scheven and Sen [44] reported their findings on the investigation of Stokes flow in random sphere packs containing glass beads of constant diameter. Although the random domains they constructed were practically homogeneous, they observed non-Fickian behaviour for advection length scales of up to more than ten times the sphere diameter. They achieved Fickian diffusion for large advective length scales when the diffusive length scale was greater than 30% of the sphere diameter. It is clear that non-Fickian dispersion is not limited to highly heterogeneous domains but can also be observed at early transport times even in homogeneous domains.

Non-Fickian dispersion is characterized by strongly skewed tracer distributions in space and break-through curves with extremely long tails. On the other hand it has been argued [33] that in the early stages of dispersion, spatial concentration distributions (so-called propagators) are strongly correlated with and mimic the velocity distribution function. Thus, it is of no surprise that early stage propagators on the pore scale - while

resembling the velocity distribution function - show non-Fickian behaviour even in non-heterogeneous materials such as random sphere packs [44]. It is therefore of inherent interest to study the formation, the dynamics in and structure of velocity distributions on the pore level.

1.2 Treating non-Fickian dispersion

For dealing with non Fickian dispersion, which is observed in the initial phase of transport through porous media or in heterogeneous porous domains, various laboratory experiments have been performed and special methods such as the use of the equation of motion of a solute have been employed in order to derive a generalized dispersion equation.

In his paper “On the Transient Non Fickian Dispersion Theory”, Hassanizadeh [12] discusses three different approaches of dealing with non fickian dispersion; namely the non Fickian equations of Scheidegger ([43]), Tompson ([52]) and Strack ([48]). He then develops and presents a general equation for dispersive mass flux which can in fact be considered a generalized form of the equations of the three afore mentioned researchers. Lowe and Frenkel [25] simulated flow in rectangular boxes randomly packed with spheres using the Lattice Boltzmann method and calculated velocity auto correlation functions and dispersion coefficients for various Peclet numbers. They observed anomalous, non-Fickian behaviours and suggest that rather than being transient the non-Fickian dispersion can persist over time. In 2000 Maier et al. [28] simulated dispersion in three dimensional regular and random sphere packs. They also obtained the pore scale velocity in the domains using the Lattice Boltzmann method and used a random walk particle tracking method to simulate the tracer evolution for various Peclet numbers. They calculated the dispersion coefficient and the velocity autocorrelation function for various variations of sphere pack and Peclet numbers and evaluated the effect of periodic boundaries, spatial resolution and packing variations on the dispersive behaviour. They investigated both the asymptotic (Fickian) and the non-Fickian dispersion and the time at which the dispersion coefficient converges to the asymptotic state.

In 2003 Levy and Berkowitz [23] performed three sets of experiments in order to observe the breakthrough behaviour of contaminants in porous media of different levels of heterogeneity. They used their findings to evaluate the classical ADE and the continuous time random walk method. They observed non Fickian behaviour even in homogeneously packed domains. They concluded that the continuous time random walk approach can yield a more accurate breakthrough curve than the classical ADE method.

In general an efficient method of dealing with dispersion is through the stochastic approach to flow and transport in porous media which aims at producing the statistical moments of quantities such as velocity and concentration in the porous medium. One method is to obtain governing equations of the statistical moments of the desired quantities with the help of known statistics of the parameters which describe the fluid and the porous domain such as permeability and log-conductivity [56] and then to solve these equations by means of low order approximations as done by for example Gelhar et al. in 1979 [9]. Gelhar et al. analysed the dispersion as a result of variations in the hydraulic conductivity field in an aquifer. They described the mass transport process using a first order approximation and

solved the resulting stochastic equation for concentration using spectral representations. The use of low order methods however is not suitable for the cases where the variance of the log-conductivity is high [33]. In 2008 Nowak et al. [36] showed the dependence of hydraulic heads and velocities on the variance of log-conductivity using Monte Carlo simulations. They resolved their three dimensional velocity fields on a large number of realizations by solving the Darcy equation using a finite element method. In their 2008 paper on this study, they offer insight into the credibility of first-order second moment (FOSM) methods for evaluating moments of hydraulic heads. They observe a large deviation of the discharge components from Gaussian distribution and suggest using more accurate methods such as extensive Monte Carlo or higher order stochastic approaches if no assumptions on the shape of distributions are justified. Directly obtaining the statistical moments of flow and transport parameters by means of Monte Carlo simulations can produce accurate statistical values for general cases of flow in porous media but accurate and sufficient Monte Carlo simulations are very expensive computationally.

In this work we present a model for dispersion based on a similar model presented by Meyer and Tchelepi [32] in 2010. Taking explicitly into account the form of the velocity *Probability Density Function* (PDF), Meyer and Tchelepi have constructed a model to describe non-Fickian and Fickian dispersion. This approach is especially attractive as dispersion is inherently connected to the velocity distribution function as previously discussed. In this approach, the evolution of a tracer cloud is represented by a random walk model in physical as well as in velocity space. The random walk model in velocity space consists of a continuous Markovian process and is equivalent to a Fokker-Planck equation for the velocity distribution function involving a drift and a diffusion term. Meyer and Tchelepi demonstrated that both, drift and diffusion in velocity space, can be obtained from velocity statistics [33]. They obtained the drift term from the averaged velocity increments conditioned on the sample space velocity while obtaining the diffusion term from the variance of the velocity increments conditioned on sample space velocity. Both of these terms were obtained by stochastic simulations and from Lagrangian displacement statistics of two-dimensional Darcy flow through random permeability fields. The main difference between the model of Meyer and Tchelepi and our model is that we calculate the drift and diffusion terms from the statistics obtained from pore scale simulations on 3D domains. Both our model for dispersion and the model of Meyer and Tchelepi will be discussed in detail at the beginning of chapter 3. A background on pore scale studies of flow and transport in porous media is presented in the following section.

1.3 Pore scale versus macro scale

In the stochastic approach to flows in porous media, the Darcy equation is almost always taken as the governing equation for the flow. However, PDFs of velocity in porous media vary with probe size down to the pore scale. This is evident when considering the simple case of a laminar flow through a circular pipe. At each wall distance, the local velocity differs from the bulk velocity, i.e. the velocity integrated over the cross section. Therefore, the sample size required to determine the PDF of the velocity in a porous medium needs to be considerably smaller than the average pore diameter. Due to experimental limitations, laboratory experiments on porous media usually deal with averaged medium properties.

There do nevertheless exist, some experimental studies involving detailed measurements of pore scale velocities and tracer concentrations in porous media such as the work of Rashidi et al. [41] who using a non-intrusive fluorescence imaging technique were able to conduct three dimensional, pore scale measurements of grain geometry, flow velocities and tracer concentrations in a sphere packed cylindrical column. Often, these studies more or less suffer from a lack of sufficient resolution or limitations in the size of observation zones. Until precise and efficient local measurement techniques are available for porous media, numerical simulations are the only means of assessing local velocity distributions on the pore level.

By directly solving the Navier-Stokes equations on the porous domain, one would not need to model the dispersion or estimate the permeability, and the only uncertainty will be due to the simplification of the complicated geometry of the pore space. Pore scale transport models are therefore very appealing. In the introduction of a paper they published in 2011 Ovaysi and Piri [38] categorize these models into two groups. In the first group the geometry is represented as an idealized network of pores connected by throats while in the second group “the equations of flow are directly solved on the pore space”. Many well-known methods such as the Lattice-Boltzmann method, finite elements, difference or volume methods, Monte Carlo method, smoothed particle hydrodynamics, moving particle semi implicit model method, etc. can be employed for solving the equations of flow on the pore space.

Here are listed a few examples of pore scale studies on flow and transport in porous media. One of the first three dimensional pore scale studies was that of Salles et al. [42] who provided numerical pore scale results for periodic three dimensional homogeneous structures containing arrays of identical unit cells. Four major possible types of these unit cells or structures were investigated. In order to obtain the velocity field they numerically resolved the Stokes equations on each local structure. They calculated the dispersion tensor for different types of porous media by various methods and investigated the dispersion behaviour for various Peclet numbers. A very comprehensive pore scale study on flows in porous media was carried out by Maier et al. [29]. They used the Lattice Boltzmann method to resolve the velocity field through various configurations of cylinders packed with spheres at different spatial resolutions and flow rates and calculated the velocity distribution functions. They investigated the effects of the spacial resolution, Reynolds number and cylinder geometry on the velocity distribution. They also calculated the permeability for different resolutions and compared their results to empirical formulas such as the Kozeny-Carman equation.

In 2000 Zhang et al. [57] performed pore scale Lattice-Boltzmann simulations to obtain parameters such as permeability and porosity at various locations and scales in a porous medium and to quantify the size of the REV for heterogeneous material. A few years later, Kainourgiakis et al. [15] reconstructed 3D porous domains and studied the transport properties of two phase flows through these structures. Their pore scale simulations were performed using a finite difference scheme together with a compressibility relaxation algorithm. They validated their resulting transport properties obtained through these simulations with existing data. In 2008 Lehmann et al. [22] attempted to identify the geometric properties which are relevant for flow (especially multiphase flow) and transport in porous media by means of pore scale simulations. They built artificial 3D porous structures with fixed geometric prop-

erties (Minkowski functionals) and performed pore scale simulations on these domains by a Lattice Boltzmann scheme. In their configurations the volume and surface of the domain appeared to have a larger impact on the permeability than the curvature or connectivity of the system. As another example of pore scale studies, Morais et al. [34] studied non-Newtonian flows in a Swiss cheese porous domain model using the finite difference method. In their paper published in 2010 Ovaysi and Piri [37] introduce a dynamic particle based method for simulating three dimensional flow on the pore scale. Their strategy is to discretize the whole domain (both solids and fluid) into particles and solve the N-S on each particle. They employ this method to simulate transport in porous media as described in their 2011 paper on this subject. In this work they perform pore scale studies on x-ray images of sandstones, calculate dispersivity tensors using the method of moments and analyse the longitudinal dispersivity in the flow field for a wide range of Reynolds numbers. They investigate the impact of inertial forces on longitudinal dispersion and the effect of grain size on solute transport at the pore level [38]. Both these papers include a rather good literature review of pore scale studies on flows and transport in porous media.

1.4 Standard discretization and random walk methods

In this work we use a standard discretization (finite volume) method for resolving the velocity field in porous media and using the results of that, we present a model for dispersion which relies on a random walk, particle tracking method for modelling the tracer behaviour in the porous medium. It is therefore appropriate to offer a brief background both on standard discretization methods and on random walk methods used for flows and transport in porous media.

The use of standard discretization methods for solving ADEs is well documented in literature. In 1995 Martys [31] investigated the applicability of computational methods in simulating dispersion in 2D random porous media. He used the finite difference method (FD) for solving both the Stokes equations and the ADE for various configurations. He then extracted effective diffusion coefficients by evaluating the obtained concentration profiles. As a further example one can point to the work of Acharya et al. [1] who used the finite volume method (FV) for studying reactive transport in a 2D porous media or to the work of Garmeh et al. [8] who utilized a finite element (FE) commercial code to model dispersion in 2D porous media and analysed the effect of porosity and heterogeneity on dispersion coefficients.

On the other hand, random walk methods have been extensively used for modelling the spreading of a tracer in porous media since the 1970s. In 1996 Labolle et al. [19] used the random walk method to simulate tracer transport in porous media and investigated mass conservation issues in the case where interpolation schemes are used when obtaining velocities. In their 2006 paper on modeling non-Fickian transport using a continuous time random walk method, Berkowitz et al. [3] present a broad overview of the CTRW approach and compare it to other methods of dealing with transport in porous media. As a more recent example Suciu et al. [49] use a mixed finite element method (MFEM) to resolve the velocity field using the Darcy and continuity equations and couple that with a global random walk (GRW) method

to track a large number of particles in a porous medium.

1.5 Objective and overview

The objective of this work is to develop and test a model describing dispersion in porous media based on a model for dispersion proposed by Meyer and Tchelepi [33] in 2010. The model is to be developed such that it describes the dispersion by the randomness of the tracer paths in the pore level rather than by the heterogeneity of the macroscopic permeability field. The aim is to reduce the geometrical complexity of the pore space to the detailed statistics of the velocity field. The basis of the model is in-depth information concerning the pore scale velocities and the conditional statistics of the velocity variation field. Validation of the model should be carried out by comparing its results to those obtained via detailed pore scale simulations of transport in porous media. *Direct Numerical Simulation* (DNS) of pore scale flow in porous media should be used to generate reliable data to quantify the different terms of the model while DNS of pore scale transport in porous media is used to obtain tracer transport data necessary for assessing the accuracy of the model.

In this work, we first present properties of flows through porous domains with periodic boundaries. We investigate the statistics and PDFs of velocity and velocity derivatives. In contrast to many other such studies which are often limited to 1D or 2D cases, homogeneous domains or oversimplified geometries where the velocity is computed using the Darcy equation, we fully resolve the velocity field by solving the Navier-Stokes equation using the DNS method. Direct Numerical simulations are performed using our in-house code MGLET to solve the Navier-Stokes equation and obtain the velocity field via a finite volume method. MGLET uses the finite volume method for space discretization, third-order Runge-Kutta for time integration and immersed boundary method for complex geometry treatment. The porous media is represented as a cube, randomly packed with spheres with periodic boundaries. Next, we investigate a stochastic velocity model for dispersion proposed by Meyer and Tchelepi [33] and venture to develop our own slightly modified version of the model. Our model is based on a method for obtaining the velocity variation field independent of the geometry of the porous media and relying solely on the pore scale velocity and velocity derivative fields. By investigating the velocity variation field and its statistics conditioned on velocity in a simple channel and in a sphere pack, we verify our model for dispersion and determine the different terms. Finally we try out different variations of our model on the flow in a channel and in a random sphere pack to appraise its validity as compared to dispersion results obtained via DNS.

2 DNS Data Base

In this chapter we present the results of our investigation of the steady flow field on the pore scale of random sphere packs by direct numerical simulations. The porous media is represented as a rectangular domain (REV), randomly or regularly packed with spheres. All boundaries are assumed to be periodic. The full Navier-Stokes equations for an incompressible, Newtonian fluid are solved by a Finite Volume method on a Cartesian grid. The irregular pore space is represented by an Immersed Boundary Method.

The geometrical modelling of the porous media and the numerical method of solving the governing equations for velocity and tracer transport are described in the following section. In the second section of this chapter we present the validation of our method. After briefly explaining and justifying our approach, we move on to presenting the results of our pore scale simulations. These results will be split into two parts and make up the last two sections of this chapter. The first part will focus on the properties, statistics and PDF of velocity and velocity derivatives in a sphere pack. In the second part we present the results of our simulation of tracer transport in a random sphere pack.

2.1 Method

In this section we present the governing equations of flow in the pore space and very briefly explain our methods for solving them. We also present our representation of the pore space geometry.

2.1.1 Solution of the Navier-Stokes and transport equations

Direct Numerical simulations are performed using our in-house code MGLET to solve the Navier-Stokes equation and obtain the velocity field. MGLET uses the finite volume method for space discretization, third-order Runge-Kutta for time integration and immersed boundary method for complex geometry treatment. The Navier-Stokes equations, i.e. the conservation equations of mass and momentum are shown below where \mathbf{u} , p , ρ and μ denote the velocity, pressure, density and dynamic viscosity, respectively.

$$\nabla \cdot \mathbf{u} = 0 \tag{2.1}$$

$$\rho \partial_t \mathbf{u} + \rho \mathbf{u} \cdot \nabla \mathbf{u} = -\nabla p + \mu \nabla^2 \mathbf{u} \tag{2.2}$$

The transport equation for a passive tracer which is also solved by a finite volume method using MGLET reads

$$\frac{\partial c}{\partial t} = -\mathbf{u}\nabla c + \Gamma\nabla^2 c \quad (2.3)$$

where c is the concentration of the tracer, \mathbf{u} is the velocity vector and Γ is the molecular diffusion.

These equations are integrated over Cartesian grid cells that are arranged on staggered positions [11]. The spatial approximations are standard central difference approximations [30]. On equidistant grids, these approximations are skew-symmetric [53] and obey advantageous numerical properties such as conservation of mass, momentum and energy. The time advancement is done by a low-storage third order Runge-Kutta method [55]. This basic solver is well validated in various flow configurations including laminar and turbulent flows (e.g. [6, 14, 39, 30, 58]). It has been shown that for viscous flow problems a second order convergence with grid refinement is achieved [39, 40].

We apply periodic boundary conditions in all three space dimensions. The flow is driven by a constant pressure gradient and advanced from rest until convergence is reached. As we only deal with Reynolds numbers which are extremely small, the time to reach convergence to steady state is mainly determined by the diffusion time scale κ/ν within the pore space, κ being the permeability.

$$t_{dif} = \frac{\kappa}{\nu} \quad (2.4)$$

Here t_{dif} is the diffusive time scale while ν denotes the kinematic viscosity of the fluid. Once the velocity field is resolved it can be used in the solution of the transport equation by MGLET.

The pore space is represented in the Cartesian grid by a so-called Immersed Boundary Method. The total space of the sphere pack (including both the pore and the solid space) is discretized by a regular Cartesian mesh with cubic grid cells. The surface of the solid material, constituting the pore space, lies in between the Cartesian grid cells. It is assumed that at this surface, the velocity is zero (no-slip condition). This is achieved by a special interpolation of the velocities in the cells adjacent to the pore surface. This interpolation uses second or higher order polynomials that assume the boundary value at the pore surface. The method has been shown to be second order accurate with respect to mesh refinement in space [40]. A special treatment of the volume fluxes during the pressure correction step of the time advancement ensures conservation of mass throughout the whole domain [39].

2.1.2 Generation of sphere packs

We represent the porous medium by rectangular sphere packs. These sphere packs were generated in three different ways to produce a dense and ordered sphere pack, an inhomogeneous random sphere pack or a homogeneous random sphere pack. All three types of

domains have periodic boundaries and are packed with spheres with a constant radius of $1mm$.

The dense sphere pack is a rectangular domain of size $(L_x, L_y, L_z) = (2\sqrt{3}, 2\sqrt{3}, 2)mm$, well packed with 13 spheres of radius $1mm$. The spheres in the domain were arranged by a hexagonal close packing method where layers of spheres are packed such that alternating layers overlie one another [54, 7, 47]. The result is a periodic and dense sphere pack with the minimum number of spheres possible. See figure 2.1. The porosity of this set-up is $\epsilon = 0.282$. In this work we use the term “dense” or “regular” when referring to this sphere pack.

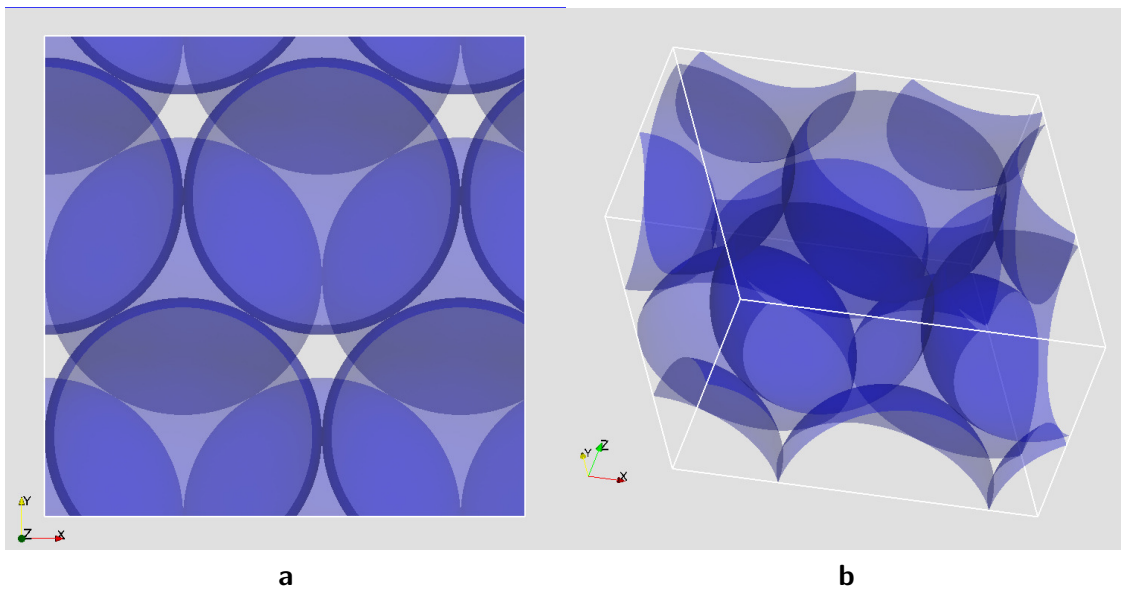


Figure 2.1: Configuration of a regular sphere pack. Top view (a) and perspective view (b).

The inhomogeneous random sphere packs are made using a simple algorithm that places spheres in a cubic domain such that no two spheres overlap. The algorithm starts by placing spheres randomly on a vertical edge of the cubic domain and then copying this edge on the other vertical edges such that the periodicity of the domain is satisfied. It then continues by filling in one vertical plane surface of the domain with spheres and copying it onto the opposite surface such that the domain remains periodic. Since the edges of the surface are pre-filled with spheres and because the spheres are not permitted to penetrate each other the centre of the surface will be more dense and between the central part and the edges there will remain an area of high porosity. This procedure is carried out for the other pair of vertical surfaces of the domain. Once all four vertical faces are packed with spheres the algorithm randomly packs the bottom surface with spheres too and then copies that to the top surface fulfilling the periodicity requirement. Finally the inside of the cube is filled randomly with spheres. Again there exists a rather more porous area between the faces of the domain and the inner region (see figure 2.2). This random sphere pack domain will simply be referred to as “heterogeneous”. The average porosity of 15 different realizations of this set-up in the case where the domain size is equal to $2.0cm$, is $\epsilon = 0.450$.

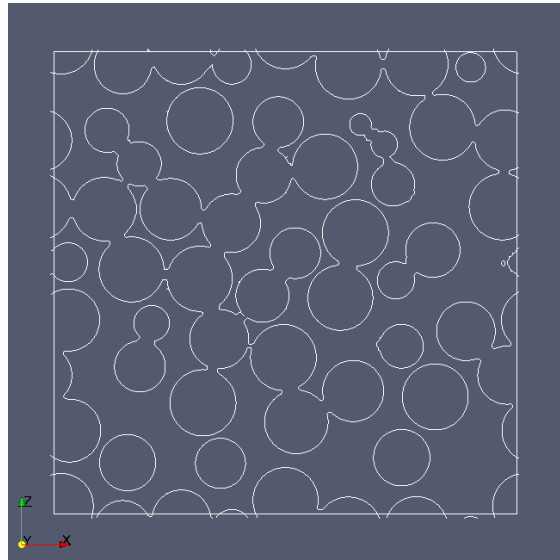


Figure 2.2: Cross section of a heterogeneous sphere pack.

For the homogeneous random sphere packs our goal was to pack the spheres as tightly as possible and to limit our porosity to less than $\epsilon = 0.430$. To do so, we used the package described by Lieb et al. in [24] which is based on the algorithm developed by Lubachevsky and Stillinger [26]. Such a randomly packed domain can be seen in figure 2.3. The average porosity of 20 different realizations of this arrangement in the case where the domain size is set to 2.0cm is $\epsilon = 0.354$. The term “random sphere pack” in this dissertation without any further explanation concerning the homogeneity or lack of in the domain refers to this type of homogeneous random sphere pack.

To better see the difference between the sphere distributions in the heterogeneous and the homogeneous random sphere packs figure 2.4 shows the porosity of cross sections normal to the x (streamwise) direction plotted against x for two different cases. The first case is one realization of random and homogeneously packed domain of size 2.4cm and the second case is one realization of random but inhomogeneously packed domain of size 2.0cm .

Notice how the porosity remains in the vicinity of its average throughout the whole length of the domain in the case of the random (homogeneously packed) domain while in the case of the heterogeneous pack the porosity is much higher near the two ends of the domain but stays close to average elsewhere due to the particular sphere packing algorithm used in making the heterogeneous domain.

2.2 Validation

In this part we aim at justifying our DNS results in terms of grid resolution, domain size and the conformity of the macro-scale parameters obtained from our pore scale simulations with empirical formulas.

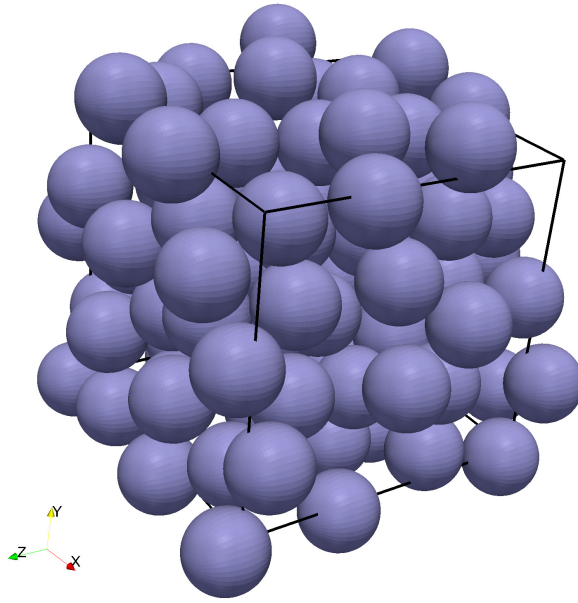


Figure 2.3: One realization of a random sphere pack.

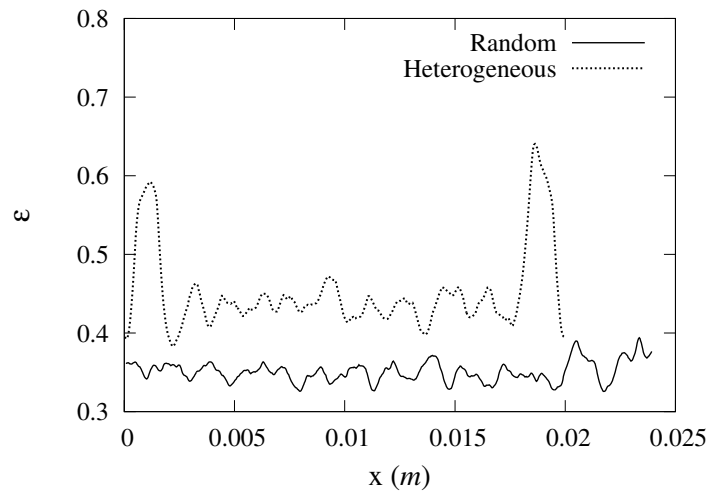


Figure 2.4: Porosity plotted over x for one realization of random and homogeneously packed domain of size 2.4cm and one realization of random but inhomogeneously packed domain of size 2.0cm .

2.2.1 Convergence study on the dense sphere pack

In order to select an efficient mesh size, a grid study was performed for water flowing through the dense sphere pack described in section 2.1.2. This domain is periodic and tightly packed with spheres of radius 1mm .

The validation was done in two steps. In the first step, we assessed the number of cells needed

per sphere diameter for the intrinsic velocity to converge. In the second step, the behaviour of the PDF of the velocity field was observed in order to determine after which level of grid refinement the general shape of the PDF curve converges.

The flow was driven by a pressure gradient of $0.025 P_a/m$ in the x -direction. The Reynolds number of this set-up was in the order of $Re = \bar{u}L/\nu = 2 \times 10^{-4}$. Where, L is a characteristic length scale (in our case the sphere diameter), and ν is the kinematic viscosity. \bar{u} is defined as the mean streamwise pore velocity in the porous domain i.e. the intrinsic velocity.

$$\bar{u} = \frac{1}{V_{pore}} \int_{V_{pore}} u(\vec{x}) d\vec{x} \quad (2.5)$$

Here V_{pore} is the volume of the pore space and $u(\vec{x})$ the local pore velocity. The average streamwise pore velocity, \bar{u} is related to the streamwise superficial or Darcy velocity U_s by

$$U_s = \bar{u}/\epsilon \quad (2.6)$$

where ϵ is the porosity. The mean transverse pore velocities in y and z direction, denoted by \bar{v} and \bar{w} , respectively, should be zero as the pressure gradient points only in the x direction.

Figure 2.5a shows the mean pore velocity, \bar{u} , versus the number of grid cells per radius of the grains. Starting from approximately 11 cells per sphere radius, the average pore velocity obeys a monotonic convergence and the error is limited to less than 6% with meshes finer than 24 grid cells per radius. The convergence is at least of second order, as figure 2.5b demonstrates. Here, we plot the error with respect to the \bar{u} obtained using 56 grid cells per radius as reference \bar{u}_{ref} .

$$error = \frac{\bar{u} - \bar{u}_{ref}}{\bar{u}_{ref}} \quad (2.7)$$

In the second part of the validation study, we assess the prediction of the velocity PDF for various grid refinements. To obtain the PDFs we divided the velocity field in the range between $-0.6\bar{u}$ to $+10\bar{u}$ in 160 bins for each case, \bar{u} being the average pore velocity for each configuration. The PDF value is normalized such that the area underneath each curve remains equal to one. One can see that with an increase in the number of grid cells the velocity PDFs converge to a certain shape, see figures 2.6 and 2.7. It appears that the PDF at low velocities, which include the peak of the PDF curve, is especially sensitive to the grid resolution. The almost singular behaviour of the PDF peak has been observed in previous studies. Notably, in their paper concerning pore scale simulations of flow through bead packs, Maier et al. come across such very sharp peaks near $u = 0$ and offer a geometric argument (assuming monotonic variation of velocity away from the sphere surface) for justifying this observation [29]. The PDFs at large velocities on the other hand, suffer from statistical uncertainties as their probabilities tend towards zero. Note that the ve-

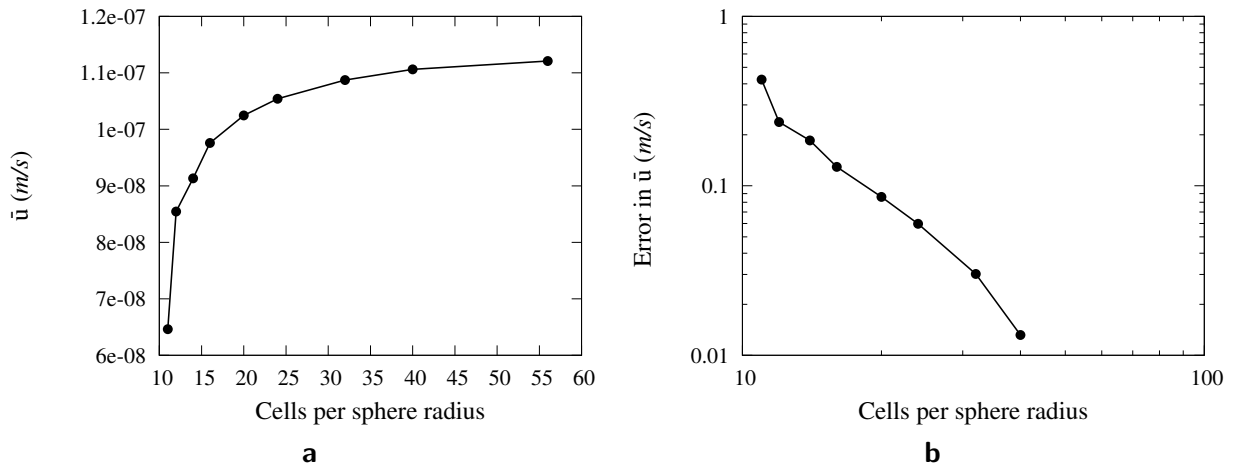


Figure 2.5: Mean streamwise pore velocity in a dense sphere pack as a function of number of grid cells per sphere radius (a). Error with respect to solution with 56 grid cells per radius (b).

velocity field is not very populated in the higher velocity range, especially when the grid is coarse.

Taking everything together, we concluded that with 32 grid cells per sphere radius it will be possible to obtain sufficiently accurate velocities and velocity PDFs. Therefore, we chose this resolution for the simulations presented for the random sphere packs. The results presented for the dense sphere pack are obtained using 56 cells per sphere radius (as the dense pack is rather small and we can afford a finer grid) while those of the heterogeneous random sphere packs are obtained using 20 cells per sphere radius.

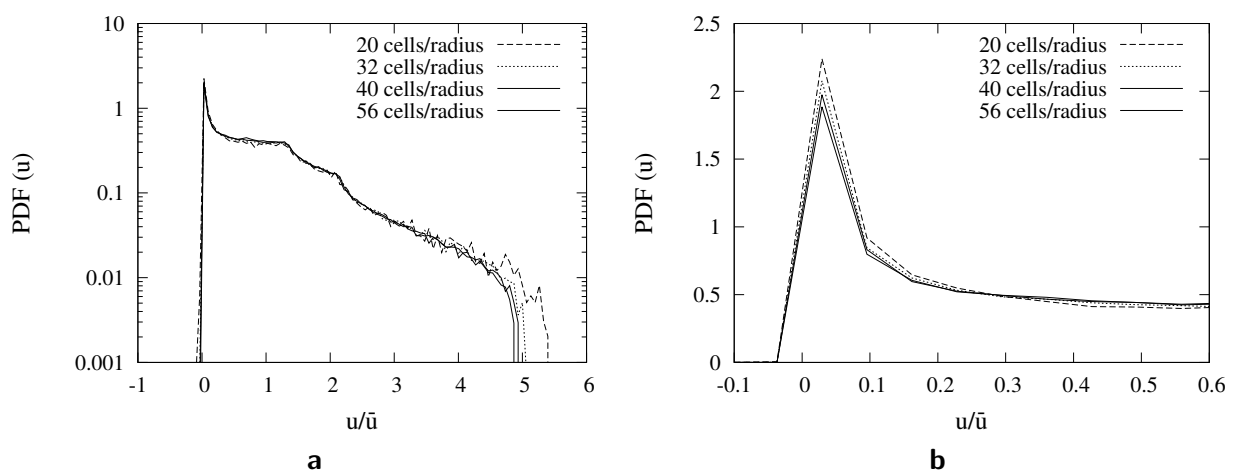


Figure 2.6: Convergence of velocity PDF's in a dense sphere pack with increasing grid resolution. Each case is normalized by its corresponding \bar{u} . Total velocity domain plotted in semi Log scale (a); zoom (b).

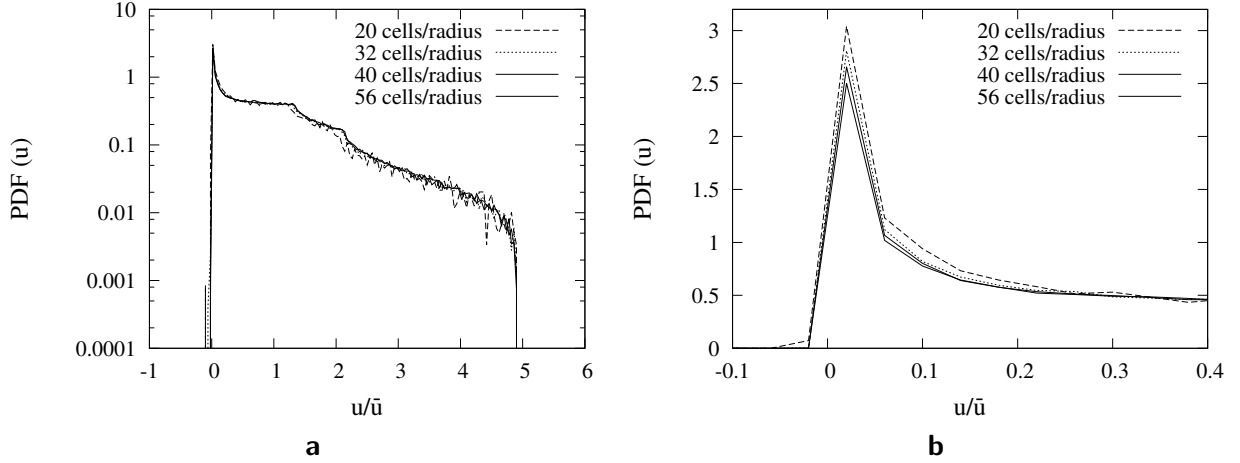


Figure 2.7: Convergence of velocity PDF's in a dense sphere pack with increasing grid resolution. Each case is normalized by \bar{u} obtained using 56 cells per radius. Total velocity domain plotted in semi Log scale (a); zoom (b).

2.2.2 Dependence of global variables on the size of the REV.

Multiple realizations of random sphere packs were generated to gather statistics and to acquire an estimation of the size of the REV. Porous domains of dimensions ranging from $(0.4cm)^3$ to $(2.8cm)^3$, equivalent to $(2D)^3$ to $(14D)^3$ were generated using the sphere pack generator of Lieb et al. [24], D being the sphere diameter ($D = 2mm$). For each domain size, 20 random realizations of sphere packs were generated using a fixed sphere radius of $1mm$. In each case the domain was meshed with elements of size $3.125 \times 10^{-5}m$ which is equivalent to 64 cells per sphere diameter. The flow was driven by a pressure gradient of $-0.025P_a/m$ in the x direction. The Navier-Stokes equations were solved by DNS and the velocity field was obtained. The permeability, κ , for each case was calculated by plugging the average streamwise superficial velocity, U_s , obtained by DNS into the Darcy equation.

$$\kappa = U_s \frac{\mu}{\nabla p} \quad (2.8)$$

The statistical properties of the streamwise mean pore velocity \bar{u} , porosity ϵ and permeability κ of the realization are given in table 2.1. As expected, with an increase in the size of the domain the standard deviations of the permeability, porosity and mean pore velocity in different realizations of the random sphere pack decrease. In other words, the global properties of different realizations become more similar. We observed that for domains of size $1.6cm$ (equivalent to $8D$) or larger, the standard deviation of the permeability of different realizations normalized by the average permeability (the coefficient of variation, CV) is limited to less than 2.2%. The coefficient of variation, CV , shows the extent of

variability of a dataset in relation to its mean.

$$CV = \frac{\sigma}{m} \quad (2.9)$$

In the above, σ represents the standard deviation of a population from its mean and m represents the average of the said population. The coefficient of variation (CV) of the porosity ϵ and mean pore velocity \bar{u} for domains of size $1.6cm$ or larger on the other hand is limited to 0.7% and 2% respectively. See figure 2.8.

Table 2.1: Hydraulic properties of random sphere pack samples.

Domain size ($D = 2mm$)	2D	4D	6D	8D	12D	14D
Number of samples	20	20	20	20	20	20
Mean number of spheres	23.712	134.732	393.420	851.357	2605.401	4081
mean ϵ	0.378	0.382	0.361	0.358	0.354	0.354
CV of ϵ	0.054	0.046	0.018	0.007	0.003	0.003
mean \bar{u} ($\frac{m}{s}$)	2.041E-7	2.008E-7	1.926E-7	1.919E-7	1.912E-7	1.916E-7
CV of \bar{u}	0.125	0.073	0.031	0.02	0.01	0.009
mean κ (m^2)	3.33E-9	3.315E-9	3.015E-9	2.980E-9	2.940E-9	2.949E-9
CV of κ	0.122	0.091	0.029	0.022	0.011	0.012

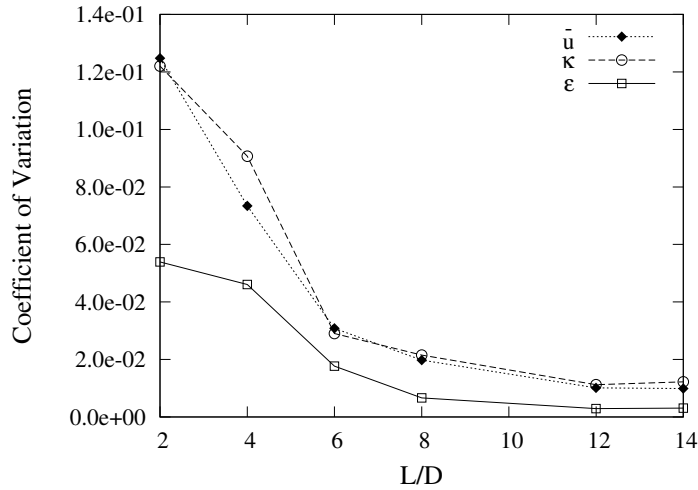


Figure 2.8: Coefficient of variation for the intrinsic velocity \bar{u} , permeability k and porosity ϵ plotted against domain size, L , normalized by sphere diameter, D .

Also with an increase in the domain size, the mean magnitude of κ , ϵ and \bar{u} will converge to certain values. The mean being the average over various random realizations of each domain size. The domain size at which sufficient convergence is achieved can indicate the size of the

REV for such porous structures. We accept a domain of size $2.4cm = 12D$ as sufficiently large to yield acceptable statistical values.

The same procedure was carried out for heterogeneous sphere packs for comparison. Multiple realizations of sphere packs with sizes ranging from $0.4cm$ to $2.0cm$ were produced and a pressure gradient of $-0.025Pa/m$ was imposed on the streamwise direction. The Navier-Stokes equations were resolved on these domains by DNS using MGLET. Table 2.2 summarizes the results of these simulations. Here also the same trends can be seen although less pronounced. For example notice how the coefficient of variation of the mean pore velocity and the permeability does not reduce as much as the random sphere packs with increase in domain size. None of the heterogeneous domains of the sizes that we have evaluated can be considered an REV. Of course in the case of the heterogeneous sphere packs a smaller number of samples were studied. However, the structure of these domains are such that as they grow in size so does the scale of their inhomogeneity.

Table 2.2: Hydraulic properties of heterogeneous sphere pack samples.

Domain Size ($D = 2mm$)	4D	5D	6D	7D	8D	10D
Number of samples	15	15	15	15	15	15
mean ϵ	0.525	0.498	0.488	0.471	0.463	0.450
CV of ϵ	0.024	0.020	0.013	0.008	0.005	0.006
mean \bar{u} ($\frac{m}{s}$)	8.961E-7	8.161E-7	7.708E-7	7.024E-7	6.474E-7	5.832E-7
CV of \bar{u}	0.185	0.107	0.089	0.072	0.063	0.038
mean κ (m^2)	2.020E-8	1.749E-8	1.625E-8	1.437E-8	1.303E-8	1.146E-8
CV of κ	0.194	0.120	0.096	0.077	0.066	0.042

For every sphere pack size, in the case of the random (and homogeneous) sphere packs, we also calculated the PDF of velocities, for each realization, in the range of $-4.15\bar{u}$ to $14.15\bar{u}$ using 90 bins of size $0.203\bar{u}$, and then averaged the PDFs over all 20 realizations. Here, \bar{u} is the average of mean pore velocities over 20 sphere pack realizations of size $2.8cm$. We observed that the shape of the PDF curves of different realizations look more and more similar as the domain size is increased. Also the average PDF of different domains converge to a certain shape with an increase in domain size.

Figure 2.9 shows the the average PDF for three different domain sizes. Figure 2.9a and 2.9b show the complete PDF and the zoom in at small velocities in linear scaling, while figure 2.9c shows the PDF in semi-logarithmic scales and figure 2.9d uses double-logarithmic scaling and concentrates on positive velocities. The width of the line for each curve at each velocity is equal to the standard deviation of the PDF value at that velocity for the corresponding domain size. In these figures it is apparent that as the domain size increases the width of the corresponding curve, which represents the variation for PDF of different realizations, decreases. However, it appears that at small domain sizes ($0.8cm = 4D$), in addition to a large standard deviation of the individual realizations, a systematic error occurs at intermediate velocities as the PDF of the small domain size lies consequently below the one of the large domain size. We therefore emphasize that a large domain size of at least

$1.6\text{cm} = 8D$ is necessary to predict the velocity PDF in a random sphere pack in a sufficiently accurate way.

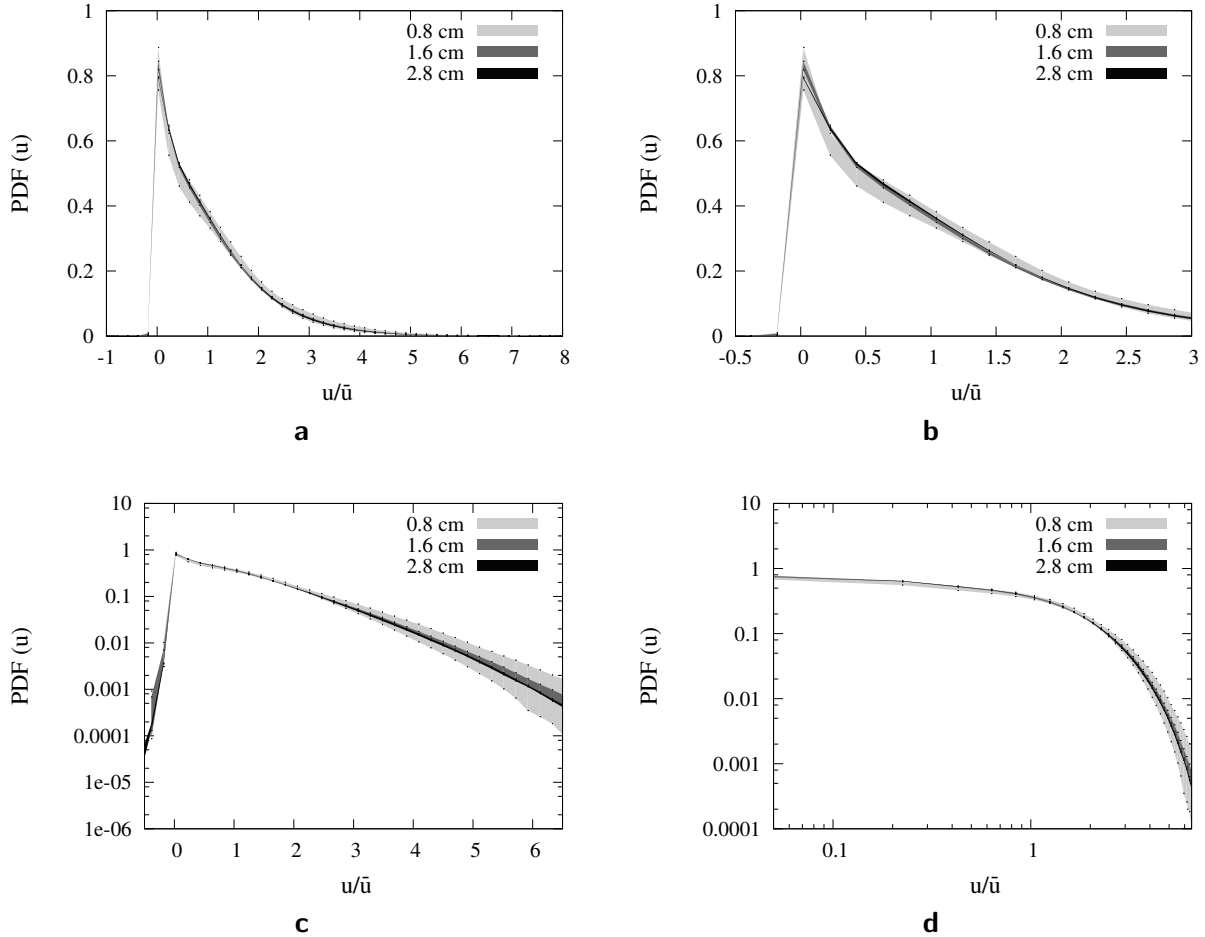


Figure 2.9: Velocity PDFs in a random sphere pack for various domain sizes. Complete PDF (a), zoom at small and negative velocities (b), semi logarithmic scale (c) and logarithmic scale for positive velocities only (d).

2.2.3 Permeability

In order to further validate our results we compared the permeability calculated using the data from our DNS results for each realization of each domain size of random sphere packs with the permeability in sphere packs predicted by the Blake-Kozeny equation. The Blake-Kozeny equation 2.10 relates the permeability κ of a grain packed domain with the porosity ϵ and the grain size D . The factor $1/150$ multiplied with these parameters is related to the ratio of the mean length of the passages a flow has to go through and the thickness of the layer that it goes through and is generally obtained by means of experiments [18, 4,

27].

$$\kappa = \frac{D^2 \epsilon^3}{150(1 - \epsilon)^2} \quad (2.10)$$

We observed that with an increase in the domain size the permeabilities obtained from our domains converge very well to the Blake-Kozeny equation. We modified the constant factor in the Blake-Kozeny equation from $1/150$ to $1/144.3$ and obtained an obvious convergence with increase in domain size.

In figure 2.10, the permeabilities calculated from the simulated average pore velocity in the domain are plotted against the porosity for various realizations of each domain size. Also the permeabilities calculated using the Blake-Kozeny and our modified Blake-Kozeny are shown. Figure 2.10b, zooms in to the points corresponding to the larger domains.

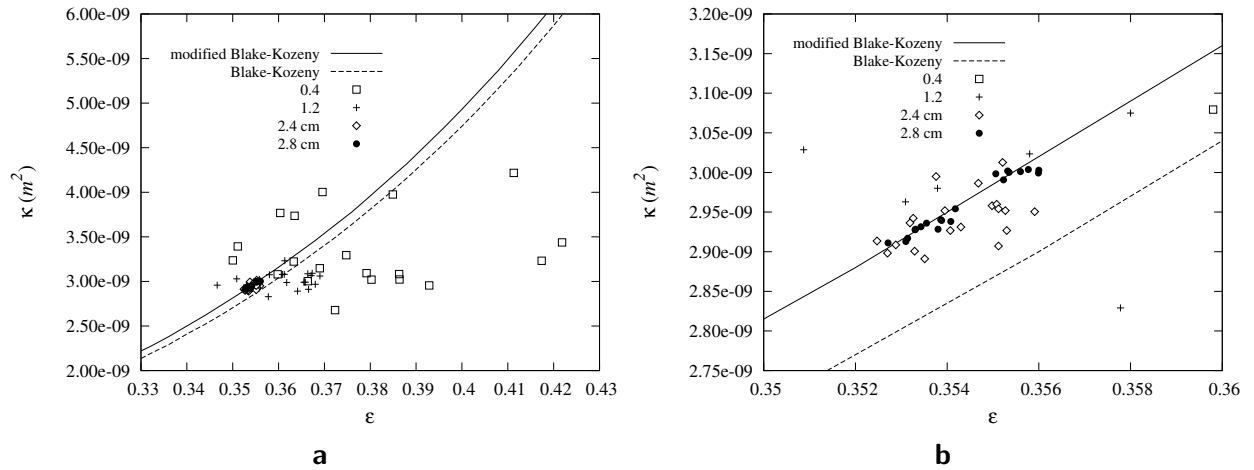


Figure 2.10: Permeability plotted against porosity for various domain sizes of random sphere pack compared to the Blake-Kozeny equation (2.10). Covering all porosities (a) zoomed in to the porosities corresponding to the larger domains (b)

2.3 Velocity field from DNS

Here we present velocity statistics and velocity PDFs obtained by DNS in random sphere packs complemented by those in a dense sphere pack or even in inhomogeneous sphere packs where suitable. For the random sphere pack, the cubic domain has a size of $(2.4\text{cm})^3$ (equivalent to 12 sphere diameters in each direction) and a porosity of $\epsilon = 0.35$ and is randomly packed with spheres of radius 1mm . The size chosen is sufficiently large to consider this domain as a rather good approximation of an REV. In the case of the inhomogeneous and random sphere pack (which we simply call heterogeneous) the domain considered is of size 2.0cm which is not large enough to be considered an REV. The dense sphere pack is packed according to a close packing hexagonal packing method as explained in section 2.1.2.

We simulated a low Reynolds number flow (in the order of $Re = 4 \times 10^{-4}$) in each of these sphere packed domains to obtain a steady state velocity field by applying a small pressure gradient of $-0.025Pa/m$ in the streamwise direction. All boundaries were assumed to be periodic.

The resolutions were 112 cells per sphere diameter for the dense sphere pack, 40 cells per sphere diameter for the heterogeneous sphere pack and 64 cells per diameter for the random (and homogeneous) sphere pack. The random sphere packed domain has a very large number of grid cells (approximately 453×10^6 cells). The results for the random sphere pack have been obtained over all grid cells in one realization. In the case of the inhomogeneous sphere pack where results are shown, they are the averages obtained over multiple realizations due to smaller than REV size of these domains. In the following we discuss some statistical variables of the velocities.

2.3.1 Velocity statistics

In tables 2.3 and 2.4 we document the minimum, maximum, average and higher statistical moments around the mean of the pore scale velocity in the dense and the random sphere pack respectively for all three velocity components. The velocity statistics of heterogeneous random sphere packs are not presented here as we do not have DNS results of heterogeneous sphere packs that are large enough to be considered an REV.

The s th statistical central moment m_s around the mean of a population of n discrete points denoted by $\theta_1, \theta_2, \dots, \theta_n$ is defined as

$$m_s = \frac{\sum_{i=1}^n (\theta_i - \bar{\theta})^s}{n} \quad (2.11)$$

where $\bar{\theta}$ is the average of the population. The mean is the first raw moment of the distribution, M_1 . The s th raw moment of a population of n discrete points denoted by $\theta_1, \theta_2, \dots, \theta_n$ is defined as

$$M_s = \frac{\sum_{i=1}^n (\theta_i)^s}{n} \quad (2.12)$$

The standard deviation is given as $\sigma = m_2^{1/2}$, the skewness is defined by $S = \frac{m_3}{m_2^{3/2}}$ and the flatness is defined as $F = \frac{m_4}{m_2^2}$.

One can see that the average cross-stream components for the random sphere pack are approximately three to four orders of magnitude smaller than its average streamwise component, \bar{u} . At a larger REV, the average of the cross-stream components should converge to zero. For the dense sphere pack, the average cross-stream components are approximately eight orders of magnitude smaller than that of the streamwise component and can be considered negligible. This of course is due to the fact that the dense sphere pack however small, is in fact an REV as the spheres in it are uniformly distributed and as mentioned the domain

Table 2.3: Statistics of local pore velocities in the x , y and z directions normalized by \bar{u} for the random sphere pack.

quantity	u	v	w
Min/ \bar{u}	-0.953	-5.976	-5.431
Max/ \bar{u}	10.451	5.581	5.317
Mean/ \bar{u}	1	-0.0004	-0.005
Standard deviation/ \bar{u}	1.016	0.646	0.659
Skewness	1.579	-0.035	-0.009
Flatness	6.213	6.9425	6.551

Table 2.4: Statistics of local pore velocities in the x , y and z directions normalized by \bar{u} , for the dense sphere pack.

quantity	u	v	w
Min/ \bar{u}	-0.005	-1.595	-2.045
Max/ \bar{u}	5.029	1.595	2.045
Mean/ \bar{u}	1	-2.614E-8	-3.264E-9
Standard deviation/ \bar{u}	0.939	0.399	0.553
Skewness	1.292	-1.291E-7	3.333E-8
Flatness	4.744	4.933	5.398

is periodic in every direction.

The standard deviations of the three velocity components are all in the same order of magnitude as the average streamwise pore velocity, \bar{u} , both for the random and for the dense sphere packs. As expected, the skewness of the cross-stream components in the random sphere pack are small compared to that of the streamwise component. The difference between the skewness of the cross-stream and streamwise components is amplified in the dense sphere pack again due to the regularity of the sphere arrangement. The flatness for both the random and the dense sphere pack, however, is similarly large for all components and much larger than the one of a Gaussian distribution which is 3.

In the random sphere pack the maximum value of the streamwise velocity is about ten times larger than its mean, the intrinsic velocity \bar{u} , while the magnitudes of the cross stream components can reach values of about five times larger than the magnitude of the intrinsic velocity \bar{u} . In the case of the dense sphere pack the value of the streamwise velocity component is approximately five times larger than that of the mean streamwise pore velocity, \bar{u} , and the cross stream components are approximately 50 to 100 percent larger than \bar{u} . The longer tail of the velocity distribution (larger maximum u) in the random sphere pack compared to that of the dense sphere pack is due to its obvious higher heterogeneity. The more heterogeneous a porous media is the more probable it is for velocities to have the opportunity to reach very high values compared to the mean velocity.

Another point to consider is that there exist negative velocities in the streamwise component for both the random and the dense sphere packs. The emergence of negative velocities will be discussed in section 2.3.3.

2.3.2 Velocity PDFs

Figure 2.11 shows the PDF of the streamwise velocity component, u for the random, the dense and the inhomogeneous sphere packs. The PDFs for all were obtained by dividing the velocities, ranging between $-2\bar{u}$ and $16\bar{u}$ (\bar{u} being the respective average pore velocity of each case), into 360 bins. The x axis is normalized by the intrinsic velocity, \bar{u} . The PDF value in each curve is normalized such that the area underneath the curve is always equal to unity. In the case of the inhomogeneous sphere pack the curve shown in the figure represents the average PDF of 15 different realizations of inhomogeneous sphere packs of size $2cm$. This is because inhomogeneous sphere packs of size $2cm$ are not large enough to be considered an REV and therefore an average of the PDFs is shown here simply to be compared qualitatively with the PDFs of dense and random sphere packs. We plot the PDF in four different scales to make several features visible.

One can see that the PDFs exhibit a maximum at a very a low velocity in all realizations. There is a long tail to large velocities, with the maximum velocities being observed at more than 10 times larger than the \bar{u} in the random, at about $5\bar{u}$ in the dense and at over $14\bar{u}$ in the inhomogeneous sphere pack. The dense sphere pack's velocity distribution is more narrow than the one from the random sphere pack, which is not surprising as the pore spacings exhibit a larger variation in the random sphere pack than in the dense sphere pack. With the same logic its is obvious that the velocity PDF of the heterogeneous sphere pack is even wider than that of the random sphere pack.

When comparing the PDFs another striking feature is that in the dense sphere pack, the PDF has two kinks, one at about $1.3\bar{u}$ and another at about $2.2\bar{u}$, best visible in the zoomed linear plot, figure 2.11b. At velocities smaller than the first kink, there is a plateau in the probability. Similar observations were made by Maier et al when studying a dense sphere pack. They divided the velocity range into several regions in order to better explain the various sections of the velocity PDF. According to Maier et al, $u/\bar{u} < 0.5$ correspond to the regions surrounding the spheres. Regions of moderate velocity which have a quasi-tubular shape with triangular cross sections correspond to $0.5 < u/\bar{u} < 1.7$ and surround the high velocity network of tubular flow structures ($1.7 < u/\bar{u}$) in the domain. They associate the second peak in their PDF curve with the contribution from the junctions of the high velocity structure [29].

For all three configurations, the PDF curves do not follow a normal or even log-normal behaviour, as can be seen in figure 2.11d. The decay of the PDFs at large velocities rather resembles an exponential decay for all three (figure 2.11c).

As expected, the PDFs of the transverse velocity components are different from those of the streamwise component. The most prominent difference is the symmetry about the zero velocity, see figure 2.12. In this figure, both transverse velocity components, v and w , are plotted. These PDFs are also obtained from DNS on the same dense, random and inhomogeneous sphere packs by dividing the velocities (ranging between -16σ and 16σ) into 360 bins. The x axis for these graphs are normalized by the standard deviation, σ , of their respective streamwise pore velocity, u . Again the curve representing the inhomogeneous sphere pack is in fact the average of PDFs over 15 different realizations of inhomogeneous sphere packs. We have also included in this figure the probability density curve of a normal distribution for compar-

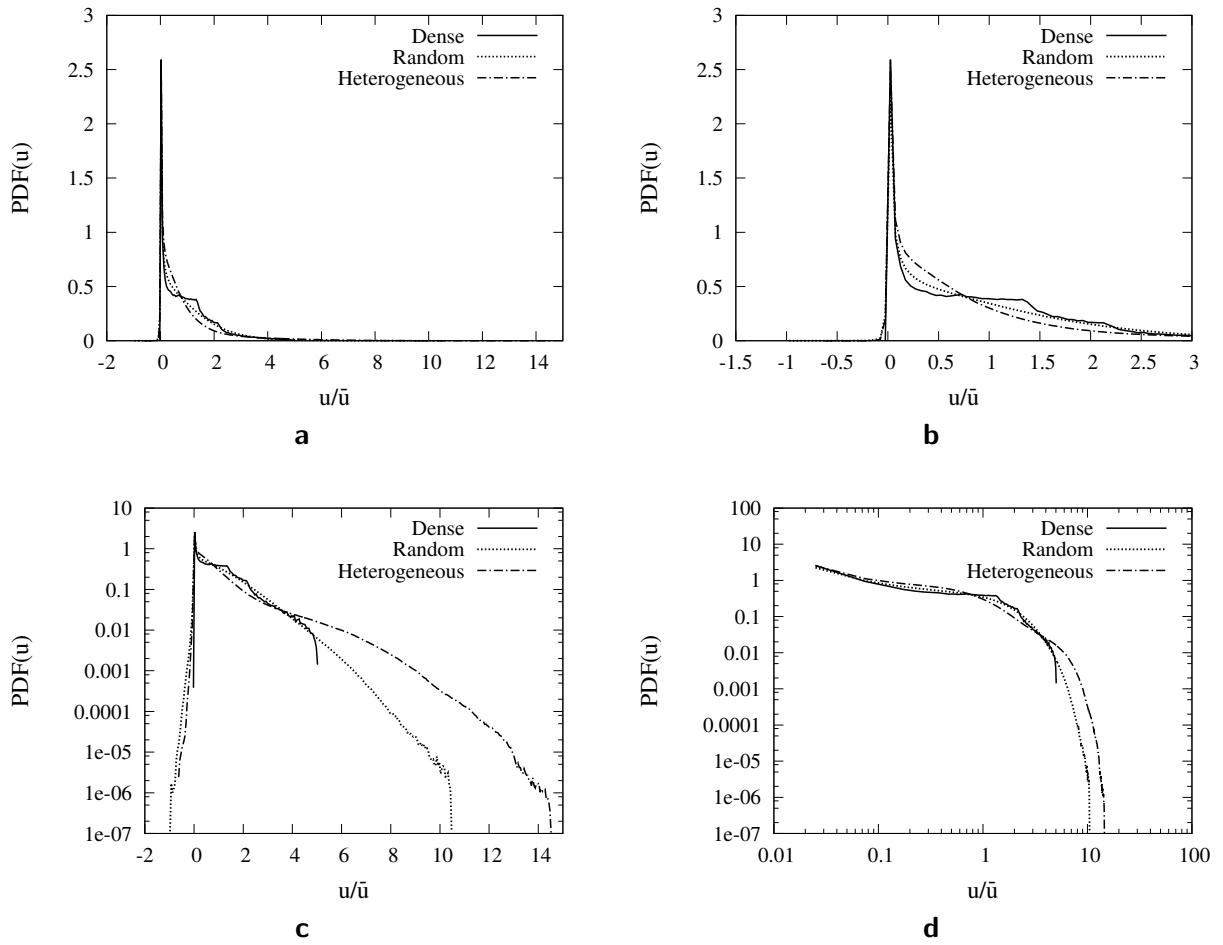


Figure 2.11: PDF of streamwise pore velocity in dense, random and heterogeneous sphere packs. Whole velocity domain (a); Zoom at small velocities (b); semi-log plot (c) and log-log plot at positive velocities (d).

ison. The probability density of the normal distribution is:

$$f(x) = \frac{1}{\sqrt{2\pi}} e^{-x^2/2} \quad (2.13)$$

Here the PDFs are symmetric and it is clear that the transverse velocities are smaller and far more prevalent around zero. There is a considerable deviation from a Gaussian distribution that has been added for comparison, which in the case of the random and dense sphere packs already could have been expected from the large flatness values, see tables 2.3 and 2.4. As expected in the case of the random sphere pack, the PDFs of v and w are identical, thus only one curve is visible. This is because the random sphere pack is isotropic and the geometry of transverse directions have no observable statistical difference with each other. The same cannot be said of the curves representing heterogeneous sphere packs. The heterogeneous sphere packs due to the method used for sphere packing are not isotropic by nature. Even

averaging over 15 different realizations does not rectify the differences between the two transverse directions. In the case of the dense sphere pack even more prevalent differences between PDFs of v and w can be seen which is of course due to the fact that the dense sphere pack arrangement is homogeneous but anisotropic by definition.

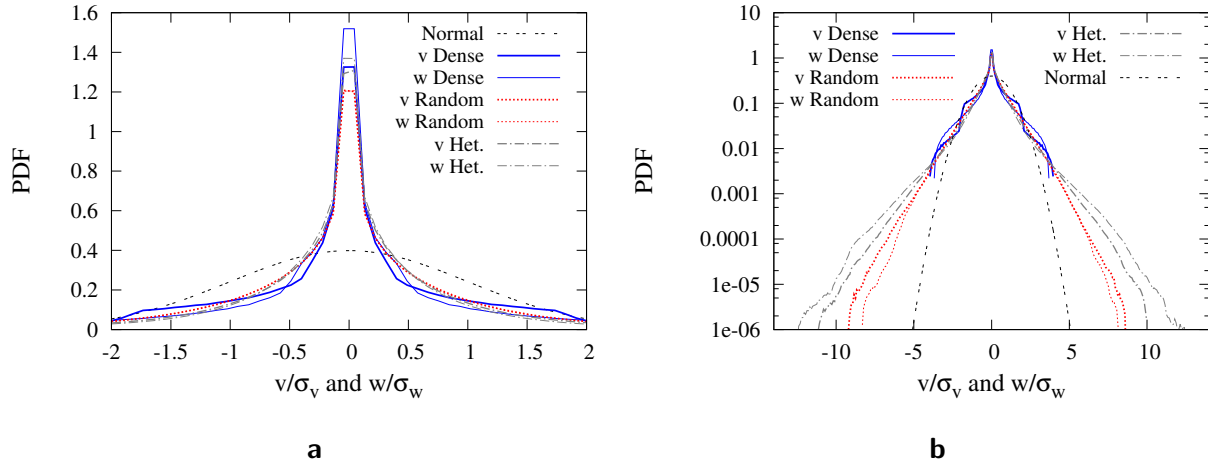


Figure 2.12: PDF of transverse velocities in random, dense and inhomogeneous sphere packs. Zoom at small velocities in linear scale (a) and semi-log scale for the complete velocity range (b).

2.3.3 Negative velocities

As can be seen in tables 2.3 and 2.4 and concluded from figure 2.11 there exist small areas of negative streamwise velocities. Negative velocities in sphere packs have also been reported by others (see [29]). These negative velocities can not be interpreted as separated flow regions which can be observed in high Reynolds number flows. The regions of back-flow appear in small pockets attached to the surfaces of the spheres, see figure 2.13. There are two possible situations which we could identify to give rise to negative velocities. The first situation appears when two spheres approach each other and form a narrow gap as indicated by the tiny spots of colour red in figure 2.13a. The second situation can be interpreted as the back-flow regions as part of streamlines attached to the sphere surfaces which point in upstream direction in the neighbourhood of stagnation points that are not centred in the front of a sphere. This is a consequence of the irregularity of the sphere distribution. Figure 2.13b shows a close up of the streamlines at such a location. Figure 2.14 visualizes the latter situation by a sketch. On the left side, we sketch streamlines in an ordered medium. The stagnation points are in the center of the spheres and streamlines departing from the stagnation point always point downstream. On the other hand, as sketched on the right hand side of figure 2.14, if a stagnation point is not located in the center of a sphere, the streamlines departing from this stagnation point would partly point in upstream and partly point in downstream direction. This simple consideration can well explain the occurrence of negative velocities at some distinct points in the random sphere pack. However, it is

important to note that at these locations, we neither observed closed separation regions in which a tracer could be trapped for a long time nor large connected regions of negative streamwise velocity in which a tracer could be transported in upstream direction over a long distance. Thus, the effect of negative streamwise velocities on tracer transport and residence times of the tracer in these pockets is expected to be small.

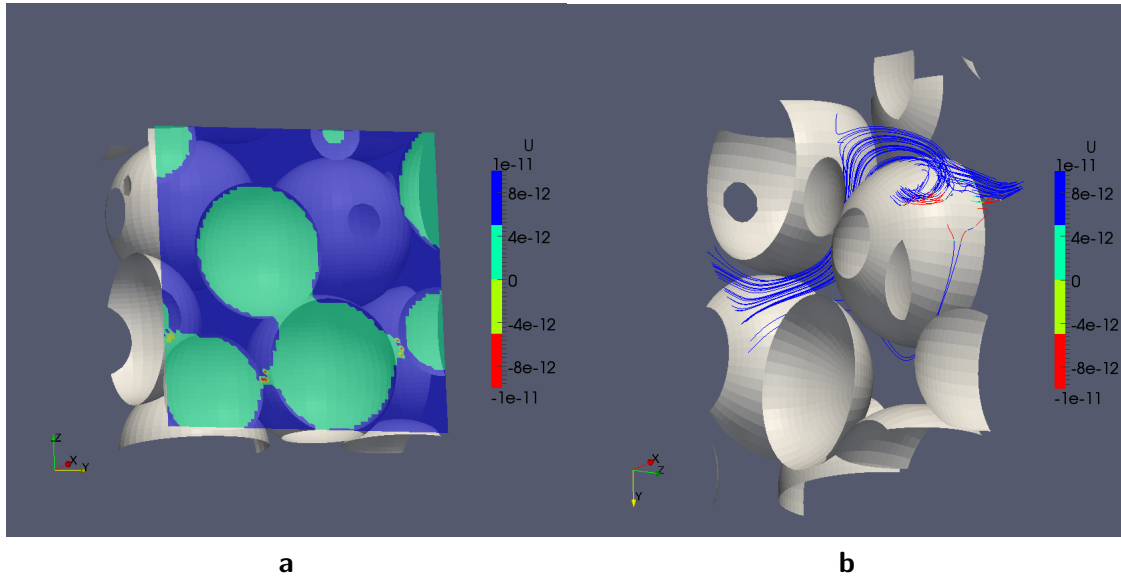


Figure 2.13: Locations at which negative velocities occur in the flow through a random sphere pack: in a cross-stream plane (a) and along streamlines (b) indicated by the colour red.

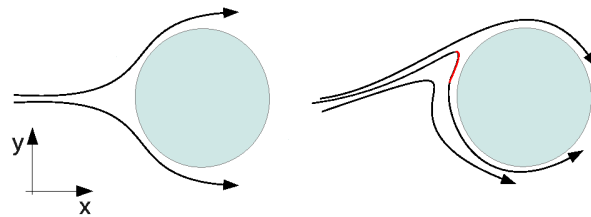


Figure 2.14: Conceptual sketch of streamlines in an ordered and a disordered sphere pack demonstrating conditions under which negative streamlines can occur.

2.3.4 Velocity derivatives

In this work we shall introduce a model for dispersion which is based on the statistics of the velocity variation field and the velocity derivatives are essential factors in the estimation of the velocity variations. Here we present the statistics and PDFs of the first and second

derivatives of pore velocity components, u , v and w in different directions of a random sphere pack of size 2.4cm .

First derivatives of velocity components

Table 2.5 summarizes the statistics of the first derivatives of the streamwise velocity component u in the three Cartesian directions, x , y and z . In order to compute the derivatives at each grid point the central difference scheme was employed.

From symmetry arguments, $\langle \partial u / \partial x_i \rangle$ should tend towards zero, which is in fact the case. The range of $\langle \partial u / \partial x \rangle$ is considerably narrower than that of $\langle \partial u / \partial y \rangle$ and $\langle \partial u / \partial z \rangle$. The skewness is very small as well, pointing to a symmetric distribution which is natural for the cross stream derivatives. For the streamwise component, it is a hint that the flow is truly linear, i.e. in the Stokes regime. The flatness is larger than the one for a Gaussian in all three directions.

Table 2.5: Statistics of first derivatives of the streamwise velocity component, u , in a random sphere pack normalized by the intrinsic velocity and the sphere diameter, \bar{u}/D .

	$\frac{\partial u}{\partial x}$	$\frac{\partial u}{\partial y}$	$\frac{\partial u}{\partial z}$
Minimum	-56.693	-125.748	-140.525
Maximum	62.061	129.374	129.916
Mean	4.831E-5	-6.070E-3	-2.234E-3
Standard deviation	6.594	11.097	11.093
Skewness	2.403E-3	-1.211E-3	3.859E-3
Flatness	5.621	8.706	8.889

Tables 2.6 and 2.7 respectively show the statistics of the first derivatives of the cross stream velocity components v and w in the three Cartesian directions. Again the average and the skewness of $\partial v / \partial x_i$ and $\partial w / \partial x_i$ are rather small and again the range which each covers appears to be narrower in its respective principal direction but not as dramatically as in the case of $\langle \partial u / \partial x_i \rangle$.

Table 2.6: Statistics of first derivatives of the cross stream velocity component, v , normalized by the intrinsic velocity and the sphere diameter, \bar{u}/D .

	$\frac{\partial v}{\partial x}$	$\frac{\partial v}{\partial y}$	$\frac{\partial v}{\partial z}$
Minimum	-84.316	-58.506	-90.709
Maximum	71.773	57.317	89.432
Mean	1.464E-3	7.956E-5	5.971E-4
Standard deviation	5.415	4.880	5.406
Skewness	-9.797E-4	-8.584E-3	1.514E-2
Flatness	9.269	7.119	11.115

Now, we turn to the probability distributions of the first derivatives of velocity components. Figure 2.15 shows the PDF of the first derivatives of u normalized by \bar{u}/D . The PDF values

Table 2.7: Statistics of first derivatives of the cross stream velocity component, w , normalized by the intrinsic velocity and the sphere diameter, \bar{u}/D .

	$\frac{\partial w}{\partial x}$	$\frac{\partial w}{\partial y}$	$\frac{\partial w}{\partial z}$
Minimum	-82.629	-75.857	-62.725
Maximum	71.165	81.163	54.008
Mean	-5.336E-4	1.114E-3	4.668E-6
Standard deviation	5.450	5.499	4.939
Skewness	6.623E-3	5.884E-3	-9.804E-3
Flatness	8.976	10.764	7.078

are normalized such that the area beneath each curve remains equal to 1. To obtain the PDFs, we used 320 bins in the range between $-142\bar{u}/D$ and $130\bar{u}/D$. We can see that the distribution of $\partial u/\partial y$ is identical to the ones of $\partial u/\partial z$ which is to be expected due to the rotational symmetry of the sphere pack. The standard deviation of the longitudinal derivative is smaller than the standard deviation of the cross stream derivatives. This leads to a more narrow distribution of the longitudinal derivative (figure 2.15b). Although we are primarily interested in the derivatives of the streamwise pore velocity component we have also plotted the PDF of the first derivatives of v and w in figure 2.16 for the sake of completeness. Notice that in general the standard deviation of the derivatives of each velocity component is narrower in its respective direction than in the direction perpendicular to it.

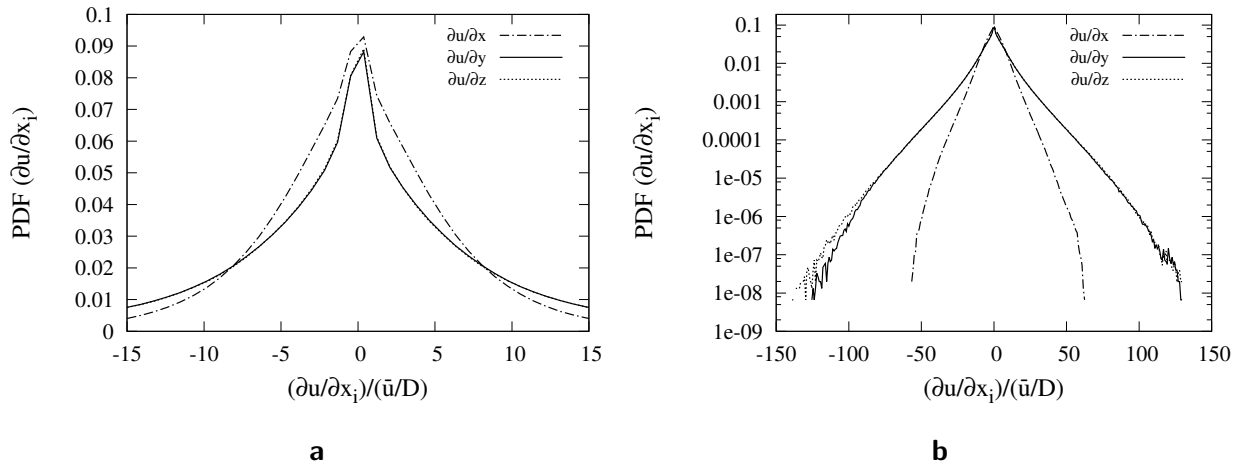


Figure 2.15: PDF of $\frac{\partial u}{\partial x_i}$ in a random sphere pack normalized by \bar{u}/D . Linear scale zoomed around small gradients (a) and semi-logarithmic scale for the complete range of gradients (b).

To compare the distribution of the first derivative of the streamwise pore velocity, u , with that of a normal distribution in figure 2.17 we show the PDF of $\frac{\partial u}{\partial x_i}$, each normalized by its corresponding standard deviation σ . Again the PDF values are normalized such that the area underneath each PDF curve is equal to one. Here we divided the derivative range between

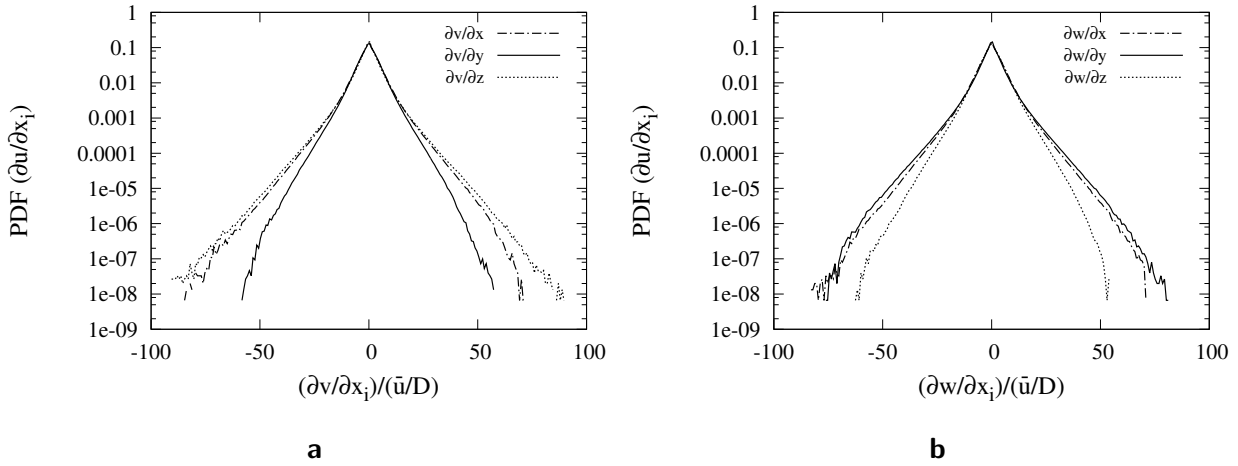


Figure 2.16: PDF of $\frac{\partial v}{\partial x_i}$ and $\frac{\partial w}{\partial x_i}$ in a random sphere pack normalized by \bar{u}/D plotted in semi-logarithmic scale for the complete range of gradients.

-13σ to 13σ into 320 bins. The distributions of the first derivatives of the streamwise velocity component are symmetric but non-Gaussian. The maximum absolute values are more than 10 times larger than the standard deviation. It is clear in this figure that the peak values are strongly pronounced - much more than in a Gaussian distribution, which is also plotted for comparison (figure 2.17b). The decay at large values is slower than the decay of a normal distribution. There is a trend towards an exponential decay, however, unlike in the distribution (PDF) of the streamwise pore velocity (figure 2.11), this trend is not fully clear.

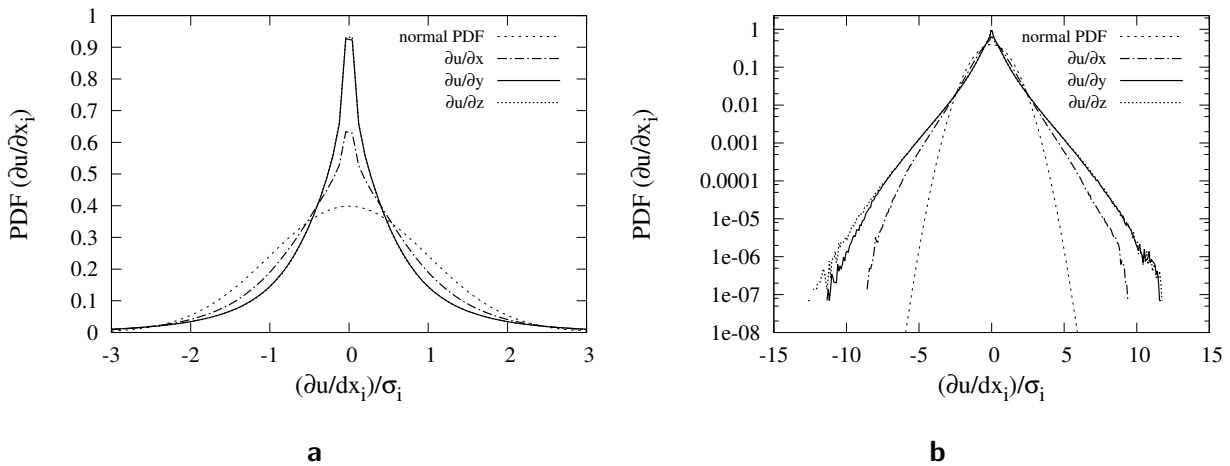


Figure 2.17: PDF of $\frac{\partial u}{\partial x_i}$ in a random sphere pack normalized by its respective standard deviation σ . Linear scale zoomed around small gradients (a) and semi-logarithmic scale for the complete range of gradients (b).

Second derivatives of the streamwise velocity component

Table 2.8 shows the second derivatives of u in all combinations of direction for the previously described random sphere pack of size 2.4cm . It is clear that the second derivatives are strongly non-Gaussian, even the mixed ones as can be deduced from the flatness factors which are even larger than the ones of the first derivatives. Also, the average value of the second derivatives of the streamwise velocity component are not necessarily tending to zero for sufficient statistics. We observe that the streamwise and the cross stream second derivatives of the streamwise velocity component are negative in the mean. This reflects the fact that at the sphere surfaces the velocity is zero while in the field, it is predominantly positive. Therefore, the curvature of the spatial streamwise velocity field is predominantly smaller than zero, as can be seen in table 2.8. This negativity of the second derivative of the streamwise pore velocity can have a subtle effect on the average of the du field the equation for which will be obtained in the next chapter.

Table 2.8: Statistics of second derivatives of the streamwise velocity component in a random sphere pack normalized by the intrinsic velocity and the sphere diameter, \bar{u}/D^2 .

	Min	Max	Mean	Std dev	Skew	Flat
$\frac{\partial^2 u}{\partial x^2}$	-1226.407	1614.642	-7.270	112.661	1.661	12.815
$\frac{\partial^2 u}{\partial y^2}$	-1727.371	1724.317	0.041	112.289	-0.046	13.915
$\frac{\partial^2 u}{\partial z^2}$	-1821.130	1841.601	-0.076	112.445	0.051	14.048
$\frac{\partial^2 u}{\partial x \partial y}$	-4016.509	3896.262	-17.369	237.792	1.464	18.092
$\frac{\partial^2 u}{\partial x \partial z}$	-2662.132	2794.736	0.006	152.737	-0.096	17.425
$\frac{\partial^2 u}{\partial y \partial z}$	-3393.494	4120.845	-17.238	237.042	1.503	18.414

The PDFs of the second derivatives of u are either normalized by \bar{u}/D^2 (figure 2.18) or by their respective standard derivation (figure 2.19). The PDFs are obtained by dividing the range between $-2700\bar{u}/D^2$ and $-3000\bar{u}/D^2$, or between -20σ and 22σ , respectively, into 320 bins. In these figures, curve **a** corresponds to $\partial^2 u/\partial x^2$, **b** to $\partial^2 u/\partial y^2$, **c** to $\partial^2 u/\partial z^2$, **d** to $\partial^2 u/(\partial x \partial y)$, **e** to $\partial^2 u/(\partial x \partial z)$ and **f** to $\partial^2 u/(\partial y \partial z)$. Curve **g** is a normal distribution for comparison.

The second derivatives $\partial^2 u/\partial x^2$, $\partial^2 u/\partial y^2$ and $\partial^2 u/\partial z^2$ have skew distributions, best seen in figure 2.18a, while the mixed derivatives are evenly distributed. However, the curvature of $\partial^2 u/\partial x^2$ is the only one at which the maximum PDF occurs at a non-zero value. The cross-stream curvatures have the highest probability at zero values, but there are considerably larger probabilities at intermediate negative than at intermediate positive values. All second derivatives have a more pronounced peak than a normal distribution at the same standard deviation, see figure 2.19a. On the other hand, all second derivatives decay much slower at large magnitudes than a normal distribution, and we observe values of more than 15σ . Maximum absolute values are about 15 times larger than the corresponding standard deviations. The mixed second derivatives are more symmetric than the unmixed ones, but are much wider than a Gaussian distribution.

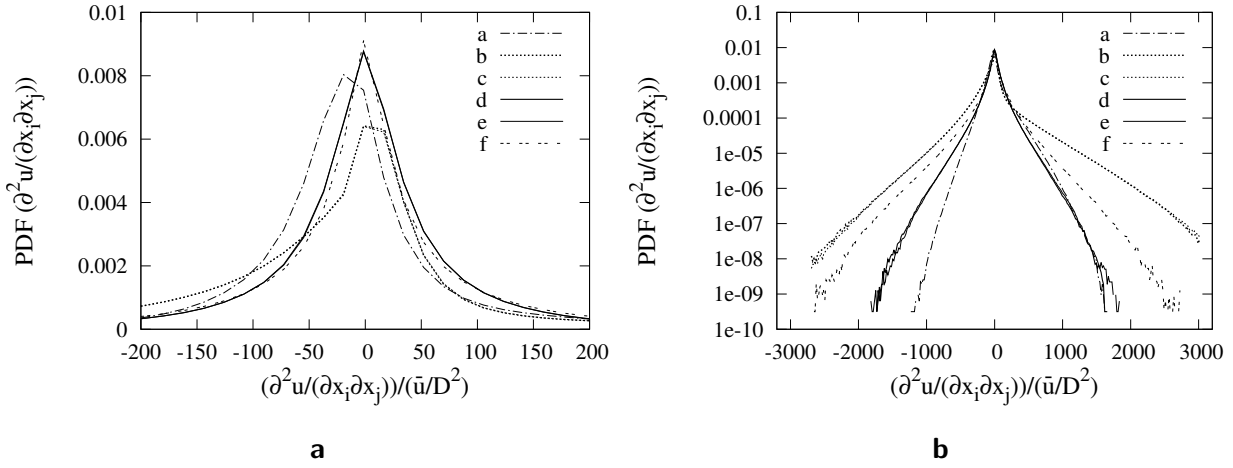


Figure 2.18: PDF of $\frac{\partial^2 u}{\partial x_i \partial x_j}$ in a random sphere pack normalized by \bar{u}/D^2 . Curve **a** corresponds to $\frac{\partial^2 u}{\partial x^2}$, **b** to $\frac{\partial^2 u}{\partial y^2}$, **c** to $\frac{\partial^2 u}{\partial z^2}$, **d** to $\frac{\partial^2 u}{\partial x \partial y}$, **e** to $\frac{\partial^2 u}{\partial x \partial z}$ and **f** to $\frac{\partial^2 u}{\partial y \partial z}$. Linear scale zoomed around small gradients (a) and semi-logarithmic scale for the complete range of gradients (b).

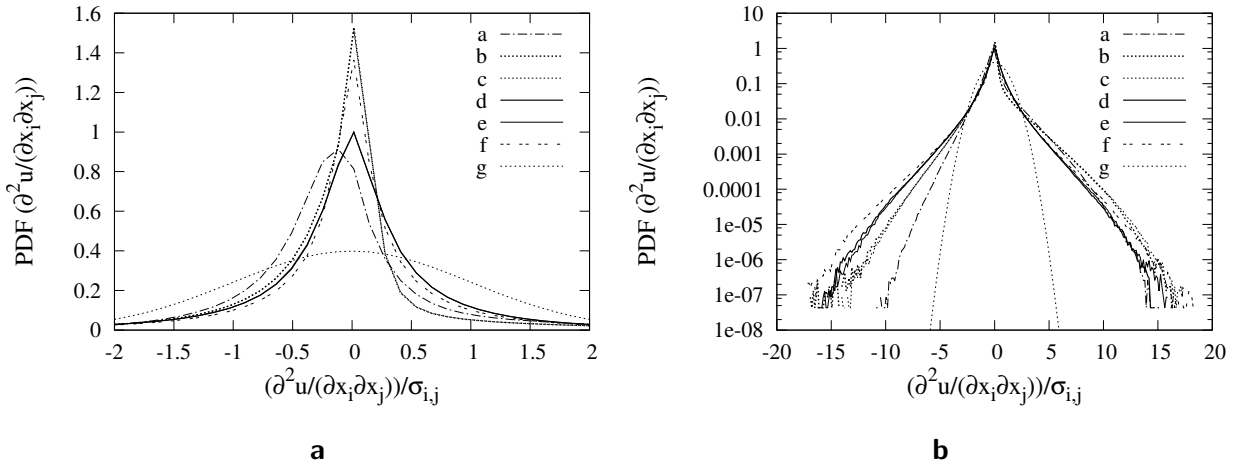


Figure 2.19: PDF of $\frac{\partial^2 u}{\partial x_i \partial x_j}$ in a random sphere pack normalized by its respective standard deviation σ . Curve **a** corresponds to $\frac{\partial^2 u}{\partial x^2}$, **b** to $\frac{\partial^2 u}{\partial y^2}$, **c** to $\frac{\partial^2 u}{\partial z^2}$, **d** to $\frac{\partial^2 u}{\partial x \partial y}$, **e** to $\frac{\partial^2 u}{\partial x \partial z}$ and **f** to $\frac{\partial^2 u}{\partial y \partial z}$. Curve **g** is a normal distribution for comparison. Linear scale zoomed around small gradients (a) and semi-logarithmic scale for the complete range of gradients (b).

2.4 Evolution of a tracer in a sphere pack

Here we report the outcome of solving the transport equation on a homogeneous random sphere pack of size 2.4cm . The velocity field resulting from an imposed pressure gradient

of $-0.025Pa/m^2$ in the sphere packed domain filled with water is obtained using MGLET as described before. The Reynolds number of the set-up is approximately $Re = 4 \times 10^{-4}$. The PDF and statistics of the velocity field were discussed in detail in sections 2.3.1 and 2.3.2.

The governing equation for transport of a passive tracer (equation 2.3) is also solved using MGLET. By passive tracer we mean the same fluid as the one which flows in the porous domain with the exact same properties but with a certain concentration value assigned to it. In other words the tracer does not react with or affect the fluid or solid phases in the domain. Since the porous domain is not very large we replicate the periodic flow field of size $2.4cm$ in the x (streamwise) direction five times in order to give room to the tracer to evolve. In this way we obtain a domain of size $(L_x, L_y, L_z) = (12, 2.4, 2.4)cm$. At every point in this domain the velocity is known. The velocity field is of course repeated five times in the length of the domain. The boundaries of the domain for the transport process are again periodic in all directions. The tracer is initialized such that on the central cross section perpendicular to the streamwise direction (at $x = 5.998cm$) the concentration of the tracer at each grid point is $c = 1kg/m^3$ and on all other points the concentration is set to $c = 0$.

2.4.1 Effect of pore space on tracer evolution

Here we compare the evolution of a tracer in a porous medium to its evolution in an empty and unbounded domain. In an unbounded domain one would expect that the shape of the tracer cloud in the streamwise direction would follow that of a normal distribution with a mean equivalent to the velocity multiplied with time, which represents the position of the center of mass of the cloud, and a standard deviation of

$$\sigma(t) = \sqrt{2\Gamma t} \quad (2.14)$$

where σ is the standard deviation of the location of tracer particles. With this definition $\sigma(t)$ represents the half width of the cloud at time t in the case of Fickian dispersion.

Considering a molecular diffusion coefficient of $\Gamma = 1 \times 10^{-11}m^2/s$ we solved the transport equation in a homogeneous random sphere pack of size $2.4cm$ for two different velocity fields. In one case the velocities at every point were set to zero and in the other we used the same velocity field explained in sections 2.3.1 and 2.3.2. We calculated the standard deviation of the concentration distribution of the tracer for these two cases and plotted them over time together with $\sigma(t)$ from equation 2.14. See figure 2.20.

It is clear that the presence of the pore space at zero velocity inhibits the growth of the tracer cloud. Maier et al. [28] report similar behaviour in the case where the Peclet number is zero and have calculated the ratio of the effective diffusivity to the molecular diffusivity for different cases. The square root of this ratio is equivalent to the ratio of the diffusive length scale in the porous medium to the diffusive length scale had the domain been non-porous and free of obstacles. This is the definition of tortuosity as defined by Bear [2]. In short, the spheres in the porous domain block the natural Brownian diffusion of the tracer. However as is evident

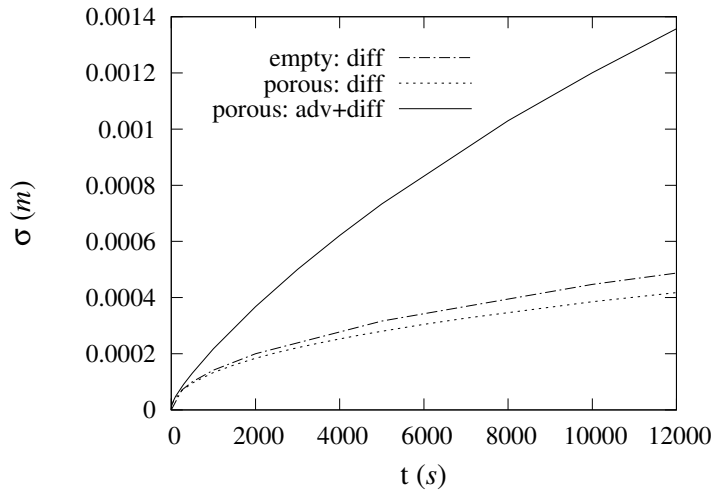


Figure 2.20: Standard deviation of the tracer positions in a non-porous domain, in a porous domain with zero velocity and in a porous domain with non-zero velocity.

in figure 2.20, in the presence of velocity the porous domain increases the growth and spreading of the tracer cloud beyond what is expected from the average pore velocity and molecular diffusion alone. This phenomena is called dispersion.

2.4.2 Effect of the Peclet number tracer evolution

The Peclet number, Pe , is a dimensionless measure of the rate of advection of a tracer to its rate of diffusion or in other words, the ratio of the diffusive time scale to the advective time scale in the transport of a tracer. The Schmidt number, Sc , is also a dimensionless measure of the ratio of the rate of viscous diffusion to the rate of molecular diffusion. The Peclet and Schmidt numbers are described in the following equations.

$$Pe = \frac{t_{dif}}{t_{adv}} = \frac{L^2/\Gamma}{L/\bar{u}} = \frac{\bar{u}L}{\Gamma} \quad (2.15)$$

$$Sc = \frac{\nu}{\Gamma} = \frac{\nu}{\bar{u}L} \times \frac{\bar{u}L}{\Gamma} = \frac{Pe}{Re} \quad (2.16)$$

In the above, L is the a length scale, \bar{u} the average pore velocity, Γ is the molecular diffusion coefficient and ν is the kinematic viscosity.

We have chosen a molecular diffusion coefficient of $\Gamma = 1 \times 10^{-11} m^2/s$ for our simulations of tracer transport in porous media. This translates to a Peclet number of $Pe = 37.11$ based on a length scale of $L = D = 2mm$, D being the sphere diameter in the porous domain. The average pore velocity, \bar{u} , in the case of the random sphere pack of size $2.4cm$ is $\bar{u} = 1.856 \times 10^{-7} m/s$. The Schmidt number of our set-up is $Sc = \nu/\Gamma = 10^5$, $\nu = 1 \times 10^{-6} m^2/s$

being the kinematic viscosity of water.

However we would first like to demonstrate the effect of the Peclet number on dispersion in the afore mentioned random sphere pack of size $12 \times 2.4 \times 2.4 \text{cm}^3$. The tracer is initialized on the central cross section of the domain perpendicular to the streamwise direction at time $t = 0$. Using the velocity field obtained via DNS (and described in section 2.3) the transport equation was solved for three different molecular diffusion coefficients. Figure 2.21 shows the centre of mass of the cloud (mean location of grid points weighted with tracer concentration) for three different molecular diffusion coefficients $\Gamma = 5 \times 10^{-12} \text{m}^2/\text{s}$, $\Gamma = 1 \times 10^{-11} \text{m}^2/\text{s}$ and $\Gamma = 1 \times 10^{-10} \text{m}^2/\text{s}$ which correspond to Peclet numbers of $Pe = 74.22$, $Pe = 37.11$ and $Pe = 3.71$ considering a length scale of $L = D = 2 \text{mm}$ and to Schmidt numbers of $Sc = 200000$, $Sc = 100000$ and $Sc = 10000$ respectively. Moreover, considering the same length scale, these molecular diffusion coefficients correspond respectively to diffusion time scales (L^2/Γ) of $t_{dif} = 8 \times 10^5 \text{s}$, $t_{dif} = 4 \times 10^5 \text{s}$ and $t_{dif} = 4 \times 10^4 \text{s}$. The advection time scale would in each case be $t_{adv} = \bar{u}/L = 1.0776 \times 10^4 \text{s}$. Figure 2.21 also includes a curve corresponding to the centre of the cloud should it have evolved in a non-porous and infinite volume following the equation

$$\bar{x}(t) = \bar{u}.t + \bar{x}_0 \quad (2.17)$$

where $\bar{x}(t)$ is the location of the centre of the cloud at time t and \bar{x}_0 is the location of the centre of the cloud at the initial time and where \bar{u} is the average streamwise pore velocity obtained via DNS (see section 2.3.1). It is evident that with an increase in the Peclet number the centre of the cloud moves faster with time even though the average streamwise pore velocity for all three cases is the same. This is due to the fact that at time $t = 0$ the tracer is initialized on a cross section of the domain perpendicular to the streamwise direction and is not spread over the whole domain. As the domain is not exactly large enough to be considered an REV the average streamwise pore velocity on this cross section ($\bar{u}_{sec} = 1.86 \text{m/s}$) is slightly different from (and in this case higher than) the average pore velocity in the whole domain ($\bar{u} = 1.856 \text{m/s}$). As time passes and the tracer spreads to more and more points in the domain the velocity PDF and therefore the average velocity of the grid points weighted by the tracer concentrations will converge to that of the total domain. This will be further elaborated upon in the next subsection.

Figure 2.22 shows the standard deviation of the tracer cloud (half width of the cloud in case of Fickian dispersion) for two different Peclet numbers. For each case the thicker curve represents the condition where both advection and diffusion occurs (using the same velocity field mentioned before) and the thinner curve represents a pure diffusion condition with zero velocity at every point in the domain. As can be observed in this figure there exists a far more significant difference between the half width of the cloud in the case of pure diffusion and that of advection plus diffusion for the higher Peclet number. It is clear that when the Peclet number is higher the varying velocity in the domain has more effect on and escalates the dispersion in the domain.

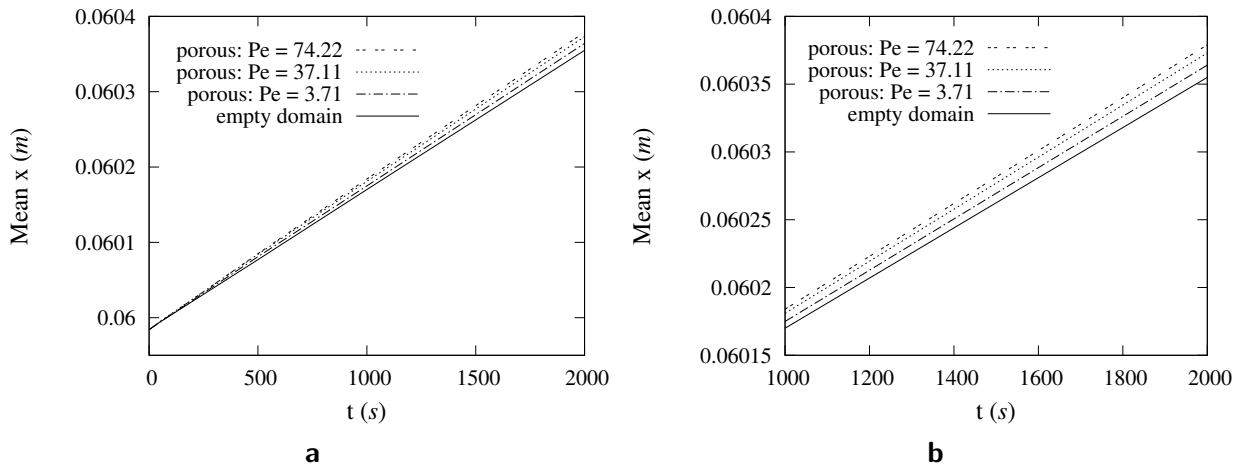


Figure 2.21: Location of centre of mass of tracer cloud over time. $t = 0$ to $t = 2000s$ (a) and $t = 1000s$ to $t = 2000s$ (b)

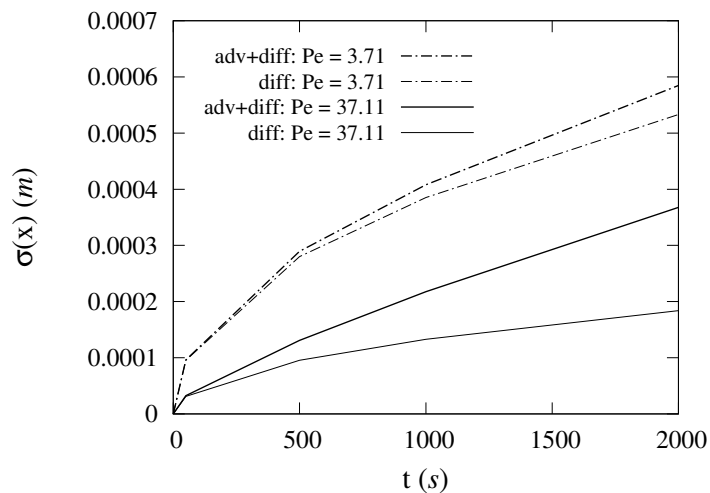


Figure 2.22: Standard deviation of the tracer cloud positions in a random sphere pack for two different Peclet numbers.

Figure 2.23 shows the shape of the cloud at time $t = 2000s$ for three different Peclet numbers. The concentration of the tracer integrated over each cross section perpendicular to the streamwise direction yields the shape of the tracer cloud. In order to obtain the shape of the cloud we calculated the PDF of the location of grid points weighted with the tracer concentration. The bins were chosen such that each bin contains exactly one grid point in the streamwise direction. Higher Peclet numbers correspond to lower diffusion coefficients and therefore the higher the Peclet number the less spread out the cloud is at a given time. In this figure however another important feature catches the eye. Notice how the skewness of the curves increase with increasing Peclet numbers. Time $t = 2000s$ is still early enough for all three configurations to be in a state of non-Fickian diffusion, i.e. for the velocities

of grid points affected by the tracer to be still correlated. On their pore scale simulations of transport in random sphere packs Maier et al. [28] report non-Fickian dispersion up until three times the advective time scale, D/\bar{u} , where D is the sphere diameter and \bar{u} the average pore velocity. In their experiment on domains packed with glass spheres Scheven et al. [44] report similar results in the same order of magnitude. They reach Fickian dispersion length scales ten times larger than the sphere diameter (which corresponds to times ten times larger than the advection time scale) and diffusion length scales larger than $0.3D$. Based on our configuration if we consider $t = 10D/\bar{u}$ as the time to reach asymptotic dispersion, non-Fickian dispersion would continue until more than $t = 100000s$. The diffusion length scale at this time for all three Peclet numbers mentioned above would be larger than $0.3D$.

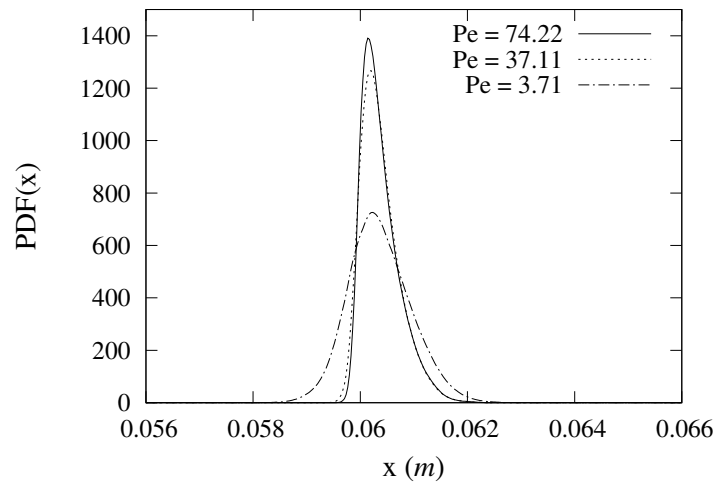


Figure 2.23: PDF of the position of tracer particles at time $t = 2000s$ in a random sphere pack for different Peclet numbers.

In order to better observe the effect of Peclet number on the skewness of a tracer cloud in the non-Fickian phase please see figure 2.24. Here the skewness of the tracer cloud is calculated at various times during the evolution of the tracer in the random sphere pack and the results are plotted for the three different diffusion coefficients (Peclet numbers). One can see that the higher the Peclet number the more skewed the the tracer cloud is or in other words the more the dispersion strays from Fickian dispersion. The ratio of diffusion effects to advection effects increase with decreasing Peclet number and more diffusion results in more jumping of the tracer from one velocity streamline to another resulting in a more homogeneous experience of the velocity field by the tracer.

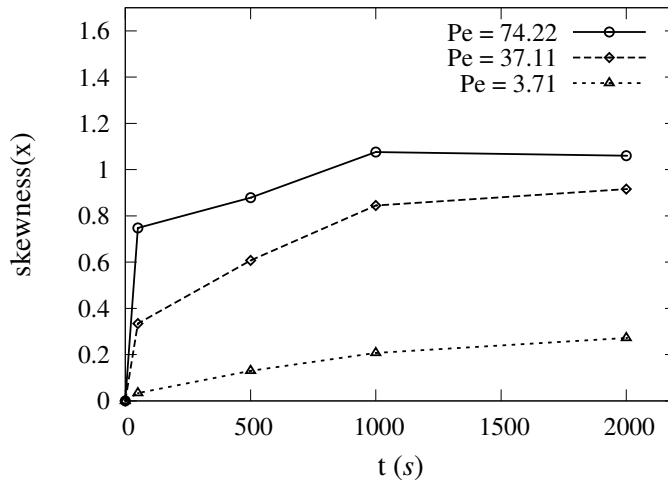


Figure 2.24: Skewness of the tracer cloud at various times in a random sphere pack for different Peclet numbers.

2.4.3 Tracer transport results

We aimed at simulating the evolution of a tracer in a homogeneous random sphere pack in order to observe and quantify the dispersion. It is clear that with a lower molecular diffusion coefficient (higher Peclet number) the dispersion would be more evident. However we were limited in our simulations in two ways. On one hand the diffusion number had to be kept well below one and on the hand the pore Peclet number had to be kept well under two in order for the finite volume simulation to stay stable. The diffusion number, δ and the cell Peclet number, Pe_{cell} , are defined by equations 2.18 and 2.19 respectively.

$$\delta = \frac{\Gamma \Delta t}{\Delta x^2} \quad (2.18)$$

$$Pe_{cell} = \frac{\bar{u} \Delta x}{\Gamma} \quad (2.19)$$

Δx here, is the grid size used in the finite volume simulation of the tracer transport. We use a grid size of $\Delta x = 3.125 \times 10^{-5} m$ in our simulations as we did also for resolving the velocity field. With this resolution if the molecular diffusion is set to $\Gamma = 5 \times 10^{-12} m^2/s$, $\Gamma = 1 \times 10^{-11} m^2/s$ or $\Gamma = 1 \times 10^{-10} m^2/s$ the cell Peclet number will be $Pe_{cell} = 1.1596$, $Pe_{cell} = 0.5798$ and $Pe_{cell} = 0.05798$ respectively and in order to keep the diffusion number below one the time step dt has to be kept well below 195.313s, 97.656s and 9.766s respectively. As the grid is rather fine it can be seen that the time step is not severely restricted by the diffusion number. However the cell Peclet number easily becomes problematic. For a diffusion coefficient of $\Gamma = 5 \times 10^{-12} m^2/s$ we were only able to run the simulation up to time $t = 6000s$ before the solution started to become unstable and affected by wiggles. In order to be able to simulate lower diffusion coefficients (and there-

for higher Peclet numbers) one would need to use a finer mesh. We decided to focus on a diffusion coefficient of $\Gamma = 1 \times 10^{-11} m^2/s$ which corresponds to a Peclet number of $Pe = 37.11$.

Figures 2.25, 2.26 and 2.27 respectively display the evolution of the centre of mass of the tracer, the standard deviation of the streamwise position of tracer particles and the skewness of the tracer cloud over time. These statistical quantities are found at every time step by calculating the statistical moments of the position of grid points, weighted by the concentration, at that time. Please note that the time necessary for the centre of mass of the tracer cloud to move, with the average pore velocity, a length equal to that of a sphere diameter is $t_{adv} = 10776s$

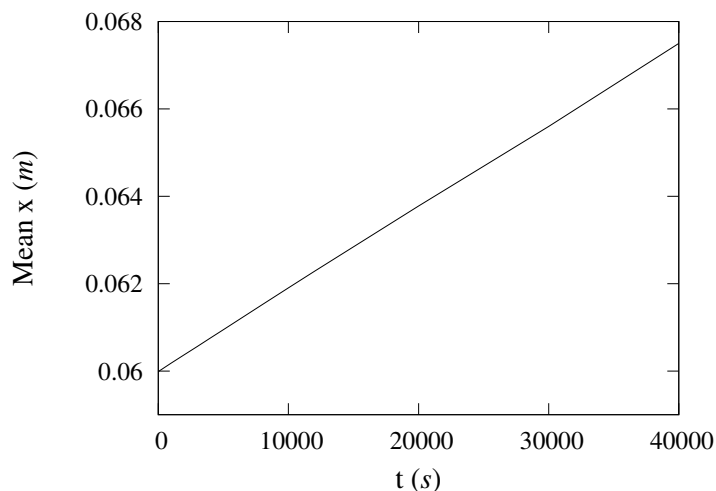


Figure 2.25: Centre of mass of the tracer cloud plotted against time in a random sphere pack for $Pe = 37.11$.

Because at the initial time all points on the cross section containing the tracer have a concentration value of $c = 1 kg/m^3$, it is clear that the initial value for the half width of the cloud has to be zero and that the tracer cloud is not skewed. In the early times when the dispersion is still non-Fickian the skewness increases with time as the cloud develops. After some time passes however the shape of the tracer cloud becomes more and more symmetric and tends towards a Gaussian profile and therefore the skewness begins to decrease. In other words the non-Fickian dispersion gradually converges to a Fickian one.

To calculate the dispersion coefficient at each time, t , from our DNS results we calculate the variance of the concentration distribution and divide that by $2t$. Figure 2.28 shows the dispersion coefficient, $\Gamma_D = \sigma^2/(2t)$, normalized by the molecular diffusion, $\Gamma = 1 \times 10^{-11} m^2/s^2$, plotted against time. σ^2 here is the variance of the concentration distribution in space. Notice that Γ_D varies over time and therefore the dispersion cannot be Fickian. Also Γ_D/Γ appears to be gradually converging towards a value pointing to a gradual transition towards asymptotic dispersion.

As previously mentioned the tracer is initialized on a cross section perpendicular to the streamwise direction. Since the domain that we use is not large enough to be considered an REV but is rather only an approximation of an REV, the velocity PDF on the cross

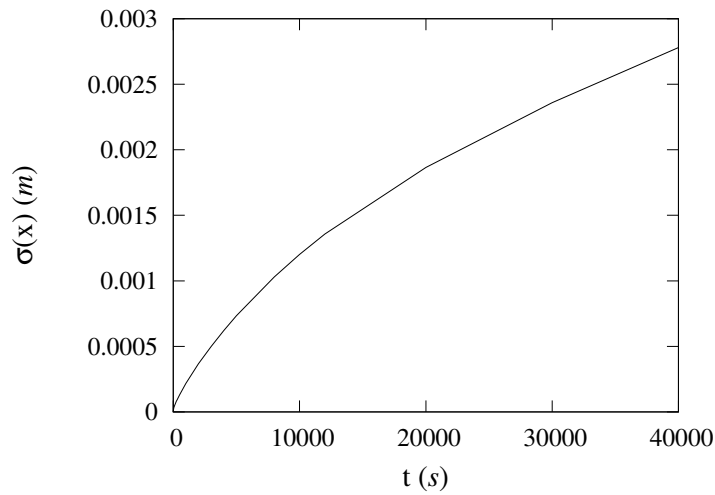


Figure 2.26: Standard deviation of tracer positions plotted against time in a random sphere pack for $Pe = 37.11$.

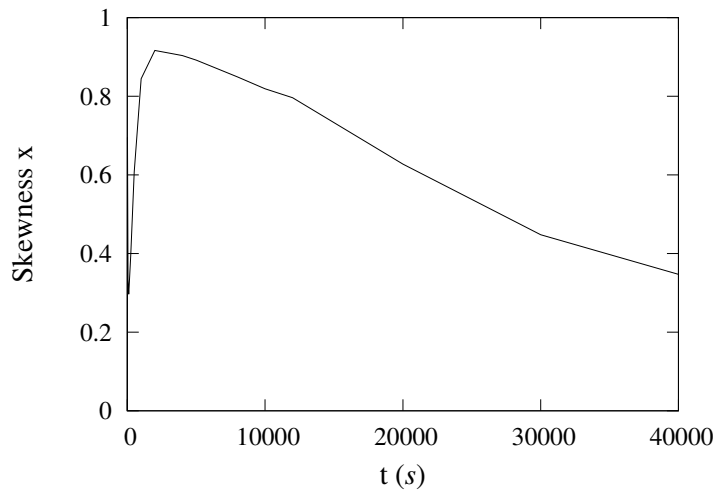


Figure 2.27: Skewness of the tracer cloud plotted against time in a random sphere pack for $Pe = 37.11$.

section does not exactly match that of the whole domain. In figure 2.29 the velocity PDF is plotted for various times. For better visibility the figure is zoomed in at velocities with higher probability. In order to obtain the velocity PDF, at each grid point the velocity is weighted by the concentration. The velocity range is between $-2\bar{u}$ and $16\bar{u}$ and is divided into 360 bins. \bar{u} is the average streamwise pore velocity in the random sphere pack domain. The velocity PDF of the total domain unweighed by the concentration is also plotted for comparison. Notice how the velocity PDF of points containing non-zero concentration values (weighted by the concentration) develops with time and converges to the PDF of the total velocity field.

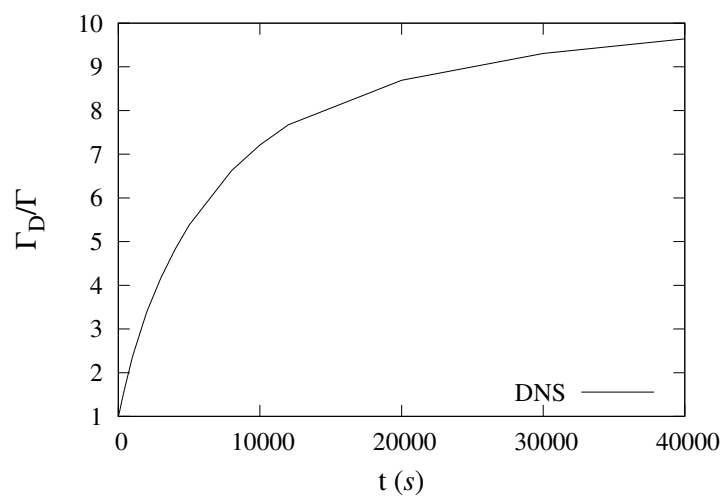


Figure 2.28: Γ_D/Γ plotted against times in a random sphere pack for $Pec = 37.11$.

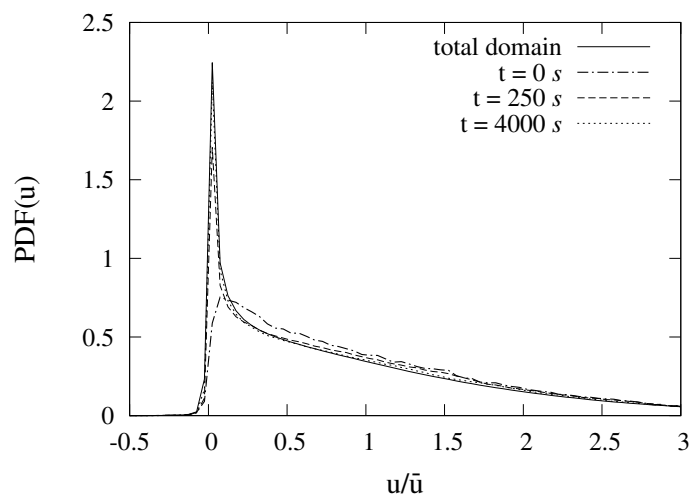


Figure 2.29: Velocity PDF of the tracer cloud at various times together with the velocity PDF of the total random sphere pack for $Pec = 37.11$.

Figure 2.30 shows the average velocity of points occupied by the tracer (weighted with the tracer concentration) which is denoted by \bar{u}_t and normalized by the average pore velocity in the total domain, \bar{u} over time. Notice how the ratio of \bar{u}_t to \bar{u} converges toward one with time.

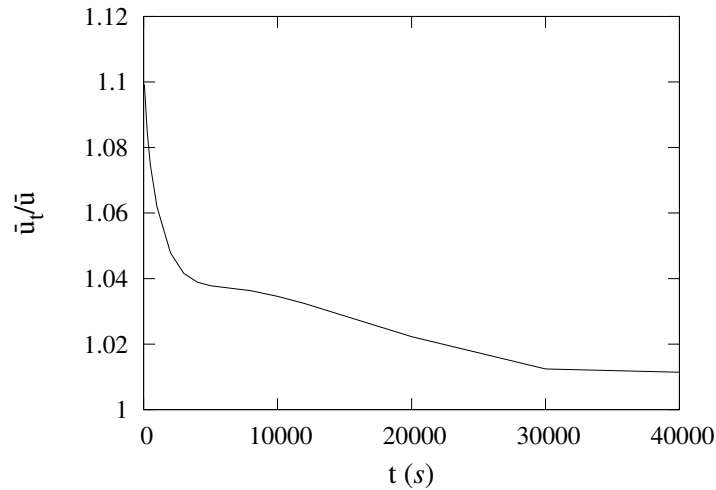


Figure 2.30: Mean pore velocity of tracer cloud normalized by the mean pore velocity, \bar{u} of the domain in a random sphere pack over time.

Figure 2.31 shows the shape of the cloud (obtained by calculating the PDF of x coordinate of grid points weighted by concentration) at various times after the release of the tracer. Notice how the skewness initially begins to increase with time and then gradually begins to decrease until the shape of the cloud becomes more and more similar to a Gaussian distribution.

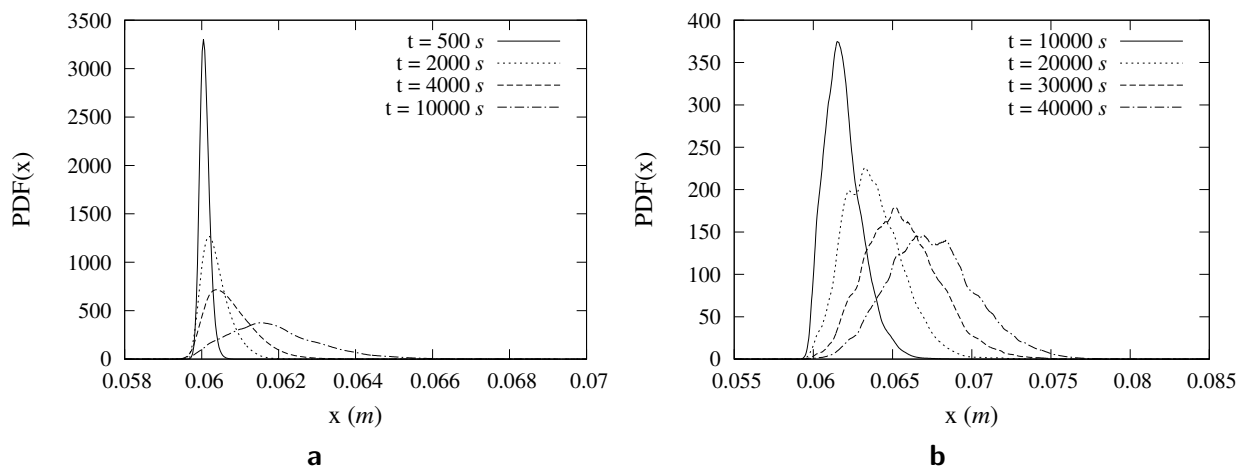


Figure 2.31: Shape of the tracer cloud over time in a random sphere pack. $t = 500s$ to $t = 10000s$ (a) and $t = 10000s$ to $t = 40000s$ (b)

3 Modelling Dispersion

In this chapter we present a model for dispersion based on the conditional statistics of the velocity increment (du) field. The statistics and PDFs of the velocity variation field will be presented and the main parameters of our stochastic velocity model will be discussed in detail. We elaborate upon both flow through a sphere pack and through a simple channel flow for comparison. We will use the model to predict the behaviour of a tracer in both a channel and a sphere pack and will compare the results to benchmark solutions.

This chapter is organized as follows. In the first section we introduce a model for dispersion based on a stochastic velocity process. This model will be used for resolving the transport of a tracer in a channel and in a sphere pack. In the second section we present the set-up of a simple channel flow. The set-up of the sphere pack, its properties and the statistics of its velocity field have been described in the previous chapter. In the third section of this chapter we describe the statistics, conditional statistics and PDFs of the velocity variation, du , field both in the channel and in the sphere pack. This section also includes the determination of the parameters (drift and diffusion terms) of our model. In the fourth and fifth sections of this chapter we present the results of tracer transport obtained from our model in the channel and in the sphere pack respectively.

3.1 A model for dispersion in porous media

In this section, we will present a stochastic process for velocities in porous media based on the model of Meyer and Tchelepi [33]. Their model has been demonstrated to reproduce the velocity distribution function well. However, the demonstration has been only conducted for two-dimensional Darcy flow in random permeability fields and is unable to account for negative velocities[33]. We then develop a link towards Eulerian statistics in three-dimensional velocity fields on the pore scale, such as the velocity fields in random sphere packs and modify the model of Meyer et al. to produce a dispersion model based on the pore scale velocity and velocity variation fields.

3.1.1 A Markovian process for velocity in porous media

Meyer and Tschelepi [33] proposed a continuous stochastic Markovian process consisting of a drift and a diffusion term in velocity space. This process is able to represent the velocity PDF if drift and diffusion are suitably calibrated. The stochastic process for velocity increments

du is formulated as follows.

$$du_0 = a(u_0)dt + b(u_0)dW(t) \quad (3.1)$$

Here $W(t)$ is a Wiener process and $a(u_0)$ and $b(u_0)$ are drift and diffusion terms respectively. In order to magnify small velocities u_0 is defined as

$$u_0 = \ln(|u|/U) \quad (3.2)$$

with u being the longitudinal velocity, and U the average longitudinal velocity. It is clear that with this configuration negative longitudinal velocities cannot be accounted for. Meyer and Tchelepi determine the drift and diffusion terms from the statistics obtained by Monte Carlo simulations where the Darcy equation is solved on 2D porous domains. In this set-up, only positive velocities occur. The drift and diffusion functions are obtained by conditioned statistics of velocity increments du_0 .

$$a(u_0) = \frac{\langle du_0 | u_0 \rangle}{dt} \quad (3.3)$$

$$b(u_0)^2 = \frac{\langle du_0^2 | u_0 \rangle}{dt} - \frac{\langle du_0 | u_0 \rangle^2}{dt} \quad (3.4)$$

This means, the drift term in velocity space of the Markovian process is determined by the conditioned average of velocity increments and the diffusion term by conditioned variances of the velocity increments. Meyer and Tchelepi [33] obtained the conditioned statistics from Lagrangian pathlines in a Monte-Carlo simulation. They also point out the similarities to the approach of [21, 20]. The transition probabilities in velocity space are therefore determined by the first and second moments of conditioned velocity increments. In the next section, we show how the velocity increments are linked to conditioned Eulerian velocity statistics.

3.1.2 Eulerian velocity increments

In this work we assess statistics of the velocity increments du in an Eulerian frame using the statistics of velocities obtained through pore scale simulations on a random sphere pack. We determine velocity increments for tracer particles moving according to Langevin's equation. The main differences with the analysis of [33] is that we do not use the mapping, equation (3.2), as the pore scale velocities can be negative and that we evaluate the velocity increments in Eulerian space using a Taylor series expansion for the velocity fields obtained by our 3D DNS in pore space. The latter allows for distinguishing between the effects of molecular diffusion and velocity variations along the streamlines on the velocity increments, as will be demonstrated in the following.

In order to obtain du we combine the Taylor series expansion for du , truncated after the

second order term,

$$du = \frac{\partial u}{\partial x_k} dx_k + \frac{1}{2} \frac{\partial^2 u}{\partial x_i \partial x_j} dx_i dx_j \quad (3.5)$$

with the Langevin equation for small tracer particles.

$$dx_i = u_i dt + \sqrt{2\Gamma dt} N_i \quad (3.6)$$

Note that $dW = \sqrt{dt}N$ where N is a Gaussian process with unit variance. In other words, N is a normally distributed random number with an average of 0 and a standard deviation of 1

After substituting dx from equation (3.6) into equation (3.5), we obtain:

$$du = \underbrace{\sqrt{2\Gamma dt} \frac{\partial u}{\partial x_i} N_i}_{\text{term 1}} + \underbrace{dt u_i \frac{\partial u}{\partial x_i}}_{\text{term 2}} + \underbrace{\Gamma dt \frac{\partial^2 u}{\partial x_i \partial x_j} N_i N_j}_{\text{term 3}} + \underbrace{\sqrt{2\Gamma dt} dt u_i \frac{\partial^2 u}{\partial x_i \partial x_j} N_i}_{\text{term 4}} + \underbrace{\frac{1}{2} dt^2 u_i u_j \frac{\partial^2 u}{\partial x_i \partial x_j}}_{\text{term 5}} \quad (3.7)$$

The Eulerian equation describing du consists of five different terms. The first two terms correspond to the first term of the Taylor expansion and the next three terms of du correspond to the second term of the Taylor expansion. The velocity variations along the streamlines are represented by terms 2 and 5. Terms 1 and 3 are due to molecular diffusion and term 4 is a mixed term. Thus, one can clearly identify which process has to be modelled in equation 3.1 if dispersion on a pore scale level is being considered. We will assess these terms together with other statistical quantities in the next sections.

After verifying that du can in fact be described by a drift and a diffusion term we attempted to enhance the model of Meyer and Tchepi by formulating a similar stochastic equation for the increments in velocity space from first principles. We define the following velocity stochastic process which is in fact the basis for a random walk process in the velocity space.

$$du = U_p dt + \sqrt{2\Gamma_p dt} N \quad (3.8)$$

Here U_p is a drift term conditioned on u and Γ_p is a diffusion term conditioned on u . The equivalent Fokker-Planck equation to this velocity stochastic process reads

$$\frac{\partial P}{\partial t} = -\frac{\partial(PU_p)}{\partial u} + \frac{\partial^2(P\Gamma_p)}{\partial u^2} \quad (3.9)$$

where P is the Probability density function of the velocity. This equation is nothing other than the continuous advection-diffusion PDE in the velocity space [51]. Notice that PU_p represents the drift flux in velocity space while $\partial(P\Gamma_p)/\partial u$ represents the diffusive flux in velocity space. In the following we attempt to determine Γ_p and U_p for a given range of u . The velocity probability density function, P , is of course easily attainable from the resolved velocity field.

Diffusion term Γ_p

In order to determine Γ_p in a given very small range of u assuming that in this range Γ_p and U_p are constant and equal to their average values in that range, $\overline{\Gamma_p}$ and $\overline{U_p}$ respectively, we evaluate the variance of du according to equation 3.8

$$\text{var}(du) = \langle U_p dt - \overline{U_p} dt + \sqrt{2\Gamma_p dt} \cdot N - \sqrt{2\overline{\Gamma_p} dt} \cdot \overline{N} \rangle^2 \quad (3.10)$$

Since Γ_p and U_p are constant and the variance of N is equal to 1 by definition, we conclude that

$$\text{var}(du) = (\sqrt{2\Gamma_p dt} \cdot \langle N - \overline{N} \rangle)^2 = 2\Gamma_p dt \langle N - \overline{N} \rangle^2 = 2\Gamma_p dt \quad (3.11)$$

and obtain Γ_p

$$\Gamma_p = \frac{\text{var}(du)}{2dt} \quad (3.12)$$

Drift term U_p

We use three different methods for calculating the drift term. The first method of finding U_p is to assume that both the drift and the diffusion terms stay constant in each small range of velocity and to simply take an average of both sides of equation 3.8

$$\langle du \rangle = \langle U_p dt \rangle + \langle \sqrt{2\Gamma_p dt} \cdot N \rangle \quad (3.13)$$

Since we assume that in the given range of u , Γ_p and U_p are constant we conclude that

$$\langle du \rangle = U_p dt + \sqrt{2\Gamma_p dt} \langle N \rangle \quad (3.14)$$

The average of N is zero by definition and therefore the second term on the right hand side can be eliminated. It follows that for each velocity range the drift term obtained via this method is simply the mean of du , in that certain velocity range, divided by time.

$$U_{p1} = \frac{\langle du \rangle}{dt} \quad (3.15)$$

The drift term obtained via this method will be denoted as U_{p1} . One must consider however, that the du field obtained via 3.7 cannot explicitly account for the bounce back at sphere surfaces. More explanation about this issue will be offered in section 3.3. Although we cannot account for the bounce back at the sphere surfaces we try to implicitly include the effects of the bounce back on the drift term by enforcing the velocity PDF as shown for the second method of obtaining U_p .

In the second method of obtaining the drift term, we assume that we are dealing with a steady flow where the velocity PDF stays constant in time. Therefore it follows from equation 3.9 that

$$\frac{\partial(PU_p)}{\partial u} = \frac{\partial^2(P\Gamma_p)}{\partial u^2} \quad (3.16)$$

As was also done in the first method we again assume that in each small range of u the drift and diffusion terms remain constant. It therefore follows that

$$U_p \frac{\partial P}{\partial u} = \Gamma_p \frac{\partial^2 P}{\partial u^2} \quad (3.17)$$

By integrating over the specific range of u , at which we want to calculate the drift term, on both sides and considering that the velocity flux remains constant at each velocity, we obtain

$$U_p P = \Gamma_p \frac{\partial P}{\partial u} \quad (3.18)$$

Finally by using the Γ_p obtained in section 3.1.2 the drift term which will be denoted by U_{p2} is determined

$$U_{p2} = \frac{1}{P} \frac{\text{var}(du)}{2dt} \frac{\partial P}{\partial u} \quad (3.19)$$

This method of determining U_p attempts at enforcing the actual shape of the velocity PDF in the stochastic velocity model. In this method a specific form of the Fokker-Planck equation is used that is based on the assumption that the diffusion term, Γ_p , remains constant in a given range of u . This assumption is not sufficiently accurate and therefore we add a correction term to the stochastic model for du (equation 3.8) to reduce the adverse affect of this simplification on our model. The stochastic velocity variation in the case where U_{p2} is used therefore reads

$$du = \left(U_p + \frac{\partial \Gamma_p}{\partial u} \right) dt + \sqrt{2\Gamma_p} dt \cdot N \quad (3.20)$$

This correction term is similar to the Itô correction term added to the random walk equation for the path of particles as described by Kinzelbach and Uffink in 1991 [16]. They observed that without the correction term the particles will accumulate in areas of lower dispersion (as cited in the paper of Kitanidis [17]). The analogy in our model would be that the velocities will be more prevalent in the ranges of velocity at which Γ_p is lower without the correction term.

The third method of obtaining U_p is similar to the second method. Again taking into account

the fact that we only deal with steady flows where the velocity PDF stays constant in time, we arrive at equation 3.16. After integrating this equation over the velocity range at which we want to find the drift term we obtain

$$U_p P = \frac{\partial(P\Gamma_p)}{\partial u} \quad (3.21)$$

Again no constant value remains after integration in the above as the velocity fluxes remain constant at each velocity. Taking the formula for Γ_p from equation 3.12 we obtain U_{p3} which denotes the drift term obtained via the third method.

$$U_{p3} = \frac{1}{P} \frac{\partial(P\Gamma_p)}{\partial u} = \frac{1}{2dtP} \frac{\partial(\text{var}(u)P)}{\partial u} \quad (3.22)$$

This method is a conservative way of enforcing the Fokker-Planck into our model. Once U_p and Γ_p are determined one can use the stochastic velocity model (equation 3.8) to obtain the velocity at each step of a random walk of a given particle.

3.2 Channel

In order to evaluate our stochastic velocity model and especially the drift and diffusion terms in the model, we consider a simple channel flow the specifications of which are shown in figure 3.1.

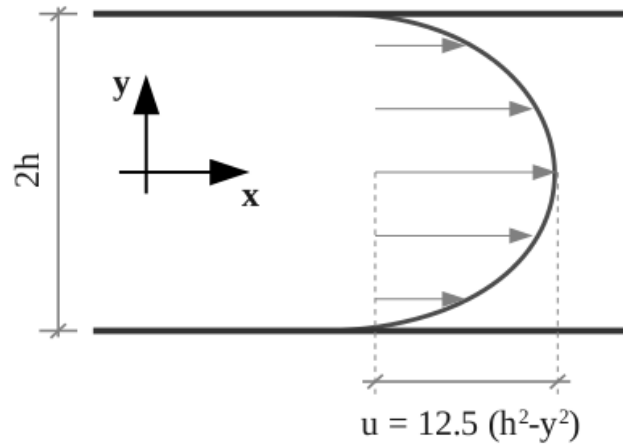


Figure 3.1: Set-up of the channel flow

The flow velocity in the x direction of the channel is defined by

$$u = -\frac{1}{2\mu} (h^2 - y^2) \nabla P \quad (3.23)$$

while the velocity in the y and z directions are zero. μ is the dynamic viscosity, h is the half width of the channel and ∇P is the pressure gradient driving the flow. We set $\mu = 0.001 \text{ kg}/(\text{m}\cdot\text{s})$ and $\nabla P = -0.025 \text{ Pa}/\text{m}^2$. The channel is infinite in directions x and z and in the y direction the width of the channel is set to $2h = 2 \text{ mm}$. We deliberately set these parameters such that the flow in the channel would be more or less comparable to the flow in a typical channel inside the sphere pack which we are interested in. The streamwise velocity profile in the channel using these parameters will be

$$u = 12.5(h^2 - y^2) \tag{3.24}$$

3.3 du and the drift and diffusion terms

It was explained in section 3.1.2 that our model of interest for dispersion in porous media relies on the statistical properties of the velocity increments in the domain conditioned on the velocity, $du|u$. Please note that we focus only on the velocities and velocity increments in the streamwise direction.

The du field can be obtained in two ways. One method is to plug in the Langevin equation for the transport of a particle into the Taylor expansion of du in order to find du as a function of velocity and velocity variations as shown in equation 3.7 for a given molecular diffusion, Γ , and in a certain time step, dt . We will refer to this method of finding du as the ‘‘LT’’ method (for Langevin and Taylor). The LT method does not allow for the explicit consideration of the boundaries imposed by sphere surfaces in the case of the sphere pack or the channel wall in the case of the channel. The other method is to evenly spread out a large number of particles into the domain (in which the velocity is known at every location), take note of the velocity that each particle has in its certain location and then allow the particles to diffuse with a given molecular diffusion, Γ and for a certain time step dt . A simple bounce back at solid surfaces is imposed. One can then simply find the difference between the new velocity and the original velocity of each particle. In this way the du field can be determined. This method will be referred to as the particle method. In some figures the results obtained via the particle method will be distinguished with the letters ‘‘RW’’ (for random walk).

The drift term, U_p , and diffusion term, Γ_p , are the building blocks of our model as explained in section 3.1.2. In order to determine these parameters we use the statistics of du conditioned on u together with information concerning the pore velocity PDF in the case of drift terms U_{p2} and U_{p3} . In the case of the random sphere pack the du is obtained using the LT method. In the case of the channel flow we have two sets of conditional statistics of du over 50 bins of u . The first set corresponds to du obtained using the particle method and the second set corresponds to du obtained from the LT method.

In this section we first present the characterisations of the du field in a simple channel and then follow that with the determination of the drift and diffusion terms of the model. The same will be presented for the flow in a random sphere pack.

3.3.1 du in a channel

Here the du field was calculated once using the particle method by evenly distributing 200 million particles in a cross section of the channel and once by using the LT method. Here, we are mainly focused on identifying the differences in the properties of du obtained by the two different methods. The particle method of obtaining the du field is straightforward. It is only important to note that when the particles are allowed to diffuse for one time step, those particle which attempt to move out of the boundaries of the channel are bounced back at the wall. For the LT method we take 200 million equidistant points on a cross section of the channel, calculate the velocity at each point using equation 3.24 and then find the du for each point from equation 3.7. Considering that the transverse velocities are zero and that the streamwise velocity is constant in the x and z directions, equation 3.7 can be simplified to

$$du = \frac{\partial u}{\partial y} \sqrt{2\Gamma dt} N + \frac{1}{2} \frac{\partial^2 u}{\partial y^2} (2\Gamma dt) N^2 \quad (3.25)$$

where N is a normally distributed random number (with a mean of zero and a standard deviation of one). The first term in equation 3.25 corresponds to the first term in equation 3.7 and the second term corresponds to the third term in equation 3.7. Using the equation for the streamwise pore velocity (equation 3.23), one can further simplify du to

$$du = \frac{\nabla p}{\mu} y \sqrt{2\Gamma dt} N + \frac{\nabla p}{\mu} (\Gamma dt) N^2 \quad (3.26)$$

For calculating the du field in both methods the molecular diffusion coefficient was set to $\Gamma = 1 \times 10^{-11} m^2/s$ and time step size was set to $dt = 1s$. Table 3.1 shows the statistics of du obtained using each method and also the statistics of the streamwise pore velocity field. All values except for skewness and flatness, which are dimensionless, are normalized by the average velocity in the channel. The average of u can also be easily found analytically by integrating equation 3.24 between $y_{min} = -1mm$ and $y_{max} = +1mm$ and then dividing by the channel width, $2h$. Considering the width of the channel as the length scale, the Peclet number of this set-up would be $Pe = 1666.667$. The Schmidt number is equal to $Sc = 100000$.

$$\langle u \rangle = \frac{1}{2h} \int_{-h}^h u dy = \frac{1}{2h} \int_{-h}^h -\frac{\nabla P}{2\mu} (h^2 - y^2) dy = -\frac{\nabla P}{4\mu h} (h^2 y - \frac{y^3}{3}) \Big|_{-h}^h = 8.333 \times 10^{-6} m/s \quad (3.27)$$

It is clear that the statistics of du differ slightly between the two methods of obtaining du . The mean du theoretically has to be zero for example, but with a finite number of points or particles at which du is calculated we are not able to achieve a complete zero. However, both methods yield a very small average du although the average du from the particle method is

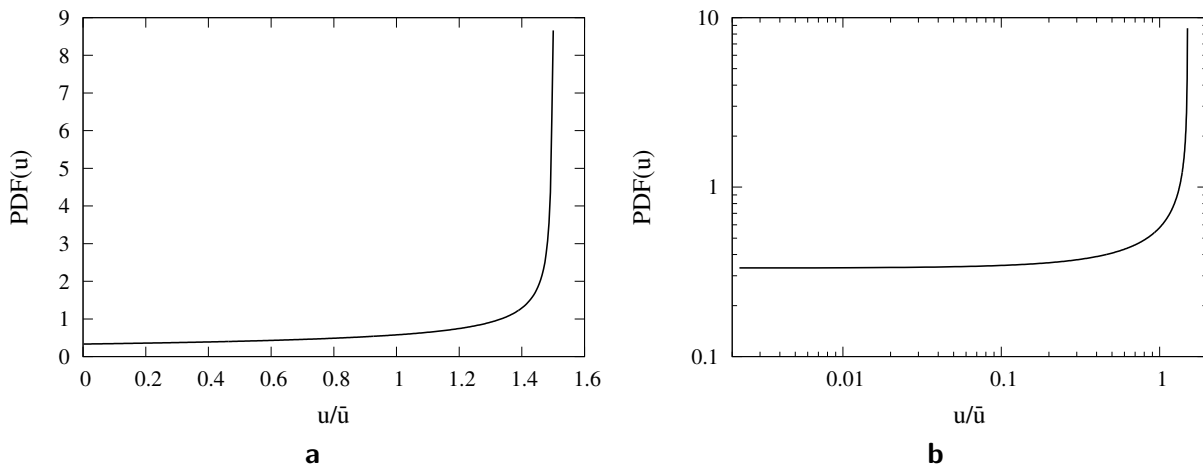
Table 3.1: Statistics of u and du in a channel

	u	du (particle)	du (LT)
Minimum $/\bar{u}$	0	-6.736E-2	-6.847E-2
Maximum $/\bar{u}$	1.5	6.979E-2	7.088E-2
Mean $/\bar{u}$	1	4.485E-7	-3.079E-5
Standard deviation $/\bar{u}$	4.472E-1	7.718E-3	7.745E-3
Skewness	-6.389E-1	1.464E-4	-2.342E-2
Flatness	2.143	5.374	5.401

two orders of magnitude smaller than the one from the LT method. Also one would expect the skewness of du to be zero. In this respect too, statistics of the particle method are more accurate. This discrepancy can be explained by the fact that by using the particle method the boundaries of the channel are accounted for through the bounce back condition placed on them. In the case of the LT method however, the boundary is not taken into account. By taking an average over equation 3.26, which describes the LT method of obtaining du , we arrive at

$$\langle du \rangle = \langle \frac{\nabla p}{\mu} y \sqrt{2\Gamma dt} N \rangle + \langle \frac{\nabla p}{\mu} (\Gamma dt) N^2 \rangle \quad (3.28)$$

It is clear that the mean du obtained via the LT method will always acquire a negative value in the channel flow. Please note that the first terms in the above equations are cancelled out due to the symmetry of the random number N and the y field.

**Figure 3.2:** PDF of u in a channel flow. Linear scale(a) and logarithmic scale (b).

The PDF of u is shown in figure 3.2 both in the linear scale and in the logarithmic scale. The PDF curve is normalized by \bar{u} and obtained by dividing the range between 0 and

$1.5\bar{u}$ into 360 bins. The PDF of du is shown in figure 3.3. These PDFs were also normalized by \bar{u} and obtained by dividing the range between $-0.071\bar{u}$ and $0.071\bar{u}$ into 360 bins. Notice how the PDF of du obtained by the two different methods are almost identical.

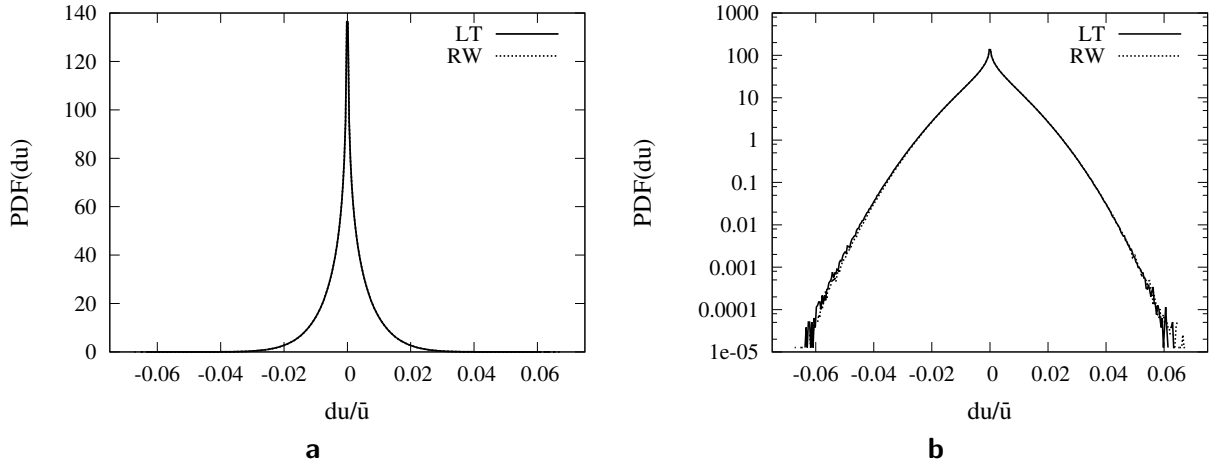


Figure 3.3: PDF of du in a channel flow. Linear scale(a) and semi logarithmic scale (b).

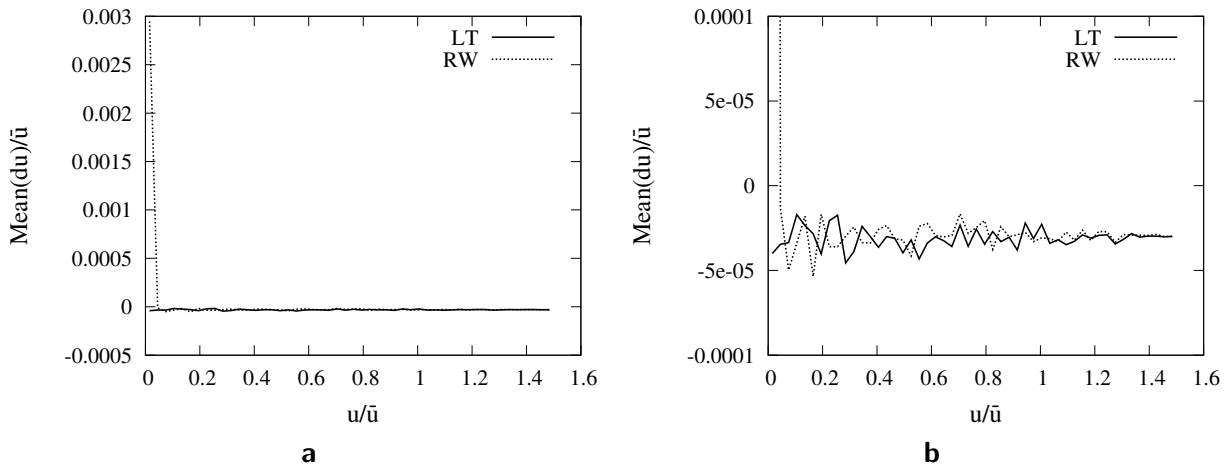


Figure 3.4: Conditional mean of du in a channel flow. Complete figure (a) and zoom in at smaller values of average du (b).

The conditional mean, standard deviation and variance of du are plotted in figures 3.4, 3.5 and 3.6. The conditional statistics were obtained by dividing the range between the maximum and minimum u into 50 bins and for each bin calculating the statistics of du values that correspond to the u values residing in that bin. Each figure shows one curve corresponding to conditional statistics of du from the particle method and one from the LT method. No curve representing the conditional statistics of the analytically obtained du is

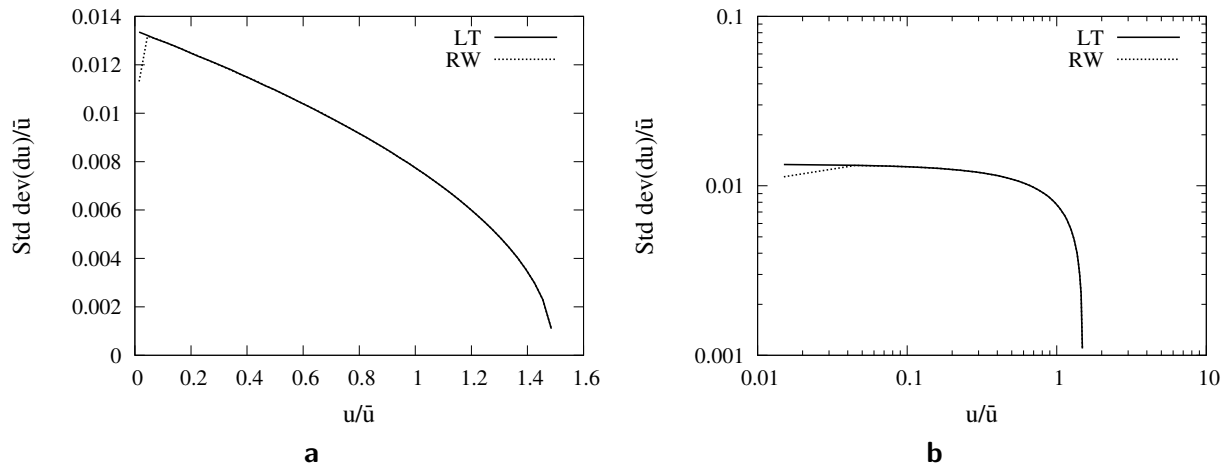


Figure 3.5: Conditional standard deviation of du in a channel flow. Linear scale (a) and logarithmic scale (b).

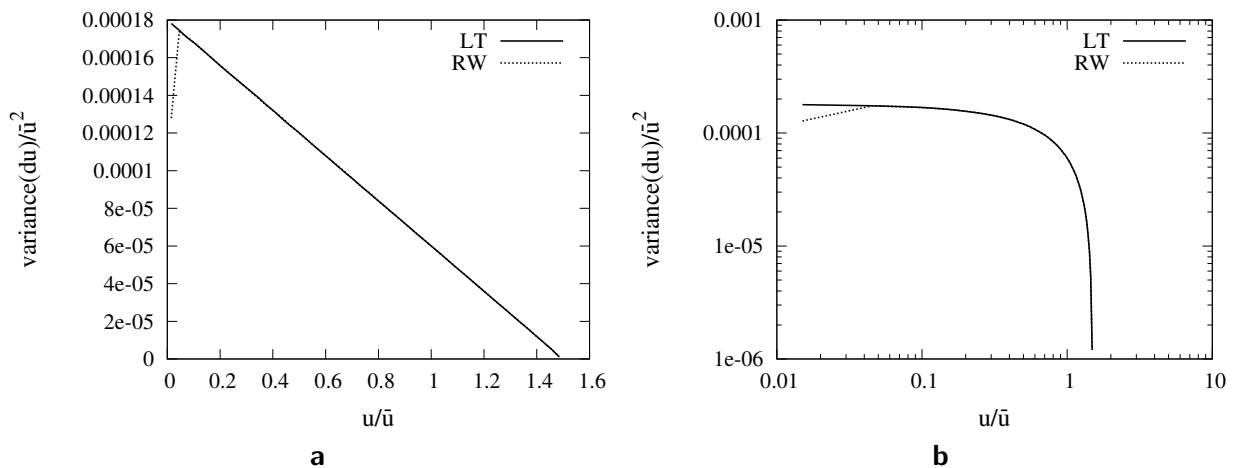


Figure 3.6: Conditional variance of du in a channel flow. Linear scale (a) and logarithmic scale (b).

presented as such curves would practically be exactly the same as the ones obtained by du from the particle method. The mean and standard deviation values are normalized by \bar{u} in the channel and the variance is normalized by \bar{u}^2 . For each bin the normalized statistical value is plotted against the median of the bin normalized by \bar{u} .

In figure 3.4 it can easily be observed that the only main difference between the conditional mean of du obtained by the LT method and that obtained by the particle method is in the first bin. This is due to the fact that the first bin of u corresponds to the boundaries of the channel which were simply ignored in the LT method and at which a bounce back was introduced for the particle method. The same is true for the standard deviation and variance of du as evident in figures 3.5 and 3.6. The difference is seen in the velocity bins

corresponding to the area near the channel walls.

The method of obtaining du appears to affect the first two bins of the conditional skewness and flatness of du . See figures 3.7 and 3.8. These conditional statistics are also obtained and plotted using the procedure explained above the only difference being that skewness and flatness are dimensionless and are therefore not normalized.

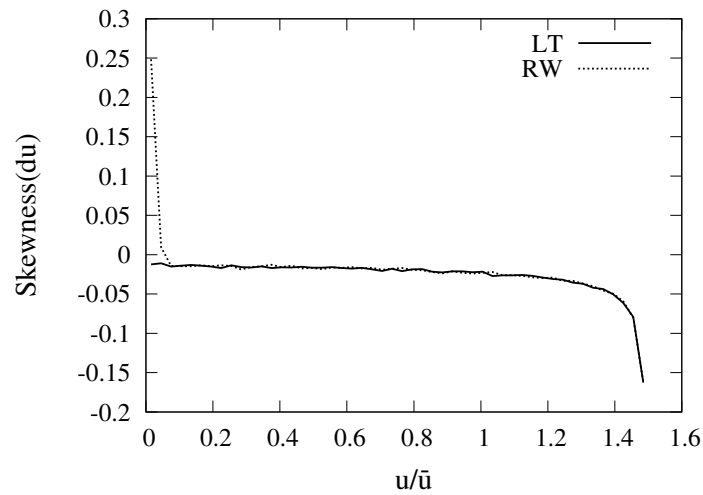


Figure 3.7: Conditional skewness of du in a channel flow.

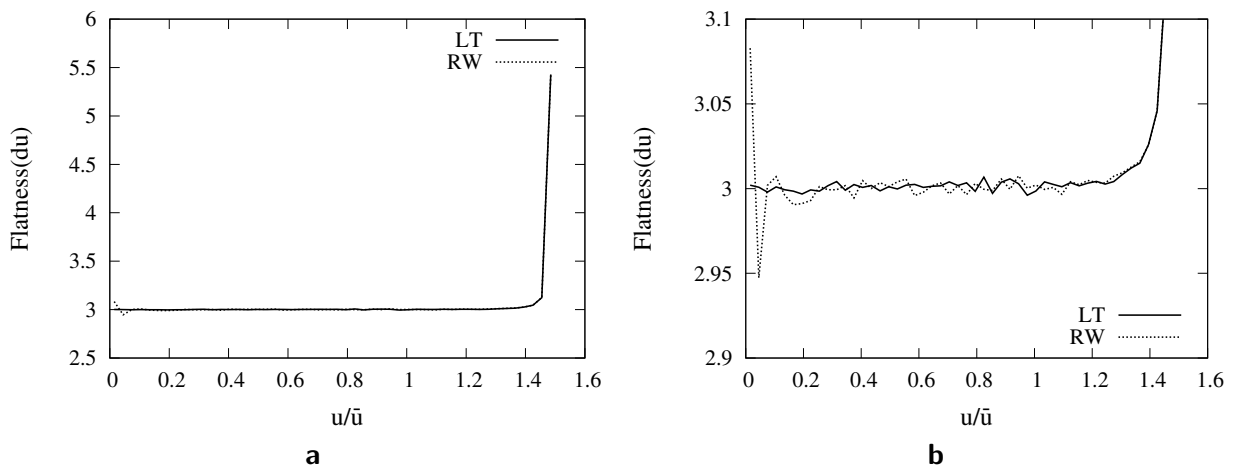


Figure 3.8: Conditional flatness of du in a channel flow. Complete figure (a) and zoom in at smaller flatness values (b).

3.3.2 Diffusion term, Γ_p , in a channel

According to equation 3.12 for each bin of u , the calculation of Γ_p is straightforward. Figure 3.9 shows Γ_p plotted over u for the channel flow. Here the number of bins is set to 50. Notice how this figure matches that of the conditional variance of du in the channel (figure 3.6). Here again it is evident that the diffusion term obtained via LT or the particle method, differ only in the first velocity bin corresponding to the channel boundaries.

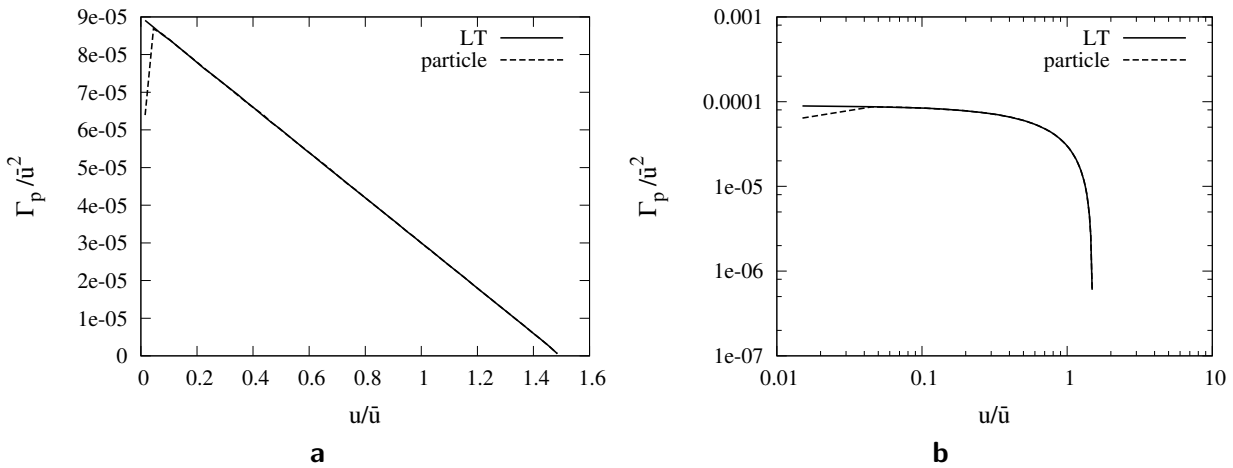


Figure 3.9: Γ_p normalized by \bar{u}^2 plotted against the median of velocity bins normalized by \bar{u} for flow in a channel. Linear scale (a) and logarithmic scale (b).

3.3.3 Drift term, U_p , in a channel

The drift term, U_p , was calculated in three different ways. According to equation 3.15 one method is to simply take the average du in each bin and divide it by the time step size dt to find the drift term of that bin. The second method relies on the PDF of u and its gradient with respect to u in each bin and also the standard deviation of du , see equation 3.19. The drift term obtained using this method ensures that the velocity PDF obtained from the model matches the velocity PDF used for finding the drift term. In order to reach equation 3.19 however, it was assumed that drift and diffusion terms remain constant in each velocity bin. A more general way of obtaining the drift term is via equation 3.22. When the drift term is found using this method the velocity PDF obtained from running the model again matches that used for obtaining U_p and the model yields more accurate results.

In the case of the channel flow, the conditional statistics of du used for determining the drift term is found using 50 velocity bins. The drift term obtained using the first method (U_{p1}) is plotted against the median of velocity bins in figure 3.10 both for du values obtained using the LT method and those obtained using the particle method. Both axes are normalized by \bar{u} . It is clear that the two curves differ due to the fact that in using the LT method the walls of the channel are not accounted for. The curves representing U_{p1} are

exactly the same as those representing $\langle du \rangle$ (see figure 3.4), as these terms are directly related.

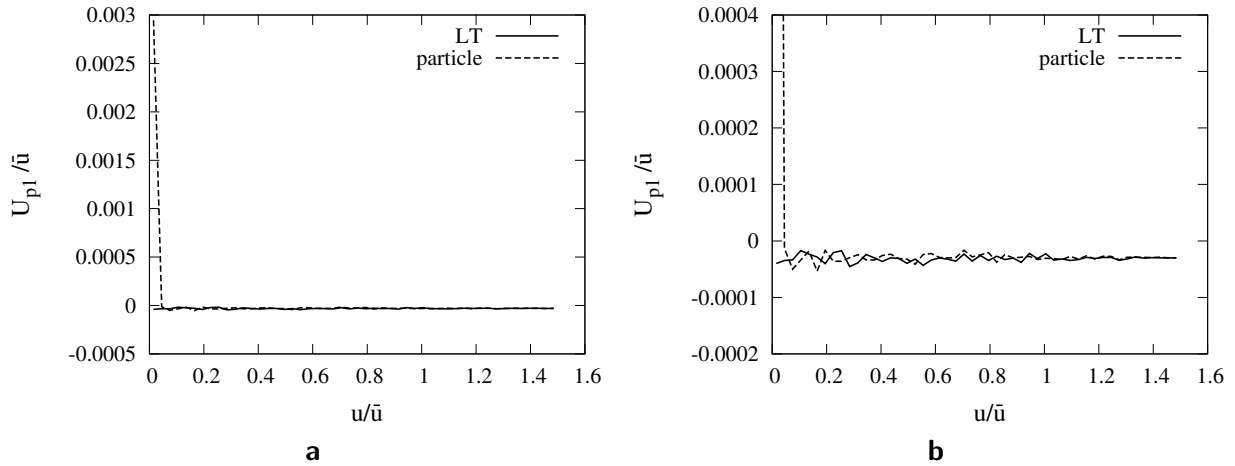


Figure 3.10: U_{p1} normalized by \bar{u} plotted against the median of velocity bins normalized by \bar{u} for flow in a channel. Complete figure (a) and zoomed in at small values of U_{p1} (b).

Figure 3.11 shows the drift term obtained using the second method (U_{p2}). Here one can see that because of using the velocity PDFs the curve representing (U_{p2}) from the LT method mimics that of the particle method except in the area of the first velocity bin. However there exists a major problem in both curves. Both curves have positive values in every bin. By examining equation 3.19 one can see that since the PDF of u in the channel and the variance of du are always positive the sign of (U_{p2}) would follow that of the gradient of the PDF which is itself always positive in the channel. This does not match the drift term obtained from the average du in each bin. It is clear that a constantly positive drift term would continuously increase the velocity rather than making it adhere to a certain distribution. Such a situation was foreseen in the process of arriving at the equation for (U_{p2}). In order to remedy this issue a correction term is added to the stochastic equation for velocity variation (equation 3.8) as shown in equation 3.20.

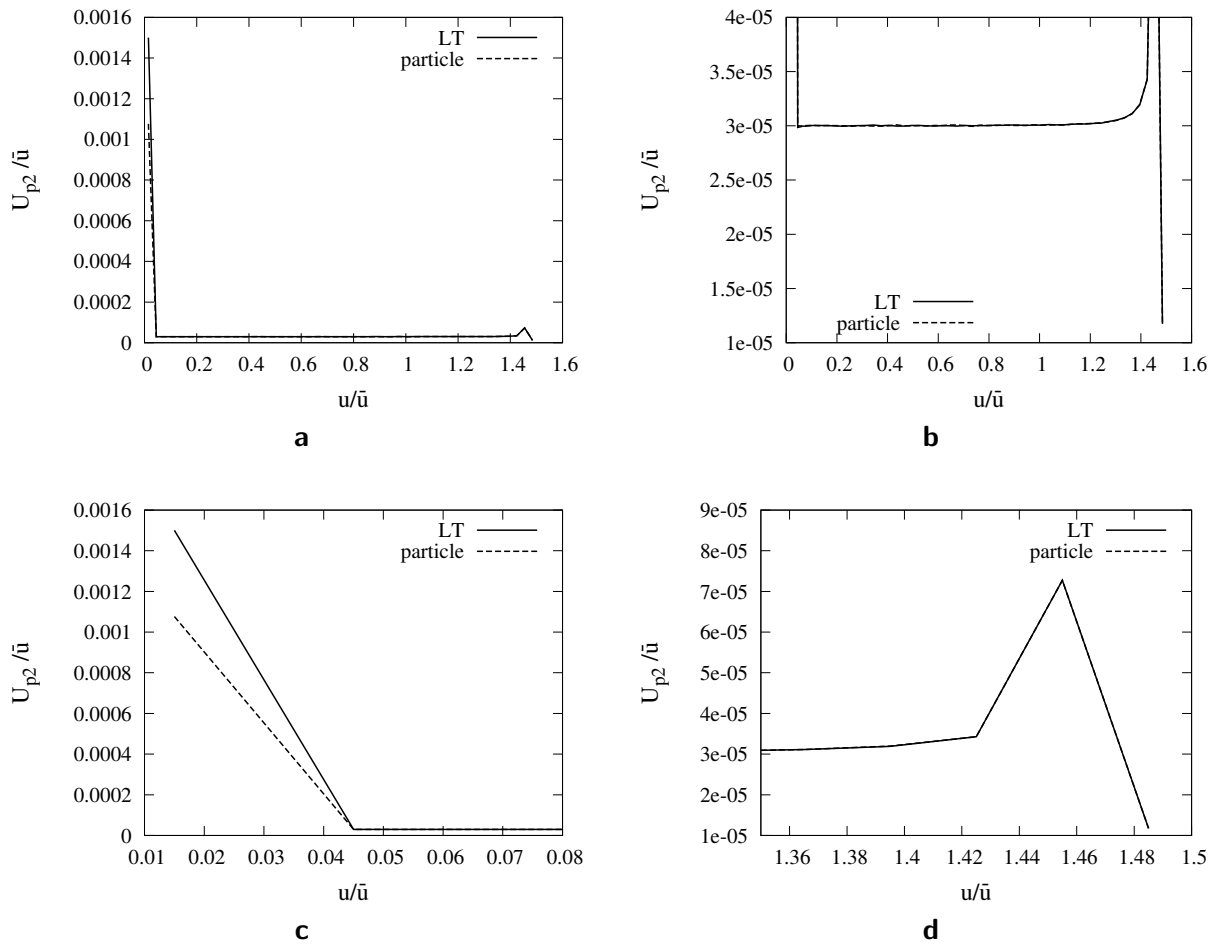


Figure 3.11: U_{p2} normalized by \bar{u} plotted against the median of velocity bins normalized by \bar{u} for flow in a channel. Complete figure (a); zoomed in at small values of U_{p2} (b); zoomed in at small values of u (c) zoomed in at large values of u (d).

It is far more accurate to use the third method of obtaining the drift term, U_{p3} , from equation 3.22, see figure 3.12. Here there is a reasonably good agreement between the curve corresponding to du from the LT method and the one corresponding to du from the particle method. Also the drift term is not continuously positive but rather fluctuates between positive and negative values over different velocity bins. The function of the drift term in each bin is to push back the straying velocities toward the mean pore velocity and to prevent the velocities from going out of the velocity extrema bounds.

To have an overview of the differences between the three methods of obtaining the drift term, figure 3.13 shows the drift terms obtained from the three different methods using the conditional statistics of du obtained by the LT method. When the LT method is used for obtaining the du field, it is clear that while the second method of obtaining the drift yields positive U_{p2} values over the complete velocity range, the first and third methods seem to create more similar drift values. The exception is at the first velocity bin where using the first method gives a very low drift term as opposed to the other two methods which are based on the velocity PDF and can to some extent account for the channel boundaries.

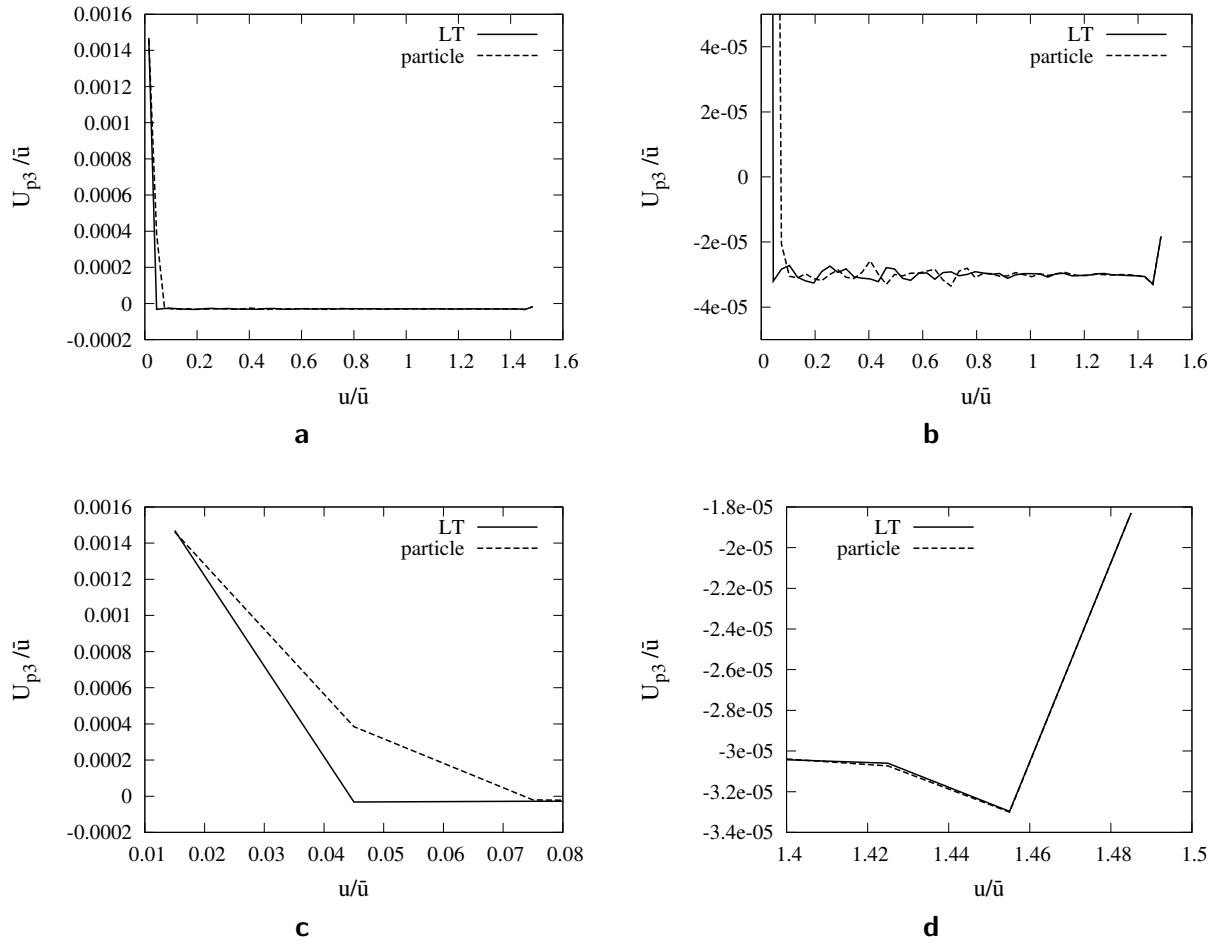


Figure 3.12: U_{p3} normalized by \bar{u} plotted against the median of velocity bins normalized by \bar{u} for flow in a channel. Complete figure (a); zoomed in at small values of U_{p3} (b); zoomed in at small values of u (c) zoomed in at large values of u (d).

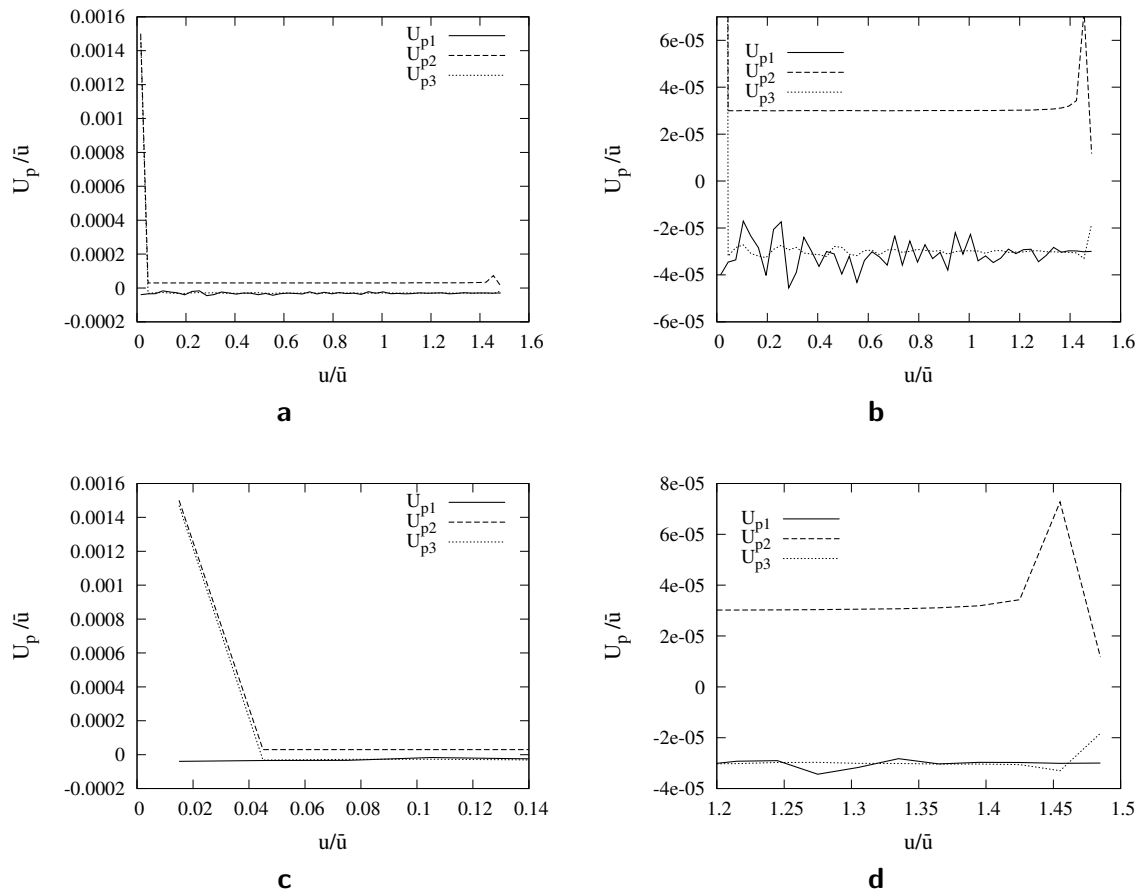


Figure 3.13: U_p obtained by the LT method normalized by \bar{u} plotted against the median of velocity bins normalized by \bar{u} for flow in a channel. Complete figure (a); zoomed in at small values of U_p (b); zoomed in at small values of u (c) zoomed in at large values of u (d).

The same is done for the particle method of obtaining the du field. Figure 3.14 shows the drift term obtained in three different ways using the conditional statistics of du obtained by the particle method. Again U_{p1} and U_{p3} seem to be more similar to each other as opposed to U_{p2} which is always positive. At the first velocity bin, which corresponds to the walls of the channel, all three drift terms acquire a large positive value that is different for each. The magnitude of this value can very well depend on the size of the velocity bins used to find the conditional statistics of du .

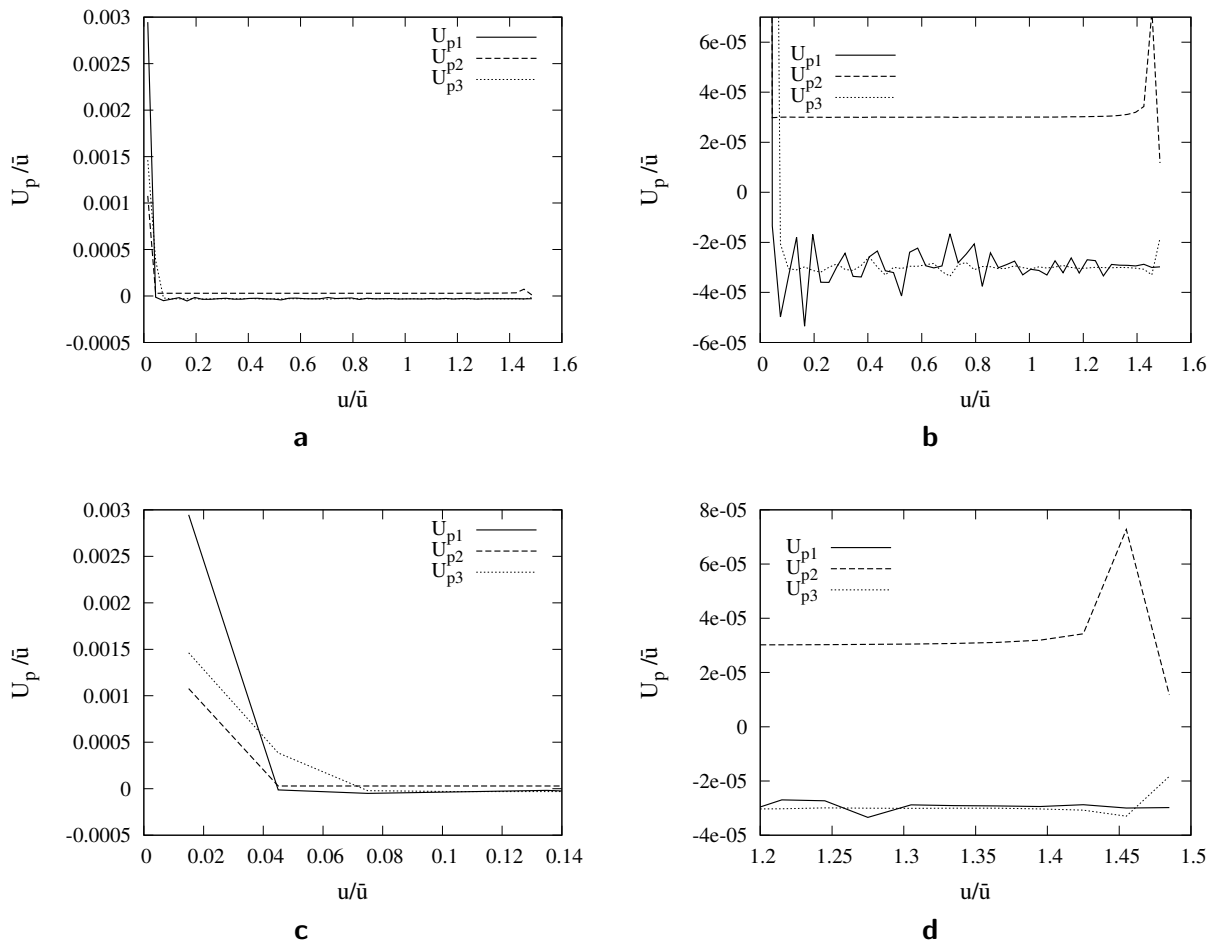


Figure 3.14: U_p obtained by the particle method normalized by \bar{u} plotted against the median of velocity bins normalized by \bar{u} for flow in a channel. Complete figure (a); zoomed in at small values of U_p (b); zoomed in at small values of u (c) zoomed in at large values of u (d).

3.3.4 du in a random sphere pack

For the flow in a random sphere pack of size 2.4cm which was characterized in detail in the previous chapter we used the LT method to obtain the du field. According to equation 3.7 du consists of five different terms. In order to evaluate the importance of each term and study their statistics we calculated each of these five terms separately at each grid point for different values of Γ and dt .

In the first step we determined the effect of dt on du . We observed that for even large values of dt the first and third terms are the main contributors to du and the other three terms can be considered negligible. Figure 3.15 shows the absolute value of the average du and the variance of du normalized by \bar{u} plotted against the time step size in log-log scale. It is quite clear that the relationship between both the average and the variance of du with time is practically linear even for large time steps up to $dt = 10\text{s}$. We choose a time step of size $dt = 1\text{s}$ for displaying our results.

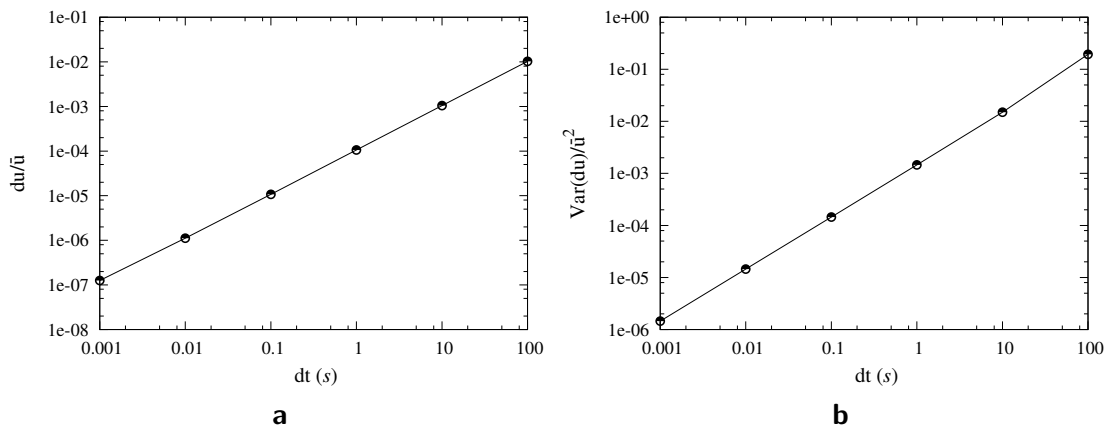


Figure 3.15: Average du plotted against time step size (a) and variance of du plotted against time step size (b).

Statistics and PDF of du in a random sphere pack

Here, in the case of the sphere pack, we only use the LT method for obtaining the du field as our initial goal was to model the velocity process and the dispersion by relying solely on the velocity and velocity derivatives fields. Using the particle method for obtaining the du requires detailed information concerning the pore geometry in order to introduce the bounce back at sphere surfaces and is beyond the scope of this work.

As the flow in the sphere pack is steady, it is clear that the average du logically has to be zero in the whole domain, but using the LT method we always end up with a small negative value for $\langle du \rangle$. As shown in the case of the channel flow, this is due to the fact that the LT method does not account for the bounce back at the surface of spheres. However as the average of du only affects the drift term, U_{p1} (when it is obtained using the first method via equation 3.15), we are more interested in the standard deviation of du and the PDF of u as these parameters affect the drift term obtained by the second and the third methods, U_{p2} and

U_{p3} respectively (equations 3.19 and 3.22). Therefore, we calculated the statistical moments (up to the 4th moment) of du and each of its components and plotted their respective probability density distributions. The diffusion coefficient is set to $\Gamma = 1 \times 10^{-11} m^2/s$ and the time step size to $dt = 1s$. The mean pore velocity is $\bar{u} = 1.85 \times 10^{-7} m/s$ and according to that the Reynolds number in the domain is approximately $Re = 3.7 \times 10^{-4}$. The Schmidt number of this set-up is $Sc = 1 \times 10^5$ and considering a length scale equivalent to the sphere diameter the Peclet number of the set-up is $Pe = 37.11$. The statistics of the five terms and du are shown in table 3.2. The values in this table are normalized by the average streamwise pore velocity, \bar{u} . Considering the range of values each of these terms cover, we concluded that the first three terms are the main contributors to the standard deviation of du while the first and third terms are the main contributors to the average du . It is evident that the first term, which contains velocity derivatives and molecular diffusion (see equation 3.7), is quite symmetric and contributes to the diffusion behaviour in the velocity space. Terms 3 and 5, both of which contain the second derivatives of velocity, on the other hand have large skewness values and point to the drift behaviour in the velocity space.

Table 3.2: Statistics of du and its components in a sphere pack with $Pe = 37.11$. The extrema, mean and standard deviation are normalized by \bar{u} and the variance is normalized by \bar{u}^2

	Term1	Term2	Term3	Term4	Term5	du
Min/ \bar{u}	-1.162	-2.937E-2	-1.155E-1	-4.557E-3	-2.021E-4	-1.094
Max/ \bar{u}	1.062	2.180E-2	1.789E-1	3.365E-3	7.135E-5	1.178
Mean / \bar{u}	1.813E-6	1.056E-8	-1.030E-4	4.220E-10	2.425E-8	-1.011E-4
Variance/ \bar{u}^2	1.402E-3	5.670E-7	4.049E-6	5.599E-10	1.140E-12	1.407E-3
Std dev/ \bar{u}	3.744E-2	7.530E-4	2.012E-3	3.366E-5	1.067E-6	3.751E-2
Skewness	-1.091E-4	-1.191E-1	3.598	-3.289E-2	-1.602E+1	1.961E-2
Flatness	1.561E+1	2.757E+1	1.080E+2	6.945E+1	1.033E+3	1.576E+1

We also plotted the PDF of the five terms plus du obtained using the same configuration, as shown in figure 3.16. The PDFs were obtained by dividing the range between -193σ and 193σ into 750 bins, σ being the respective standard deviation of each term or du . The PDF curve of each is normalized by its respective standard deviation and the PDF of a normal distribution is also plotted in the figure. Please note that the PDF curves for Term1 and du are not easily distinguishable as they are very similar. Term1 of course is the main contributor to du . Also notice that neither du nor any of its components have a normal distribution. As expected, the third and fifth terms appear very skewed and account for the drift pattern in the velocity space. A drift term aids at pushing back the velocity towards its average. The other terms seem more symmetric and rather than drifting the velocity toward its mean, will diffuse the velocity.

Conditional statistics of du in a random sphere pack

In the next step we calculated the statistics of du and each of its terms conditioned on the longitudinal velocity, u . This was done by dividing the velocity field into a certain number

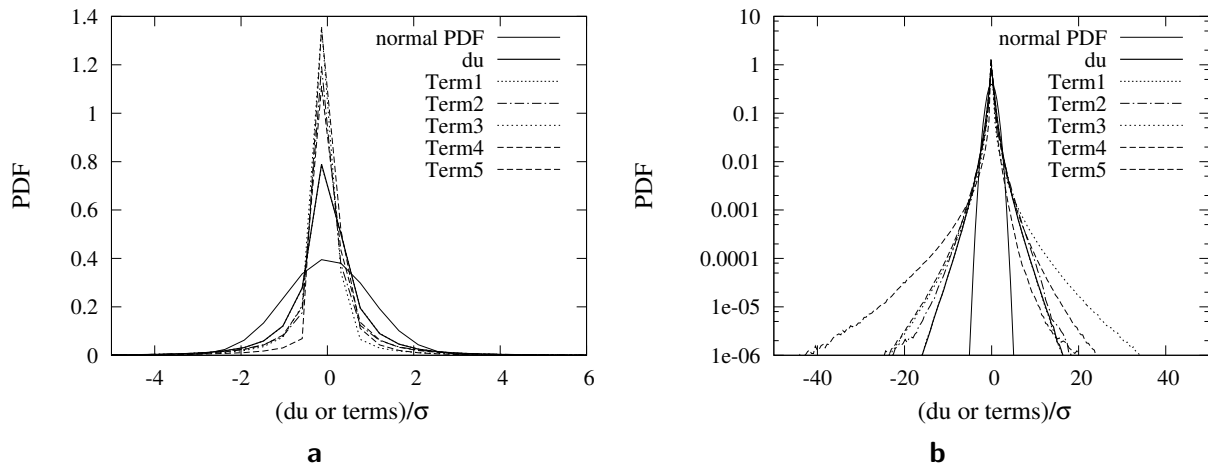


Figure 3.16: PDF of du and its components each normalized by its respective standard deviation. Figures are zoomed in at areas of higher probability for better visibility. Linear scale (a) and logarithmic scale (b).

of bins. We will first demonstrate the sensitivity of the conditional statistics to the number of velocity bins. Figure 3.17 shows the median of the most populous velocity bin for each case plotted against the number of bins. These points demonstrate the velocity at which the peak of the velocity PDF occurs should we use the corresponding number of bins to find it.

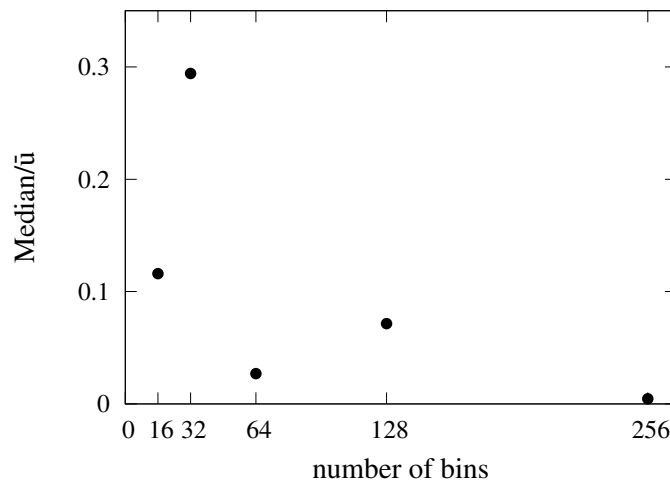


Figure 3.17: Median of the most populous velocity bin for each case plotted against the number of bins.

It is quite clear that the location of the peak of the velocity PDF is very sensitive to the bin size. In calculating the drift terms U_{p2} and U_{p3} (equations 3.19 and 3.22) we rely on the slope of the velocity PDF which of course can vary greatly at the point of maximum velocity PDF depending on the bin size. Also, in order to find the conditional statistics of du (necessary

for obtaining both drift and diffusion terms) at the most frequently occurring velocities, it is necessary to use very fine velocity bins. However increasing the number of bins is very problematic due to the very long and sparse positive tail of the velocity PDF. As the number of bins increases the bins at the edges of the domain (those corresponding to negative or large positive velocities) will contain less and less data points and the statistics of du found on these bins will be unreliable due to the low data population.

This is evident in figures 3.18 and 3.19 which show the conditional mean and variance of du for various number of bins respectively. In these figures the x axis shows the median velocity of each bin normalized by \bar{u} . The average du and variance of du are normalized by \bar{u}/t and \bar{u}^2/t respectively. The time scale t is equivalent to the time step size. As the time step size is $dt = 1s$, from here onward both in the text and in figures we will simply mention normalization by \bar{u} and \bar{u}^2 . Again as is observed in these figures, when we zoom in to the most populated velocity bins the curves differ quite a lot from each other depending on the number of bins used for getting the conditional statistics. However, as the number of bins increase the curves become more similar.

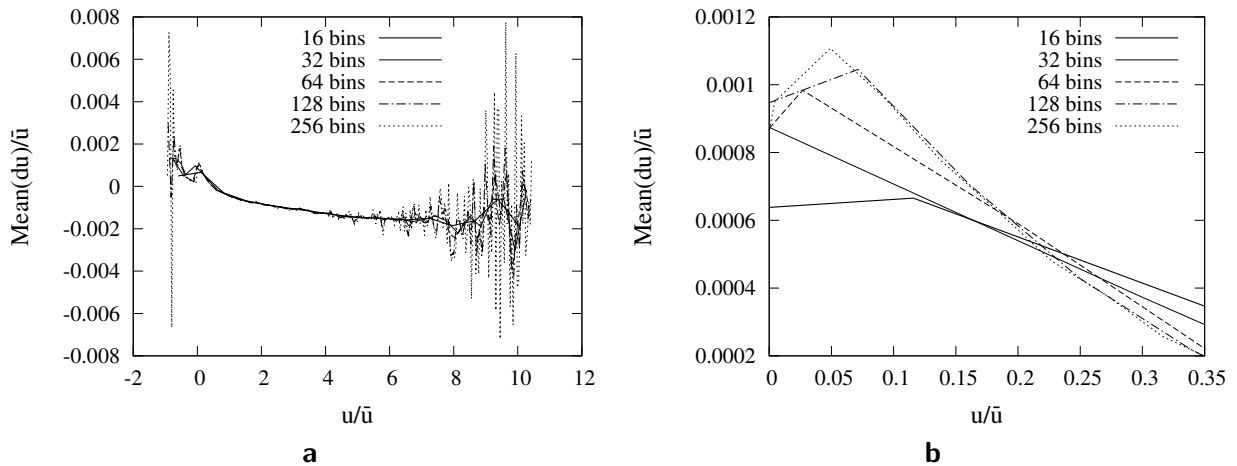


Figure 3.18: Mean du conditioned on u plotted against median of velocity bins in sphere pack. Both axes are normalized by \bar{u} . Complete velocity domain (a) zoomed in at most probable velocity bins (b).

For presenting the conditional statistics of du in the following we use 32 velocity bins, as this will provide a sufficiently accurate qualitative representation of the behaviour of du conditioned on u and we can avoid the scattering which results from using finer bins to some extent.

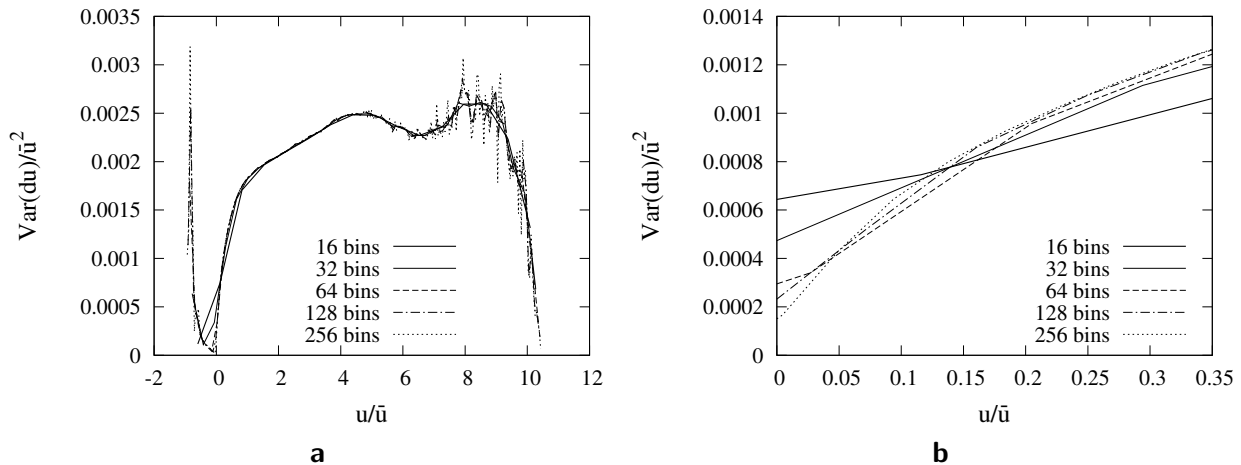


Figure 3.19: Variance of du conditioned on u plotted against median of velocity bins in sphere pack. Variance values are normalized by \bar{u}^2 while the x axis is normalized by \bar{u} . Complete velocity domain (a) zoomed in at most probable velocity bins (b).

Figure 3.20 shows the extrema of du and its components normalized by the average pore velocity, \bar{u} , plotted against different velocity ranges. The values on the x axis of this figures and the next 4 figures in this section are the median of the velocity bins normalized by the average pore velocity \bar{u} . Figure 3.21 shows the average value of the different terms and du normalized by \bar{u} as a function of velocity, while figure 3.22 displays the variance normalized by \bar{u}^2 . The skewness of du and its components plotted as a function of velocity can be seen in figure 3.23. The flatness of all terms plus du plotted against velocity can be seen in figure 3.24. These 6 figures (figures 3.20 to 3.24) are plotted from the data obtained using the velocity field and assuming a molecular diffusion coefficient of $\Gamma = 10^{-11} m/s^2$ and a time step size of $dt = 1s$. The Peclet number, in this set-up, based on a length scale of one sphere diameter is $Pe = 37.11$.

In all the above figures concerning the conditional statistics of du and its terms, the curve representing term 1 is very similar to (and often indistinguishable from) the one representing du . From figures 3.20 and 3.23 it is again evident that terms 3 and 5 are skewed and point to a drift behaviour in the velocity space as opposed to the rest of the terms which are more or less symmetric and contribute more to a diffusion behaviour in the velocity space. This reconfirms what was already observed in the statistics and PDFs of the different terms of du . A drift in the velocity space works at pushing back the velocity towards the average pore velocity, \bar{u} . This drift and diffusion behaviour point to the validity of the stochastic velocity model, as described by Meyer and Tchelepi [33].

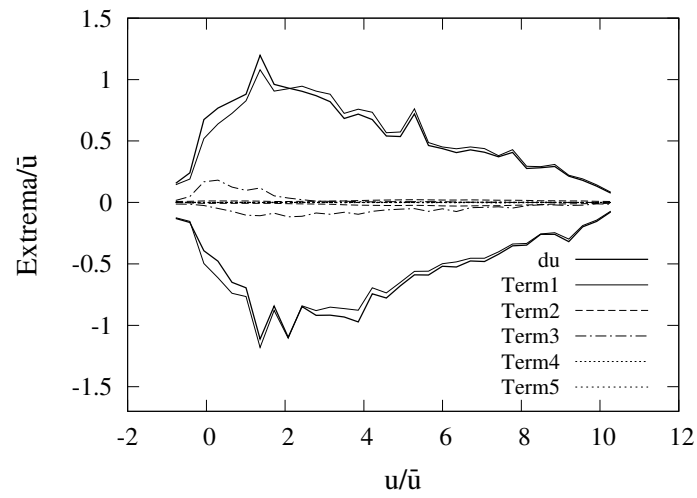


Figure 3.20: Normalized extrema of all terms and du plotted against median of velocity bins normalized by average pore velocity in a sphere pack.

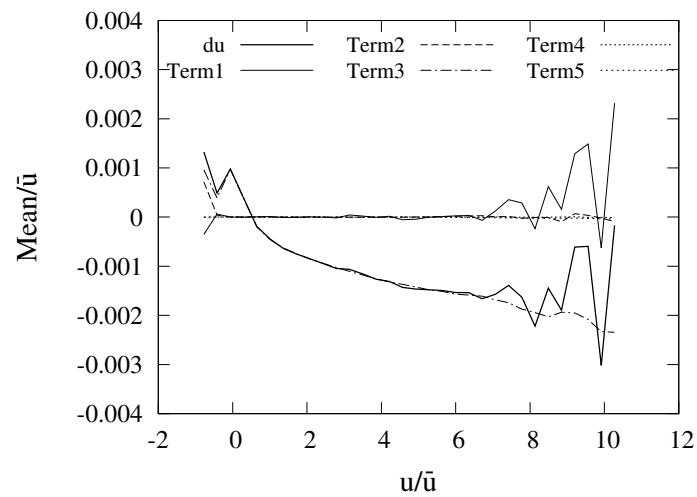


Figure 3.21: Normalized mean of all terms and du plotted against median of velocity bins normalized by average pore velocity in a sphere pack.

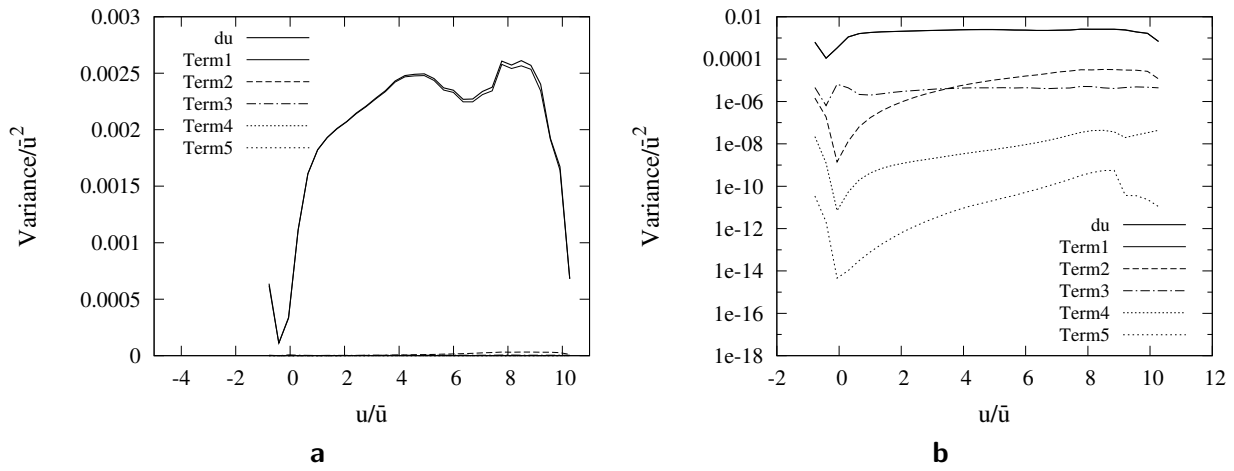


Figure 3.22: Variance of all terms and du conditioned on u plotted against median of velocity bins in a sphere pack. Variance values are normalized by \bar{u}^2 while the x axis is normalized by \bar{u} . Normal scale (a) and semi-log scale (b).

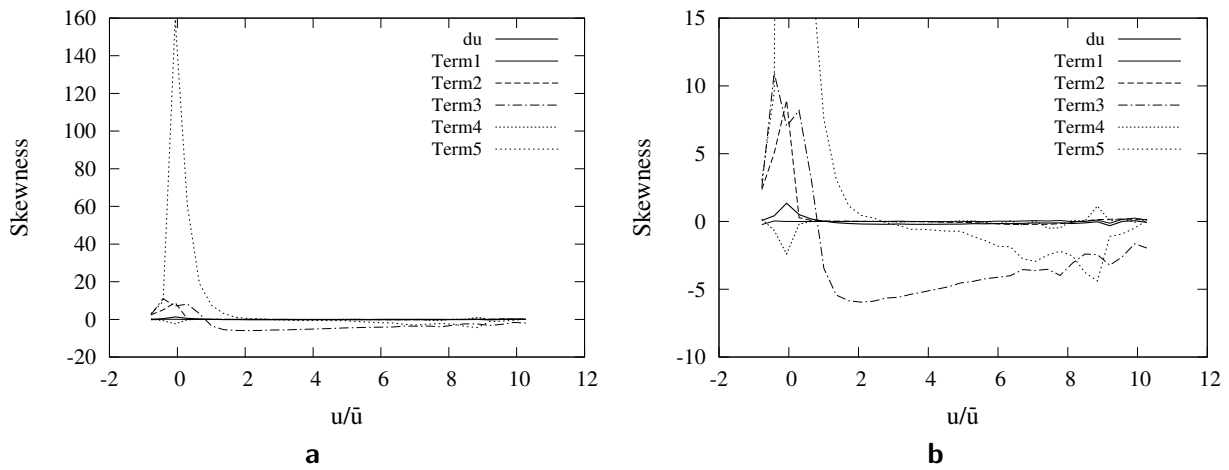


Figure 3.23: Skewness of all terms and du conditioned on u plotted against normalized median of velocity bins in a sphere pack. Complete figure (a) zoomed in at smaller skewness values (b).

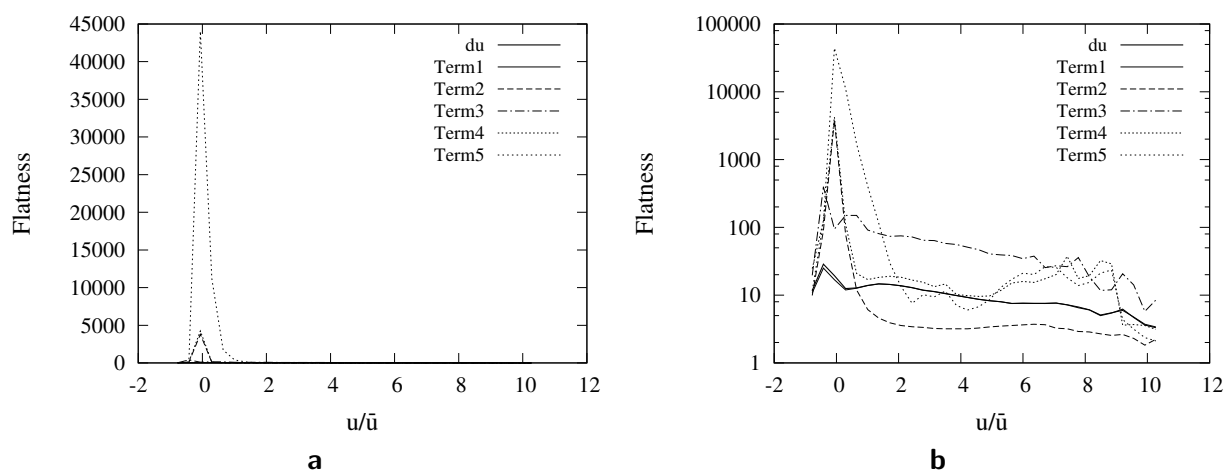


Figure 3.24: Flatness of all terms and du conditioned on u plotted against normalized median of velocity bins in a sphere pack. Normal scale (a) and semi-log scale (b).

3.3.5 Diffusion term, Γ_p , in a sphere pack

In the case of the sphere pack we are also interested in the effect of the number of bins on the diffusion term. Here again we calculated Γ_p using equation 3.12. Figure 3.25 shows Γ_p plotted over u for the random sphere pack under study. In this figure the x axis is normalized by the average pore velocity, \bar{u} , of the whole domain. Each curve represent a different number of velocity bins. At each bin the value of Γ_p is plotted against the median of the bin divided by \bar{u} . Notice how similar this figure is to figure 3.19. This is of course to be expected as Γ_p is directly related to the conditional variance of du . As the number of bins increase the population of each bin decreases and the statistics of the bins corresponding to the lower and higher end of the velocity range become less reliable due to the lower number of data points. The bins that each contain 0.1 percent or more of the total velocity points roughly lie between $-0.33\bar{u}$ and $5.83\bar{u}$. Figure 3.25b shows a zoom in at the more populated bins. This figure demonstrates that as the number of bins increase the areas of the curves corresponding to the more populous velocity bins become more similar while the other parts of the curves diverge.

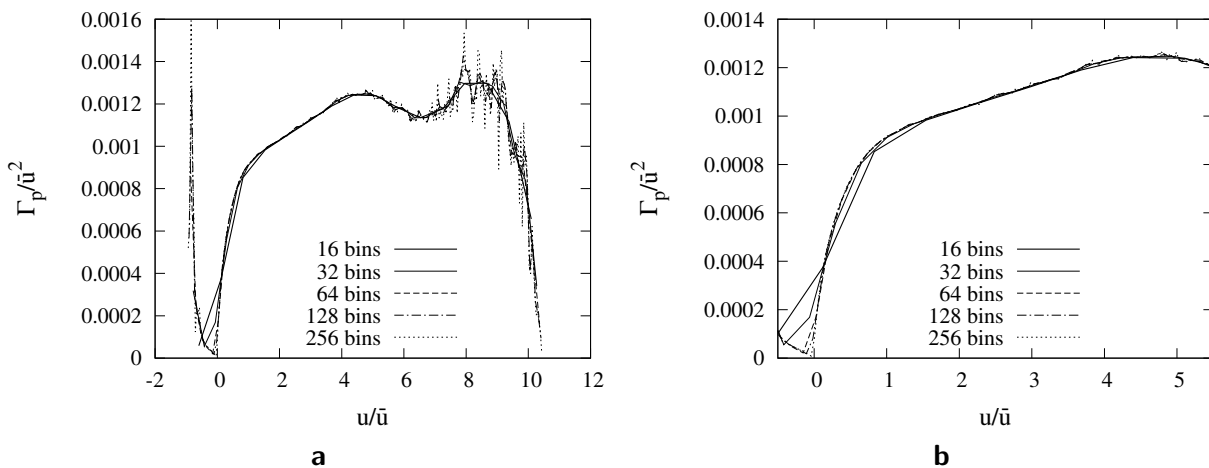


Figure 3.25: Γ_p normalized by \bar{u}^2 plotted against the median of velocity bins normalized by \bar{u} for flow in a sphere pack. Complete figure (a) and zoom in at more probable bins (b).

3.3.6 Drift term, U_p , in a sphere pack

Here again the three methods of obtaining the drift term, U_p , are presented. In the case of the sphere pack however we have only the data points corresponding to du obtained via the LT method. To find the drift term with either one of the three methods the statistics of du conditioned on u is used. The conditional statistics of du have been found using different numbers of velocity bins.

Figures 3.26 shows the drift term obtained using the first, second and third method (equations 3.15 , 3.19 and 3.22) for various numbers of bins. The bins which include 0.1 percent or more of the total data points lie between $-0.33\bar{u}$ and $5.83\bar{u}$ and the figures on the right

hand side are zoomed in to this range. Note that both axes are normalized by the average pore velocity in the domain, \bar{u} .

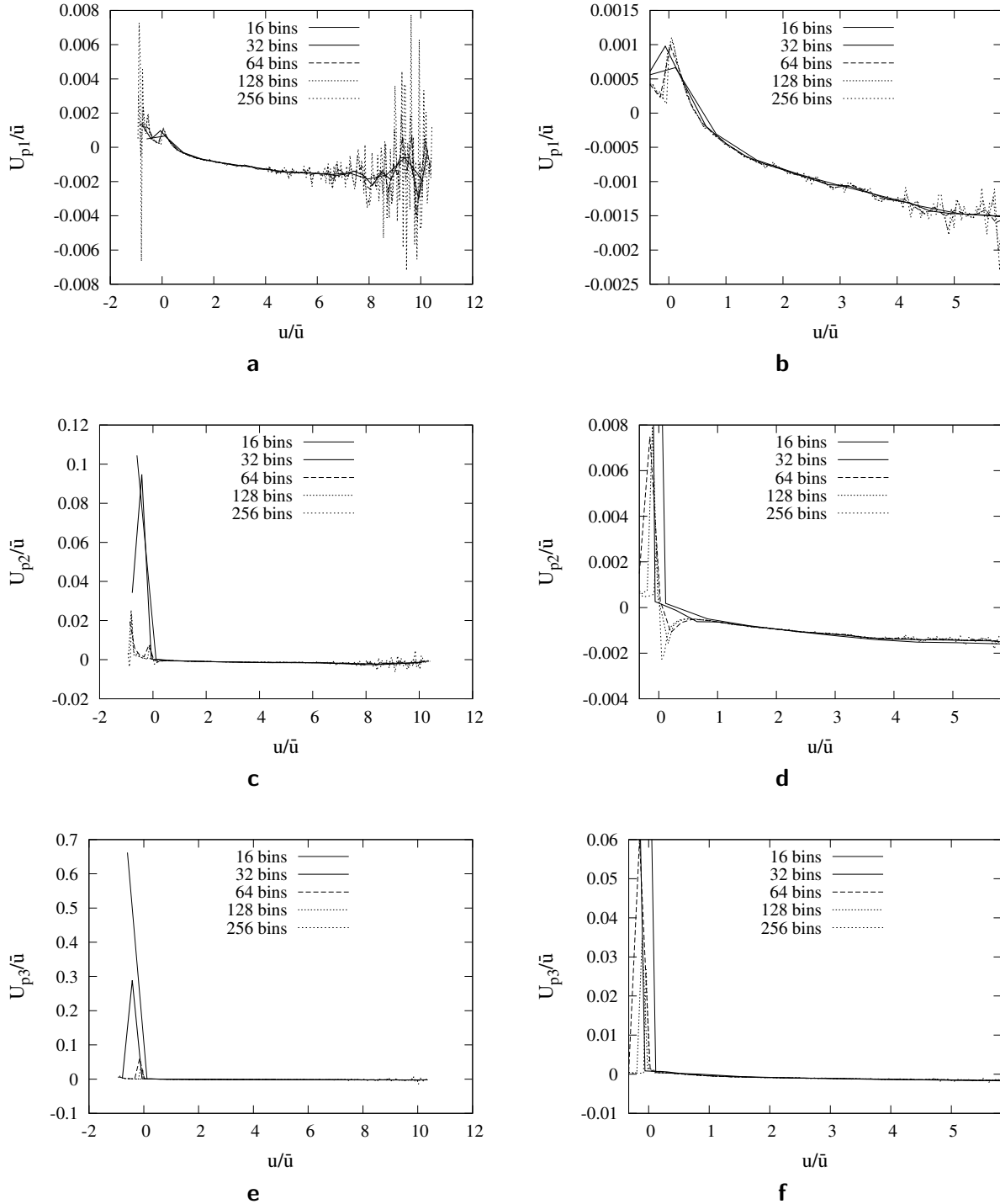


Figure 3.26: From top to bottom U_{p1} , U_{p2} and U_{p3} obtained by the LT method plotted against the median of velocity bins for flow in a sphere pack. Both axes are normalized by \bar{u} . Figures on the right hand side are zoomed in at the more populated velocity bins.

What instantly catches the eye in the graphs of figure 3.26 is that using 16 or 32 bins cannot give an accurate description of the behaviour of the drift term, U_p , over different velocity ranges. However, as the number of bins increases, the curves become somewhat more similar. We were not however, able to increase the number of bins enough to obtain a convergence due to the fact that small bins especially at the areas near the extrema of the velocity space will not be sufficiently populated to yield acceptable conditional statistics as our velocity data base does not contain many points in these areas.

Another point of interest is the considerable differences between the different methods of obtaining U_p . It is of course expected that the first method for finding U_p (equation 3.15) cannot be accurate. This is due to the fact that the conditional statistics of du which are used to find the drift term cannot account for the bounce back at sphere surfaces and that the first method offers no remedy for this problem as was seen in the case of the channel flow. The second and third methods of obtaining the drift term, U_p , yield slightly more similar results as both these methods aim at overcoming the bounce back issue by enforcing the velocity PDF. The differences seen between these two methods are not necessarily critical since the drift terms obtained by them will eventually be used in different stochastic processes for velocity. In the case of U_{p2} the stochastic process described via equation 3.20 will be used which contains a correction term. In the case of U_{p3} however, no correction term is necessary. Using this argument one would expect U_{p1} and U_{p3} to be actually more similar since in the case of U_{p1} no correction term will be used either. This however is not true when the du field is obtained via the LT method due to the inability of U_{p1} to account for the bounce back issue. The similarity between U_{p1} and U_{p3} was shown for the channel flow when the particle method (which accounts for bounce back at the walls) was used for obtaining the du field.

As it appears that using 16 or 32 bins is far too coarse and that U_{p1} will potentially yield poor dispersion results we will now focus exclusively on U_{p2} and U_{p3} obtained using 64, 128 and 256 velocity bins. Figure 3.27 shows U_{p2} normalized by \bar{u} plotted against the median of velocity bins normalized by \bar{u} .

Figure 3.27a shows the complete curves. It is quite evident that with an increase in the number of bins the drift curves becomes more and more jagged. Figure 3.27b zooms in at the velocity bins that each approximately contain at least 0.1 percent of the velocity points. The differences between the curves obtained via different number of velocity bins is less pronounced in the velocity range where the bins are more populated. However, even here major differences can be seen in the bins corresponding to lower velocities which are in fact the most probable velocities and correspond to the peak of the velocity PDF. Figure 3.27c zooms in at the lower end of the velocity spectrum. Here it is evident that qualitatively the three curves behave in a similar manner. The peaks and valleys of the curves however, are shifted with respect to each other. It must be noted that the drift terms corresponding to the lowest velocities (below $-0.33\bar{u}$) cannot be relied upon since the velocity bins that correspond to them are severely underpopulated. The main point of interest here for each curve is its most populated bin and the few adjacent bins to that on either side. The most populated bin as was mentioned before is dependent on the number of bins (See section 3.3.4 and figure 3.17). When 64, 128 or 256 bins are used the median of the most populated bin lies at $0.027\bar{u}$, $0.071\bar{u}$ and $0.004\bar{u}$ respectively. Figure 3.27d zooms in at the upper end of the velocity spectrum. Here due to a lack of sufficient data points in the velocity bins the

drift curves become very jagged. Of course the higher the number of the velocity bins the less populated the bins at the end are. The overall average behaviour of the curves however are quite similar.

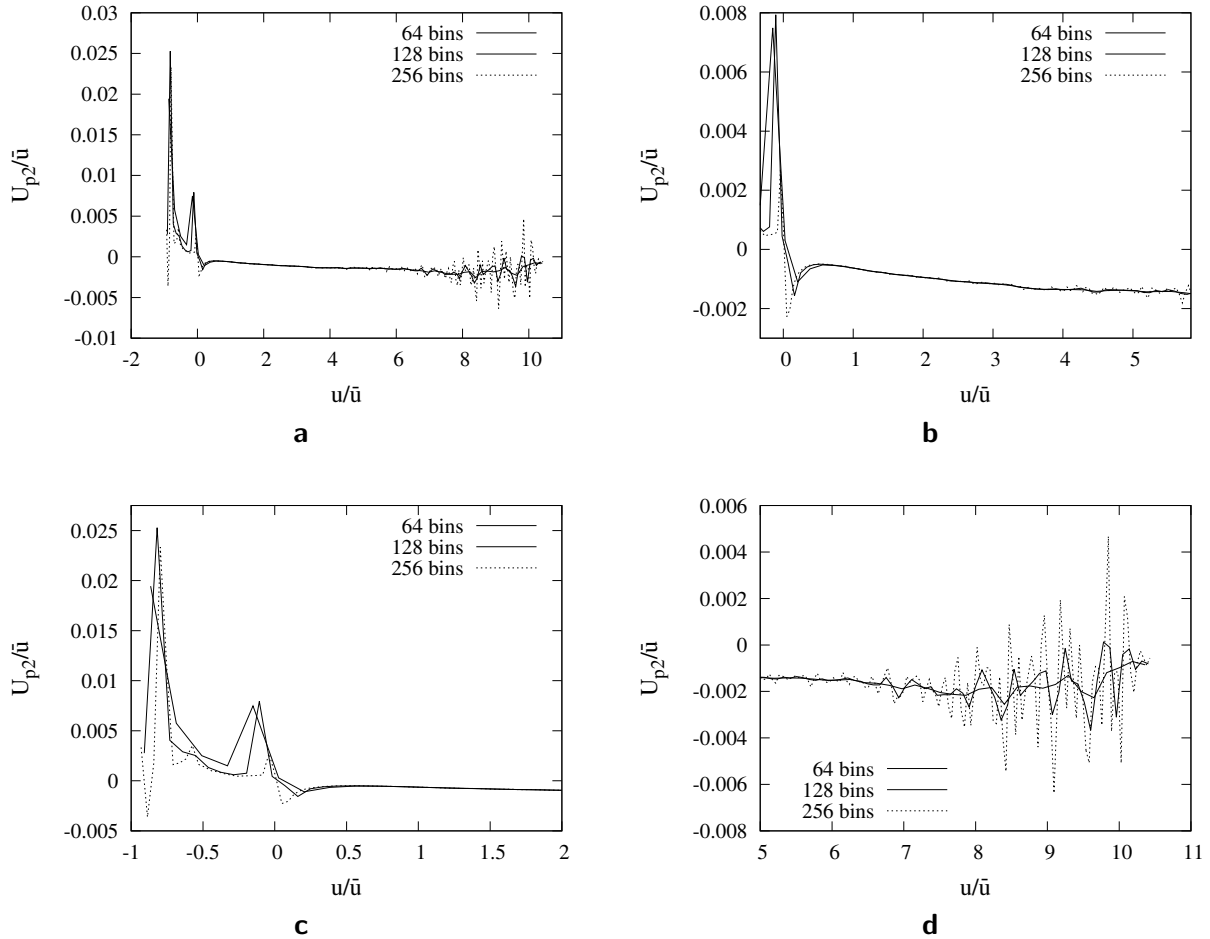


Figure 3.27: U_{p2} obtained by the LT method plotted against the median of velocity bins for flow in a sphere pack. Both axes are normalized by \bar{u} . Complete figure (a), zoomed in at more probable velocities (b), zoomed in at smaller velocities (c) and zoomed in at larger velocities (d).

Figure 3.28 shows the same for U_{p3} . All that was said of the effect of number of bin sizes on the drift for U_{p2} applies to U_{p3} also, even though the shape of U_{p3} curves are significantly different from those of U_{p2} . This difference will however be accounted for in the stochastic velocity process by adding a correction term in the case where U_{p2} is applied. U_{p3} is affected by the velocity PDF. When less bins are used for obtaining the velocity PDF, the peak of the PDF at small velocities is underestimated and instead the velocities closer to the mean pore velocity will become slightly more probable. It is to be expected that the drift term which pushes the velocities toward the mean velocity will have a higher peak when less bins are used.

We will now take a deeper look at the differences of the various methods of determining

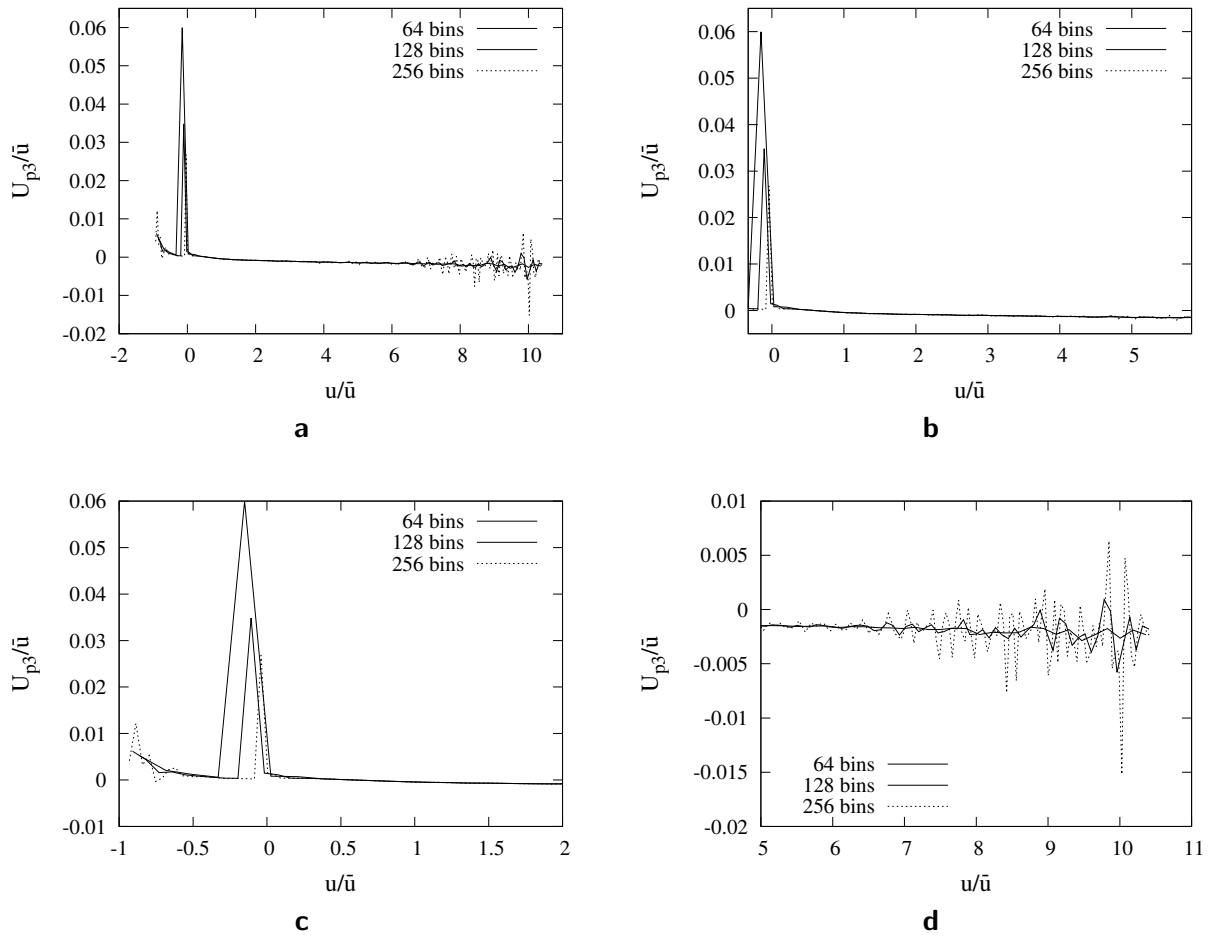


Figure 3.28: U_{p3} obtained by the LT method plotted against the median of velocity bins for flow in a sphere pack. Both axes are normalized by \bar{u} . Complete figure (a), zoomed in at more probable velocities (b), zoomed in at smaller velocities (c) and zoomed in at larger velocities (d).

the drift term, U_p . Figure 3.29 shows the drift term obtained via the statistics of du (from the LT method) and using 128 velocity bins plotted against the median of the velocity bins. Both axes are normalized by \bar{u} . The three curves correspond to the three different methods of finding U_p . Here again it is clear that the three methods result in significantly different drift terms especially at the lower and most probable velocity bins. U_{p2} and U_{p3} look qualitatively comparable while U_{p1} is completely different from them both as it does not consider the boundary conditions. The differences between U_{p2} and U_{p3} in the vicinity of zero velocity can be due to the different interpretation of the diffusive flux considered for deriving these drift terms. This is comparable to what was observed in the channel at very small velocities.

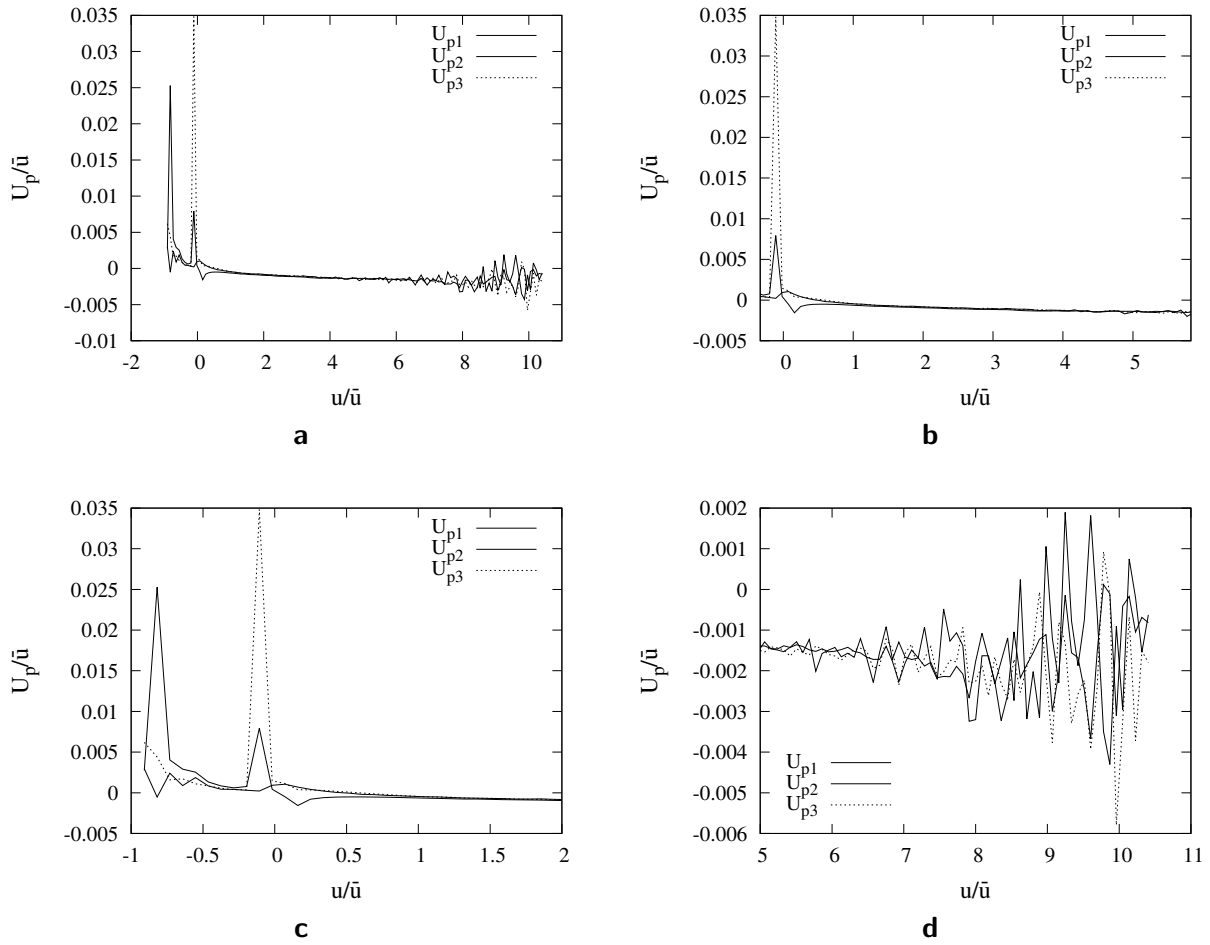


Figure 3.29: U_p plotted against the median of velocity bins for flow in a sphere pack. Both axes are normalized by \bar{u} . Complete figure (a), zoomed in at more probable velocities (b), zoomed in at smaller velocities (c) and zoomed in at larger velocities (d).

3.4 Tracer transport in a channel

In this section we present the results of our transport model for various configurations of U_p and Γ_P in the channel flow introduced in section 3.2. The transport model was run using the U_p and Γ_p values explained in the previous section. The statistics of the transport model for each method of obtaining du (LT or particle method) and for each of the three methods of obtaining U_p are compared to our benchmark solution of tracer transport in the channel.

The benchmark solution of tracer transport in the channel is obtained by releasing 4000001 particles uniformly in a cross section perpendicular to the streamwise direction and at position $x = 0$. Each particles is then allowed to both diffuse with a Brownian motion ($\Gamma = 1 \times 10^{-11} m^2/s$) and to move with its velocity with time steps of size $dt = 1s$. Then according to the new vertical location, y , of the particles their new velocity is cal-

culated (equation 3.24) and the process is repeated in order to get a time evolution of the spreading of the particles. At the boundaries a simple bounce back condition is imposed.

The same procedure is carried out for the tracer transport using our model. The only difference is that at each time step the new velocity of each particle is calculated, not according to the particle's position, but instead using the stochastic velocity process (equation 3.8 or in the case where U_{p2} is used equation 3.20). In this model regardless of how the parameters of the model were found, the geometry of the channel is not explicitly accounted for (we do not even consider the vertical locations of the particles) meaning that we do not have any bounce back of the particles at the walls of the channel. Our model is based on the velocity rather than on position. If at any step the velocity of a particle goes beyond the velocity bounds it is simply put back at the velocity boundary.

3.4.1 Characteristics of the tracer cloud

We will start this subsection by presenting the results obtained using the drift term, U_{p1} . Figure 3.30 shows the mean location, x , of particles in the channel plotted against time in the case where U_{p1} is used. For the first curve in this figure, U_{p1} is obtained using the statistics of du from the LT method. The second curve corresponds to the statistics of du from the particle method and the third curve demonstrates the benchmark solution for transport of particles.

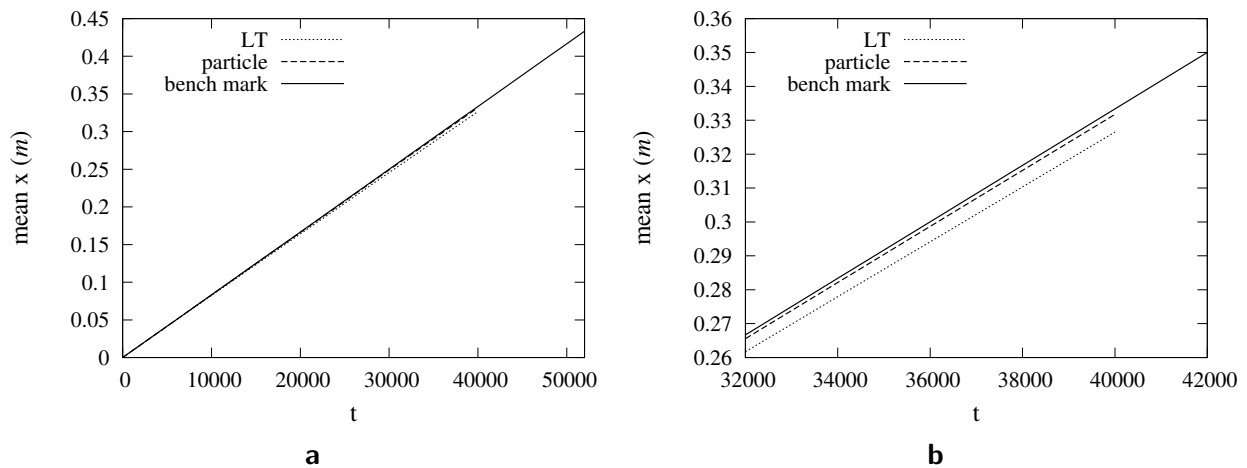


Figure 3.30: Mean position (x) of particles plotted against time for flow in a channel. Model uses U_{p1} from both the LT method and the particle method. Results of the benchmark solution are included for comparison. Complete figure (a) and zoomed in at later times (b).

When the drift term, U_p , for each velocity range is found by taking the average du in that velocity range it is clear that if the du is obtained using the LT method the average du of the smallest velocity range corresponding to the channel walls will be much smaller than expected as the LT method uses no bounce back at the wall. It is therefore not surprising

that the heart of the cloud of particles moves slower when the du is taken from the LT method than when it is calculated using the particle method. Figure 3.30 however shows that even when du is calculated using the particle method using U_{p1} does not yield an exact velocity for the tracer cloud. This slight inaccuracy, which is most probably due to the limited number of bins used for calculation of the conditional statistics of du , is magnified for the higher statistical moments of the particle positions. This can be observed by looking at figures 3.31 and 3.32. These figures show the standard deviation of the location of tracer particles (which represents the width of the cloud) and the skewness of the cloud of particles respectively at various times.

In the case of the standard deviation it surprisingly appears that U_{p1} obtained via the LT method yields better results than U_{p1} from the particle method. Concerning the skewness values, neither the LT method nor the particle method seem to have any particular advantage over each other when U_{p1} is taken as the drift term in the velocity process.

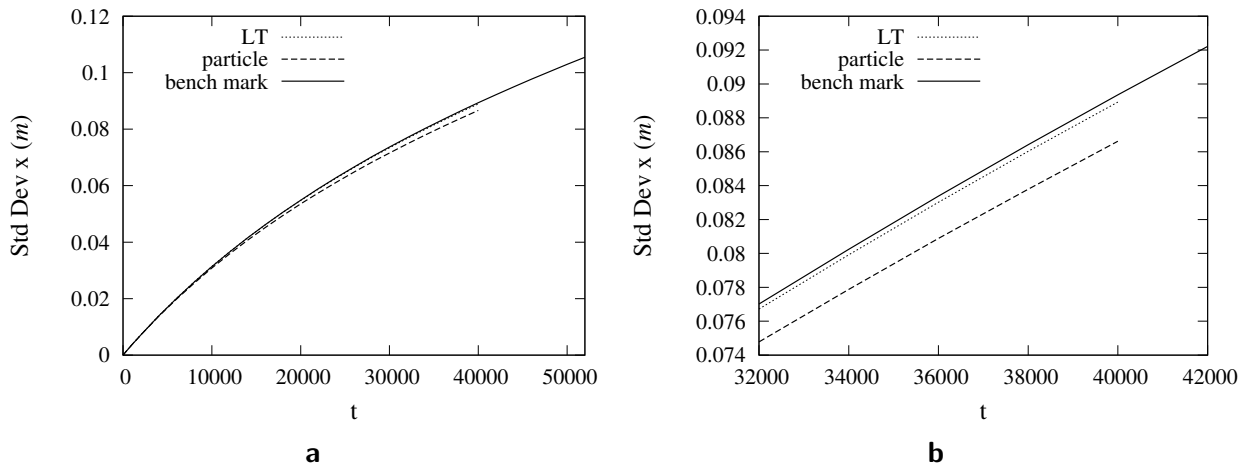


Figure 3.31: Standard deviation of location (x) of particles plotted against time for flow in a channel. Model uses U_{p1} from both the LT method and the particle method. Results of the benchmark solution are included for comparison. Complete figure (a) and zoomed in at later times (b).

We now turn to the results obtained using the drift term, U_{p2} . Figure 3.33 shows the mean location, x , of particles in the channel plotted against time in the case where U_{p2} is taken as the drift term in the model. It is clear that using U_{p2} both the LT method of obtaining du and the particle method overestimate the velocity with which the cloud moves forward. As explained before U_{p2} , which is obtained using equation 3.19, is positive for all ranges of u in the channel. However, a correction term is added to equation 3.8 which counteracts the constant positive drift in the velocity field to some extent. From figure 3.5 it is evident that the correction term, seen in equation 3.20, is negative in the channel flow. As can be seen in figure 3.33, the mean location of tracer particles obtained via U_{p2} from the LT method is practically identical to that from the particle method.

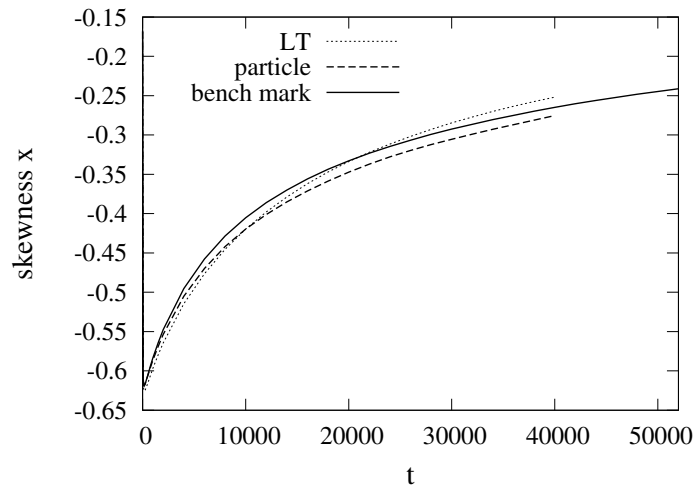


Figure 3.32: Skewness of location (x) of particles plotted against time for flow in a channel. Model uses U_{p1} from both the LT method and the particle method. Results of the benchmark solution are included for comparison.

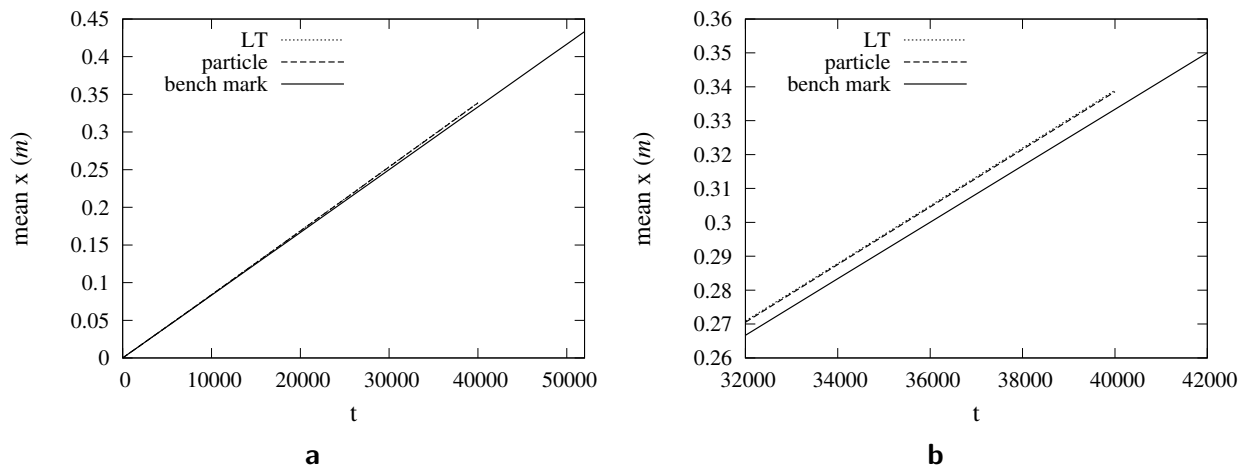


Figure 3.33: Mean location (x) of particles plotted against time for flow in a channel. Model uses U_{p2} from both the LT method and the particle method. Results of the benchmark solution are included for comparison. Complete figure (a) and zoomed in at later times (b).

Figures 3.34 and 3.35 demonstrate the standard deviation of the location of tracer particles and their skewness respectively at various times. The drift term U_{p2} from both the LT method and the particle method of obtaining du , equally overestimate the standard deviation of particle positions. The skewness is also comparable for the two methods although the particle method of obtaining the du field yields a U_{p2} which can predict the skewness values slightly more accurately. However the skewness is visibly underestimated regardless of how the du field is obtained when U_{p2} is used.

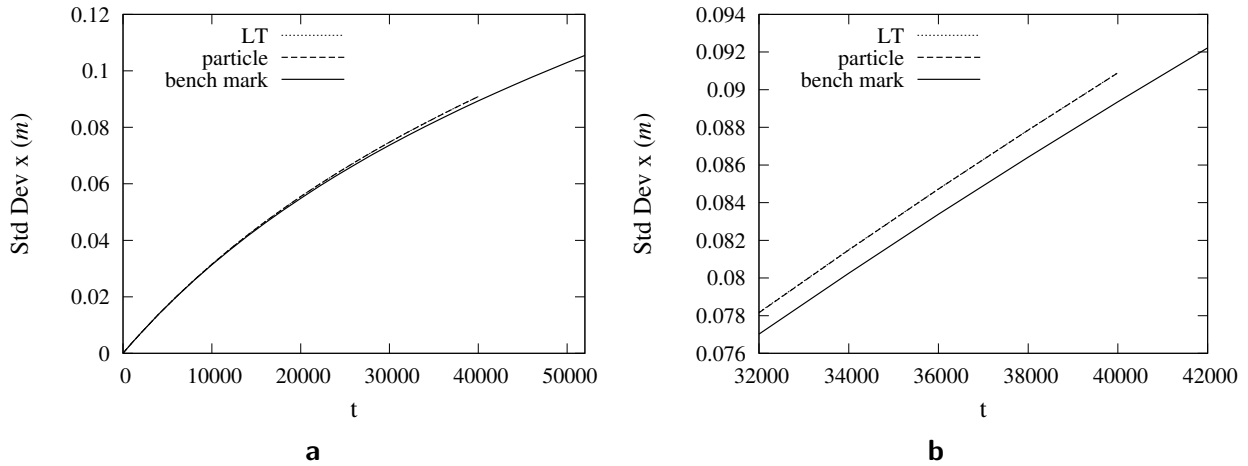


Figure 3.34: Standard deviation of location (x) of particles plotted against time for flow in a channel. Model uses U_{p2} from both the LT method and the particle method. Results of the benchmark solution are included for comparison. Complete figure (a) and zoomed in at later times (b).

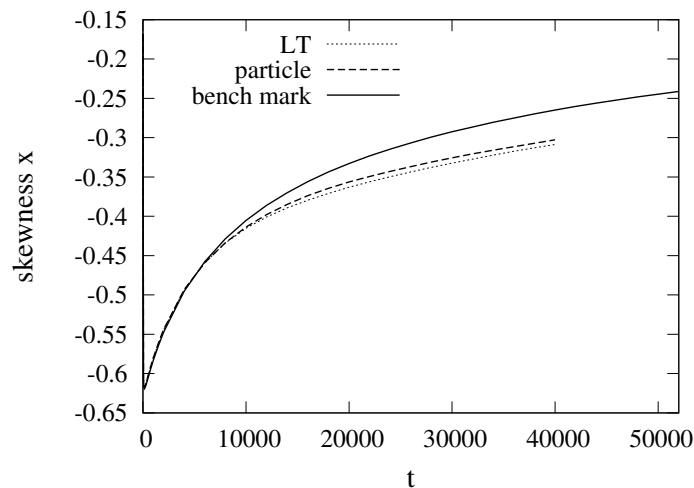


Figure 3.35: Skewness of location (x) of particles plotted against time for flow in a channel. Model uses U_{p2} from both the LT method and the particle method. Results of the benchmark solution are included for comparison.

One can conclude that the first two methods of determining the drift in velocity can to some extent and up to a certain time predict the evolution of tracer in the channel. The results are however not accurate. Neither U_{p1} nor U_{p2} appears to have an advantage over the other. Also neither the LT method of finding du nor the particle method appear to have any clear cut advantage over the other. One can postulate that 4000001 particles cannot yield a large enough data base to predict the behaviour of a cloud of particles or more conceivably that using only 50 bins for the velocity is not sufficient for finding accurate statistics of du conditioned on u . This coarseness in dealing with the statistics is however necessary as our main goal is to predict the evolution of tracers and the dispersion phenomenon in a random sphere pack in the case of which we are limited in the number of data points in the velocity field and consequently in the number of velocity bins that can be used. In studying the dispersion in a channel we would like to determine the best method in the case where data points are limited.

The third method of finding the drift term for the evolution of velocities yields considerably better results. Here we have also run the model for longer times to make sure that the better results persist over time. Please note that the advective time scale considering a length scale equal to the width of the channel $L = 2h = 2mm$ and the mean velocity of $\langle u \rangle = 8.333 \times 10^{-6} m/s$ is $t_{adv} = 240s$. Figure 3.36 shows the mean location, x , of particles in the channel plotted against time in the case where U_{p3} is used. It is clear that by using U_{p3} , which is obtained using equation 3.22, both the LT method of obtaining du and the particle method predict the velocity with which the cloud moves forward exceptionally well. In this case as in the case of using U_{p1} no correction term is used in the stochastic equation for du (equation 3.8).

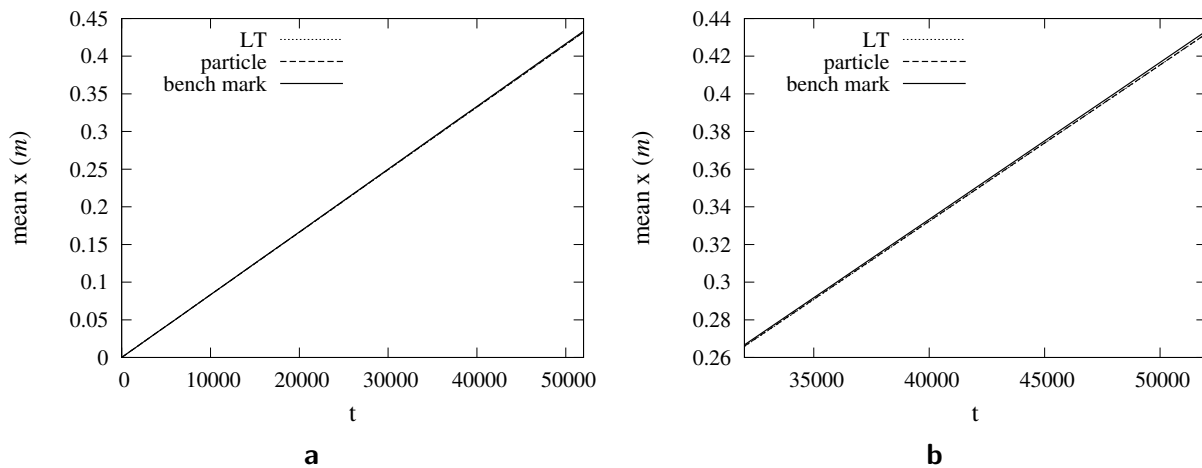


Figure 3.36: Mean location (x) of particles plotted against time for flow in a channel. Model uses U_{p3} from both the LT method and the particle method. Results of the benchmark solution are included for comparison. Complete figure (a) and zoomed in at later times (b).

Also notice how well the standard deviation and the skewness of the location of particles from the model matches that of the benchmark solution as evident in figures 3.37 and 3.38.

Both the LT method of obtaining the du field and the particle method yield drift terms, U_{p3} , which can produce practically the same mean, standard deviation and skewness values of the particle positions.

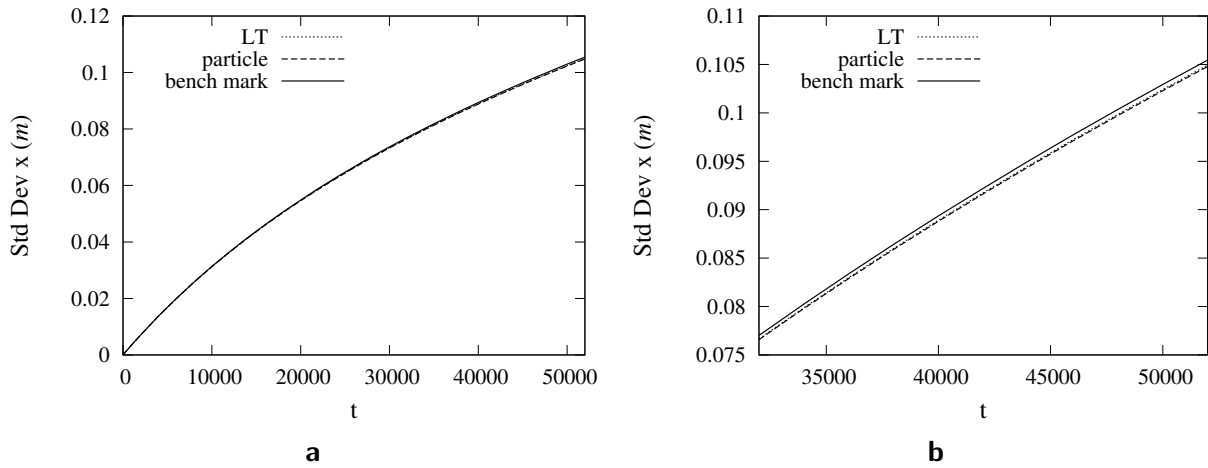


Figure 3.37: Standard deviation of location (x) of particles plotted against time for flow in a channel. Model uses U_{p3} from both the LT method and the particle method. Results of the benchmark solution are included for comparison. Complete figure (a) and zoomed in at later times (b).

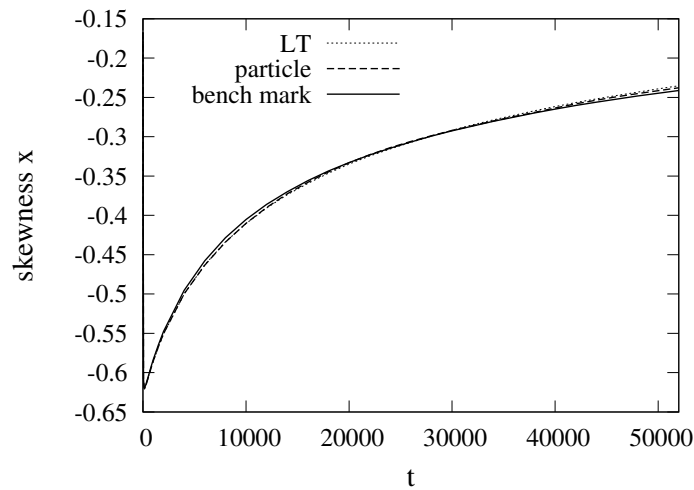


Figure 3.38: Skewness of location (x) of particles plotted against time for flow in a channel. Model uses U_{p3} from both the LT method and the particle method. Results of the benchmark solution are included for comparison.

To better compare the results obtained via different drift terms we present the following. Figures 3.39 and 3.40 show the mean of particle positions obtained via the model using the three different drift terms in the case where du is obtained from the LT method and

particle method respectively. Concerning the average particle positions, it is evident that U_{p3} both from the particle method and from the LT method produces the best results. U_{p2} from both the LT and the particle method yields equally inaccurate results. U_{p1} from the particle method however gives considerably better average position values than U_{p1} from the LT method.

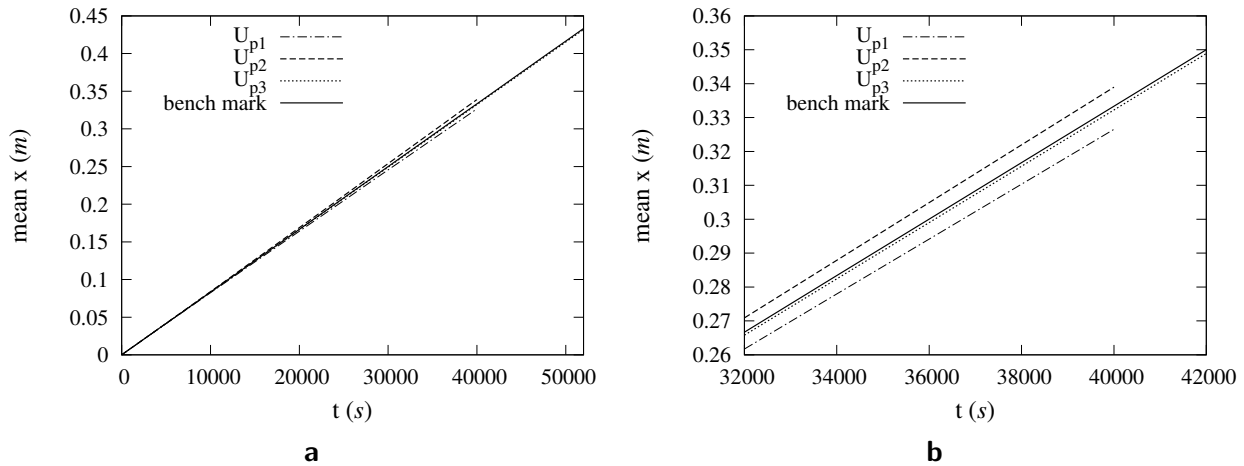


Figure 3.39: Mean location (x) of particles plotted against time for flow in a channel. U_p and Γ_p are extracted from the statistics of du obtained from the LT method. Results of the benchmark solution are included for comparison. Complete figure (a) and zoomed in at later times (b).

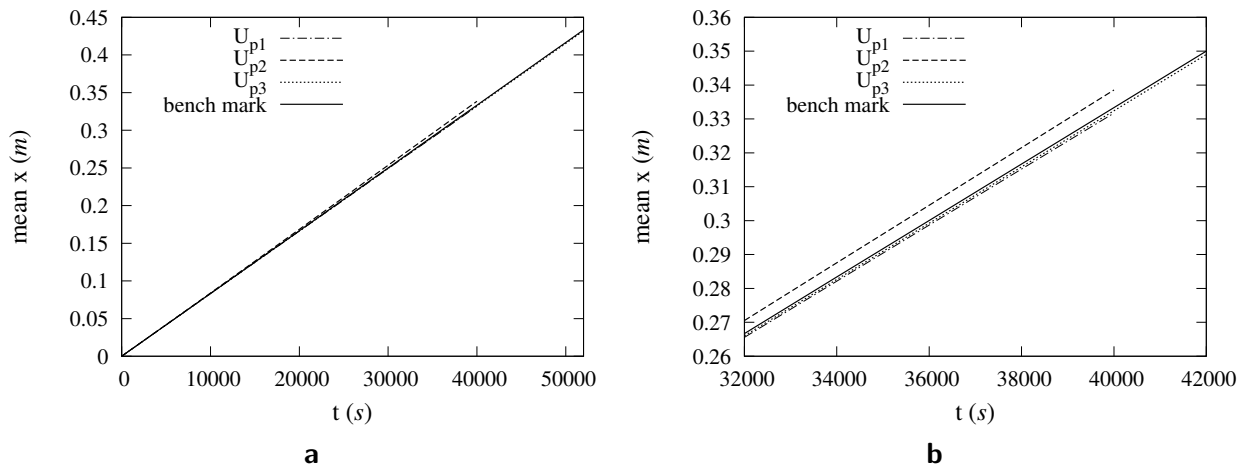


Figure 3.40: Mean location (x) of particles plotted against time for flow in a channel. U_p and Γ_p are extracted from the statistics of du obtained from the particle method. Results of the benchmark solution are included for comparison. Complete figure (a) and zoomed in at later times (b).

Figures 3.41 and 3.42 show the standard deviation of particle positions obtained via the

model using the three different drift terms in the case where du is obtained from the LT method and particle method respectively. Again in general U_{p3} appears to produce the most accurate standard deviation values. Results obtained using U_{p2} are not very good both for U_{p2} from the particle method and from the LT method. Surprisingly U_{p1} from the LT method produces accurate results comparable to that from U_{p3} while U_{p1} from the particle method does not produce acceptable standard deviation values.

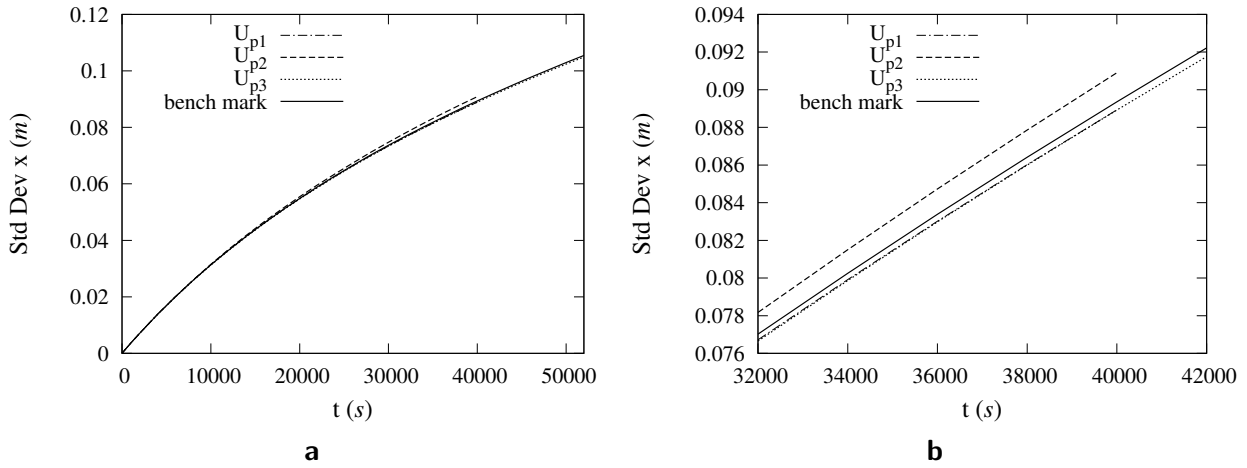


Figure 3.41: Standard deviation of location (x) of particles plotted against time for flow in a channel. U_p and Γ_p are extracted from the statistics of du obtained from the LT method. Results of the benchmark solution are included for comparison. Complete figure (a) and zoomed in at later times (b).

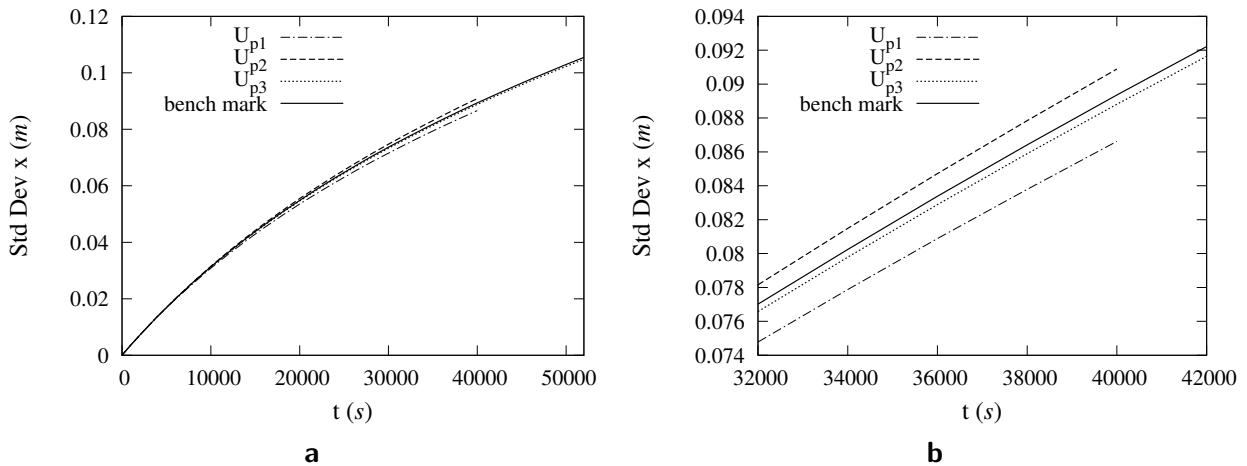


Figure 3.42: Standard deviation of location (x) of particles plotted against time for flow in a channel. U_p and Γ_p are extracted from the statistics of du obtained from the particle method. Results of the benchmark solution are included for comparison. Complete figure (a) and zoomed in at later times (b).

Figures 3.43 and 3.44 show the skewness of particle positions obtained via the model using the three different drift terms in the case where du is obtained from the LT method and particle method respectively. Again both for the LT method and the particle method of obtaining the du field, U_{p2} performs poorly while the results when U_{p3} is taken as the drift term matches those of the benchmark solution very closely.

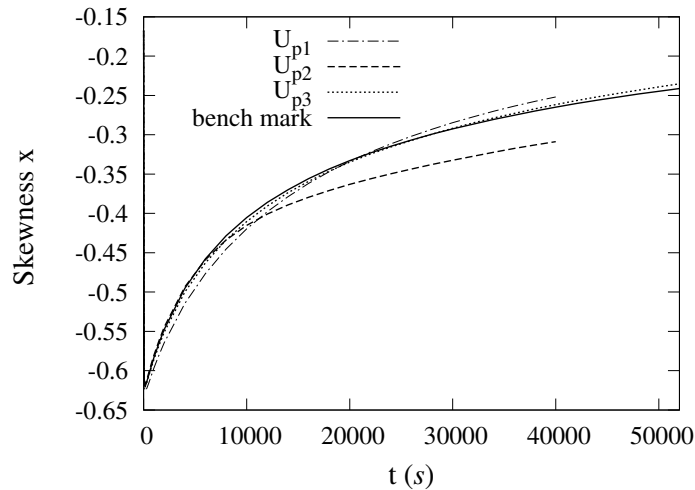


Figure 3.43: Skewness of location (x) of particles plotted against time for flow in a channel. U_p and Γ_p are extracted from the statistics of du obtained from the LT method. Results of the benchmark solution are included for comparison.

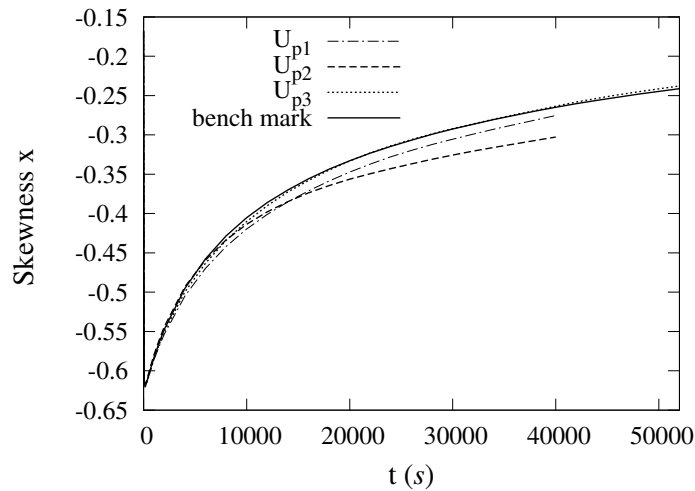


Figure 3.44: Skewness of location (x) of particles plotted against time for flow in a channel. U_p and Γ_p are extracted from the statistics of du obtained from the particle method. Results of the benchmark solution are included for comparison.

In summary regardless of whether the particle or the LT method is used for obtaining the du field, the drift term U_{p3} yields very accurate statistical results in the case of the channel

flow. U_{p1} however, which is equivalent to the drift term used by Meyer and Tchelepi ([33]) produces inaccurate statistics both when it is obtained from the LT method (in terms of mean particle positions) and when obtained from the particle method (in terms of standard deviation of particle positions).

3.4.2 Velocity PDFs

In order to have a better overview of the quality of each method of determining the parameters in our stochastic model for velocity we also examine the velocity PDF at various time steps when the tracer is transported via our model and compare it with the velocity PDF of the benchmark solution. Figure 3.45 shows the streamwise velocity PDF at very early time ($t = 1s$). Figure 3.45a shows the PDF resulting from velocity drift and diffusion terms obtained from the LT method while figure 3.45b shows those obtained by the particle method.

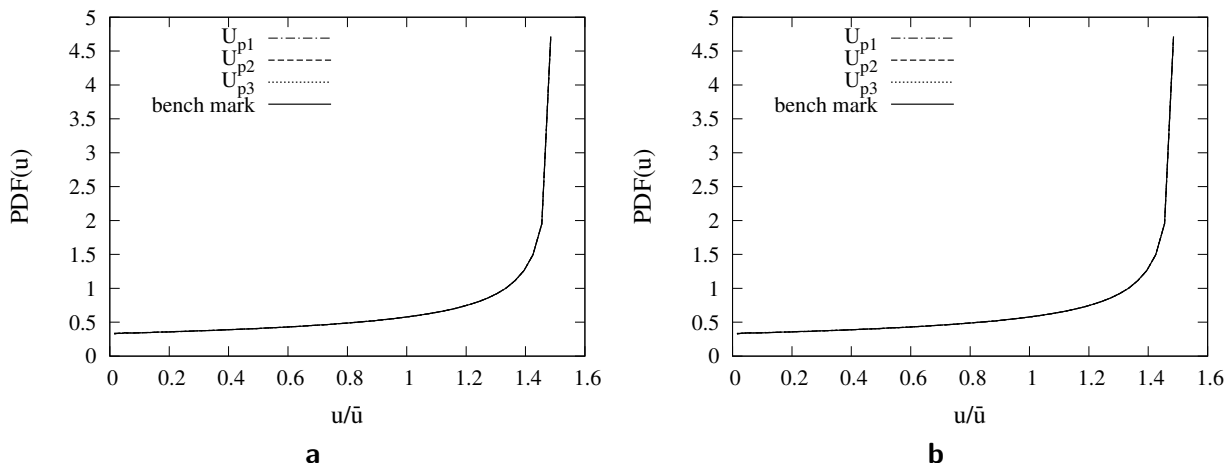


Figure 3.45: Velocity PDF for flow in a channel at time $t = 1s$ for different methods of obtaining U_p . Results of the benchmark solution are included for comparison. U_p and Γ_p obtained by the LT method (a) and particle method (b).

It is clear that at very early times all the PDF curves lie on each other since the particles almost exactly have the same velocity as their initial state. However, as time passes particles will acquire new velocities depending on the way they evolve which is in turn dependent on the transport model. The benchmark PDF of course does not change over time. The difference seen between the benchmark PDF in figures 3.45 and figure 3.2a is due to the fact that to get the velocity PDF in figure 3.2, we used 360 bins while here only 50 bins are used. This is because the drift and diffusion terms in our model are based on the statistics of du conditioned on 50 velocity bins and therefore can at best mimic the PDF obtained using 50 bins.

Figure 3.46 shows the streamwise velocity PDF at a later time, $t = 10000s$, for both the LT and the particle methods. With the average velocity in the channel ($\bar{u} = 8.333 \times 10^{-6} m/s$), the tracer cloud can be displaced a length of more than 40 times the width of the chan-

nel ($2h = 2mm$). Notice that at this time the PDF curves found using different versions of the model differ slightly from each other and from that of the benchmark solution.

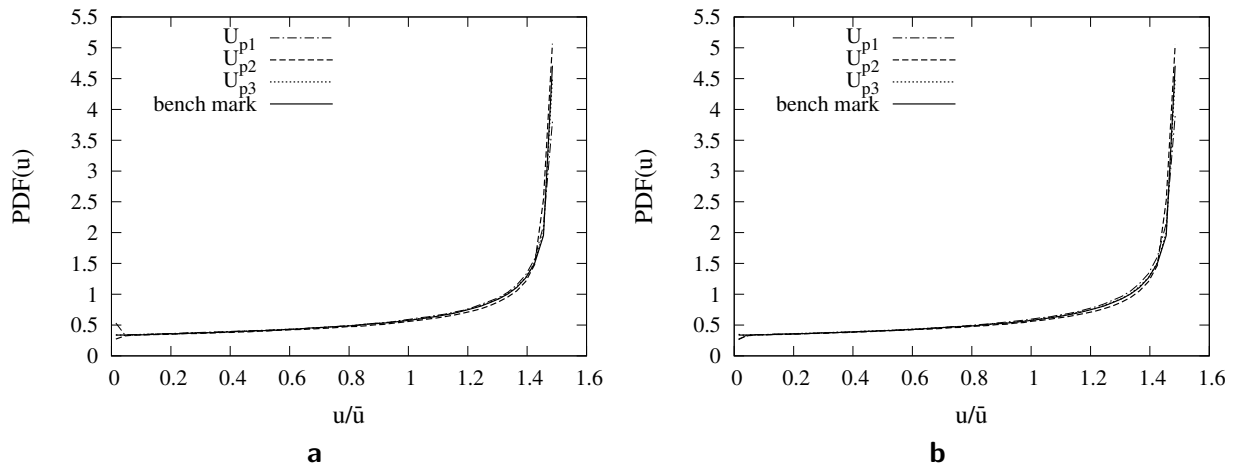


Figure 3.46: Velocity PDF for flow in a channel at time $t = 10000s$ for different methods of obtaining U_p . Results of the benchmark solution are included for comparison. U_p and Γ_p obtained by the LT method (a) and particle method (b).

In order to better see the differences we zoom in at smaller velocities as shown in figure 3.47 and at larger velocities as shown in figure 3.48.

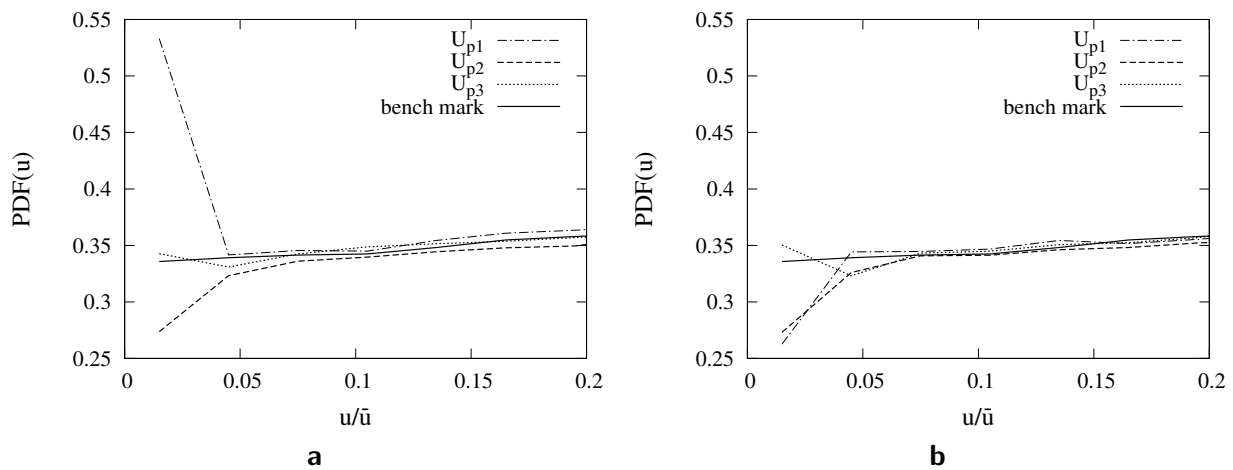


Figure 3.47: Velocity PDF for flow in a channel at time $t = 10000s$ for different methods of obtaining U_p zoomed in at smaller velocities. Results of the benchmark solution are included for comparison. U_p and Γ_p obtained by the LT method (a) and particle method (b).

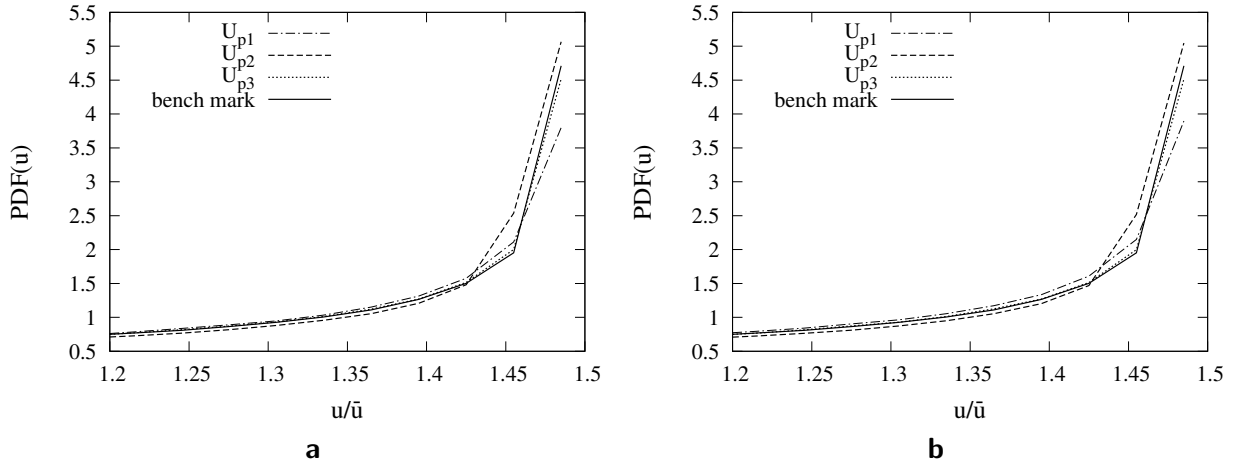


Figure 3.48: Velocity PDF for flow in a channel at time $t = 10000s$ for different methods of obtaining U_p zoomed in at larger velocities. Results of the benchmark solution are included for comparison. U_p and Γ_p obtained by the LT method (a) and particle method (b).

It is evident that except for the case where U_{p1} (which does not enforce the velocity PDF) is used and even then only for the smaller velocities that occur near the walls of the channel, using the LT or the particle method for obtaining the statistics of du makes no significant difference in the quality of the velocity PDFs obtained. In conclusion these figures show that the PDFs obtained from the model match that of the benchmark solution very well even at later times. Also it can be seen in figure 3.48 regardless of whether the LT method is used for finding the du field or the particle method, the peak of the velocity PDF which occurs at the highest velocities is underestimated by U_{p1} and therefore it is to be expected that the centre of mass of the tracer cloud should move more slowly when the model is used with U_{p1} than what the benchmark results show (see figures 3.39 and 3.40). Similarly U_{p2} overestimates the percentage of the largest velocities as can again be seen in figure 3.48 and therefore it is clear that the mean location of particles when U_{p2} is used will move faster than it would with the benchmark results (see again figures 3.39 and 3.40).

3.4.3 Tracer cloud

We will now present the actual shape of the tracer cloud in the channel over time. To do so we calculate the probability density of the particle locations (x) at different times. The range of x is between $x = 0$ and $x = 1m$ and is divided into 4000 bins. The percentage of particles residing in each bin is calculated and from that the PDF is obtained. This PDF represents the shape of the tracer cloud. Figure 3.49 shows the evolution of the tracer cloud from the benchmark solution over time. It is clear that as time passes the cloud both spreads and moves forward in the streamwise direction. Also, the shape of the cloud smooths out with time.

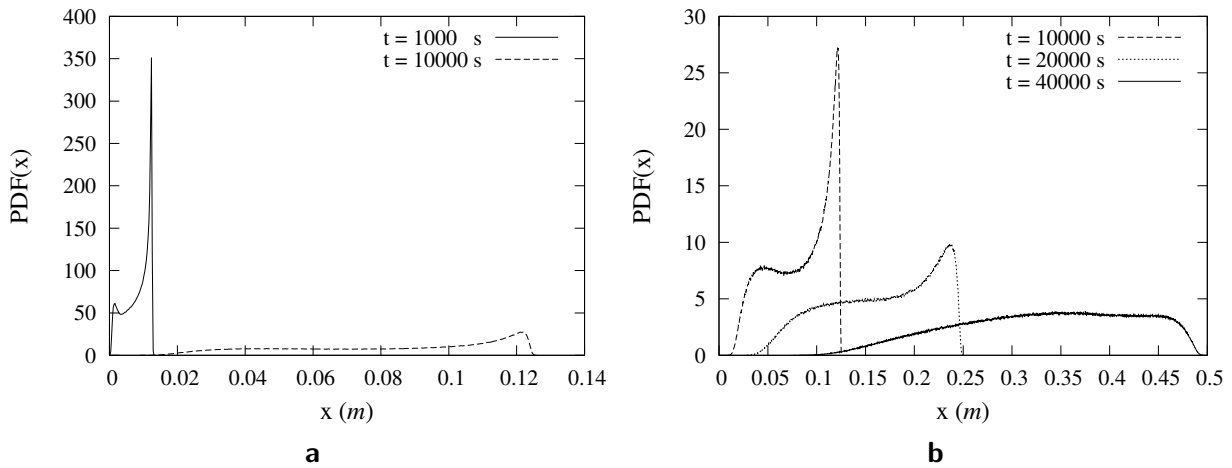


Figure 3.49: Shape of the tracer cloud in a channel flow at various times from the bench mark solution. Early times (a) and later times (b).

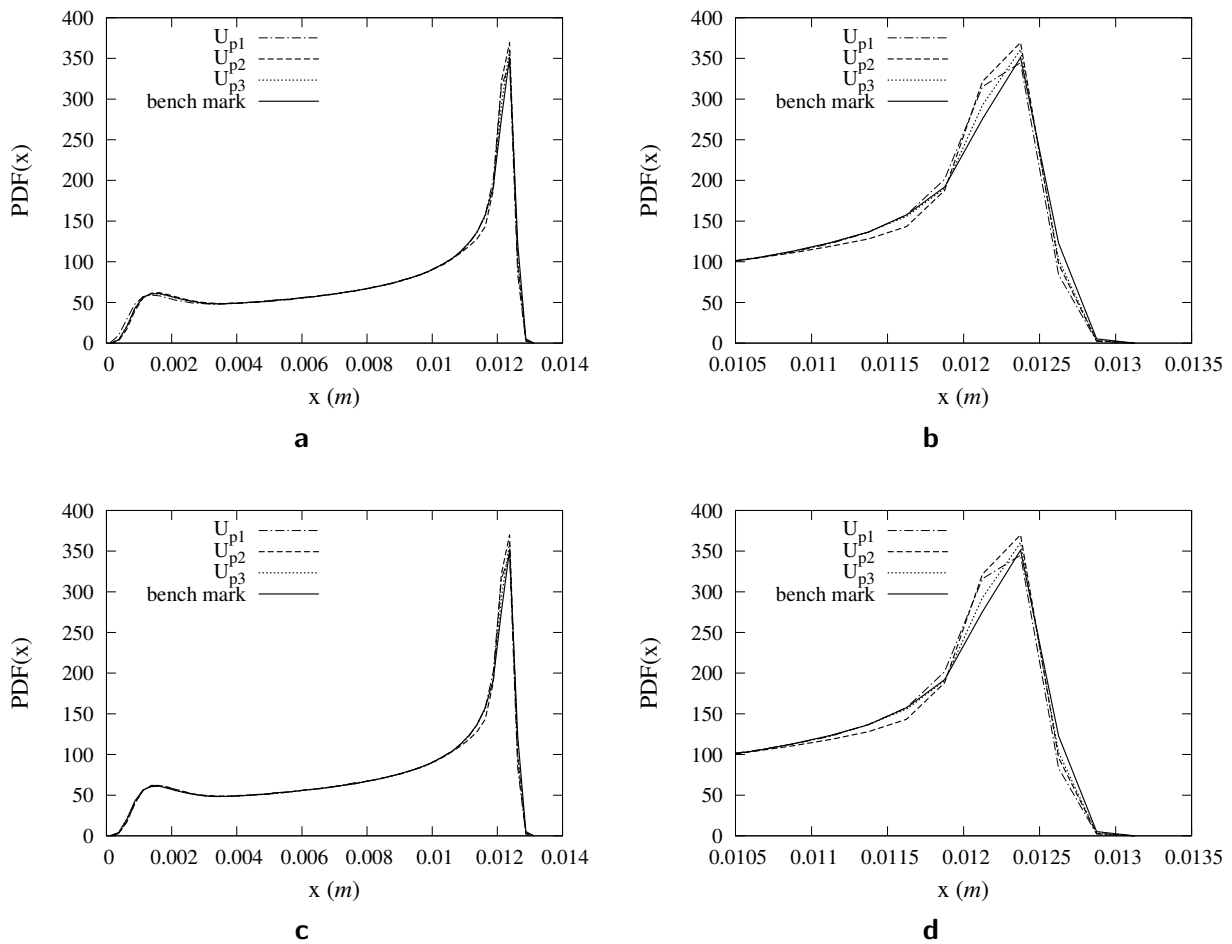


Figure 3.50: Shape of the tracer cloud in a channel flow at time $t = 1000$ s. Curves for which the drift terms are calculated from the LT and the particle method are displayed on the top (a,b) and on the bottom (c,d) respectively. The left hand side shows the complete PDFs while the figures on the right are zoomed in at farther locations.

Figure 3.50 and 3.51 show the PDF of particle locations at times $t = 1000s$ and $t = 10000s$ respectively. Each figure includes the PDFs obtained through the conditional statistics of the du field from the LT and from the particle method and also distinguishes between the results from different methods of calculating the drift term, U_p . It is clear that at the early time $t = 1000s$ there is no obvious difference in whether the LT method is used for obtaining the du field or the particle method. The curves for the different methods look almost exactly alike. Differences in the results obtained from the two methods are more obvious at much later times.

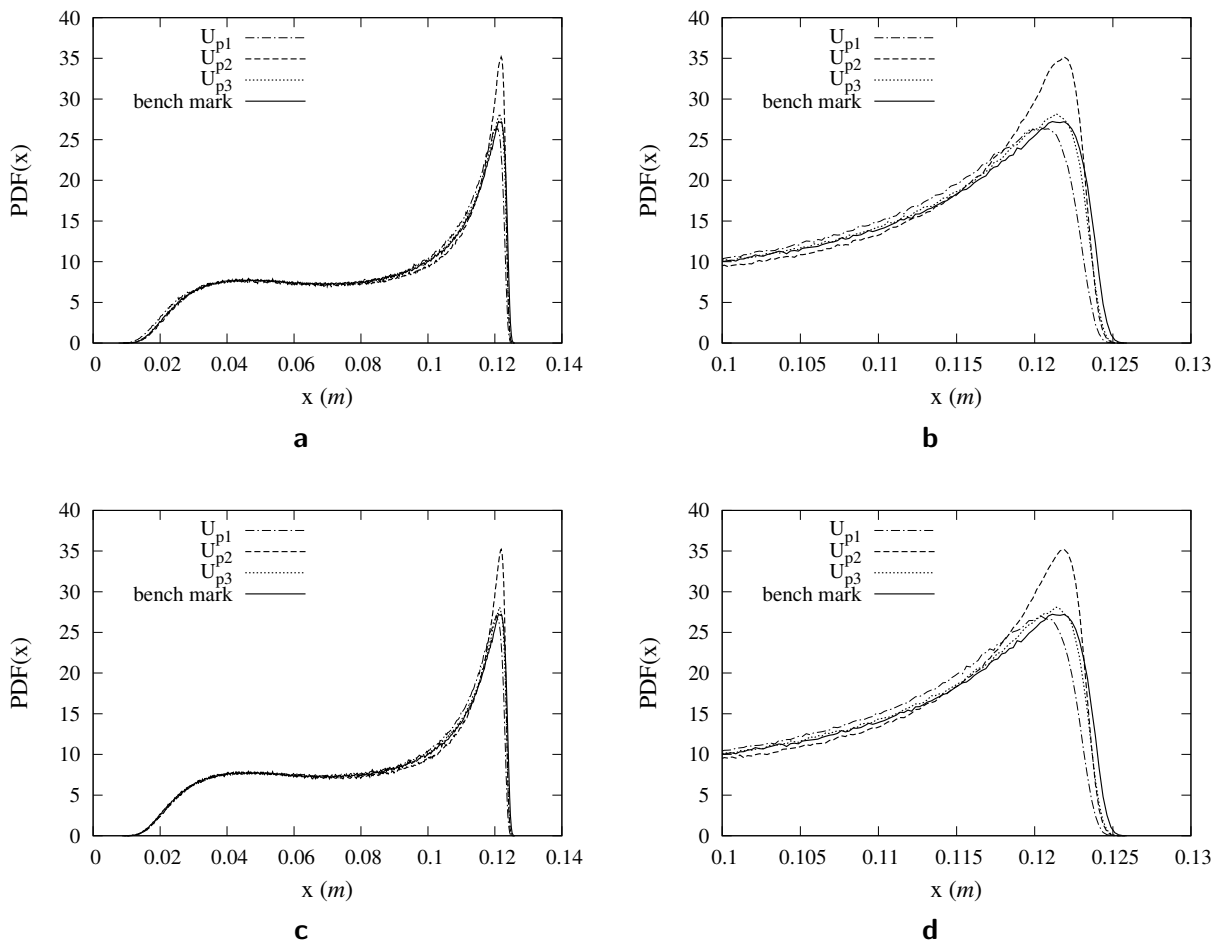


Figure 3.51: Shape of the tracer cloud in a channel flow at time $t = 10000s$. Curves for which the drift terms are calculated from the LT and the particle method are displayed on the top (a,b) and on the bottom (c,d) respectively. The left hand side shows the complete PDFs while the figures on the right are zoomed in at farther locations.

It is evident from figure 3.51 that even at later times ($t = 10000s$) there exists no particular difference between using the particle method or the LT method for obtaining du . The only rather slight difference is limited to the case where the drift term U_{p1} (equation 3.15) is used and even in that case the differences can only be observed in the first part of the PDF curves (corresponding to lower velocities). It can also be observed that U_{p2} cannot yield

reliable results at later times. Another observation is that the third method of obtaining the drift term (equation 3.22) yields the most accurate results. In order to better observe the behaviour of the model the shape of the cloud at a much later time, $t = 40000s$, is plotted in figure 3.52. Because very fine bins are used for calculating the PDFs the resulting curves become very jagged as the particles spread out away from each other with time. Therefore the probability in each bin is shown with dots in figure 3.52 for better visibility. At this time the differences between the LT and the particle methods become more visible. Here again it is quite clear that U_{p3} produces the most reliable results regardless of whether the LT or the particle methods have been used for obtaining the du field.

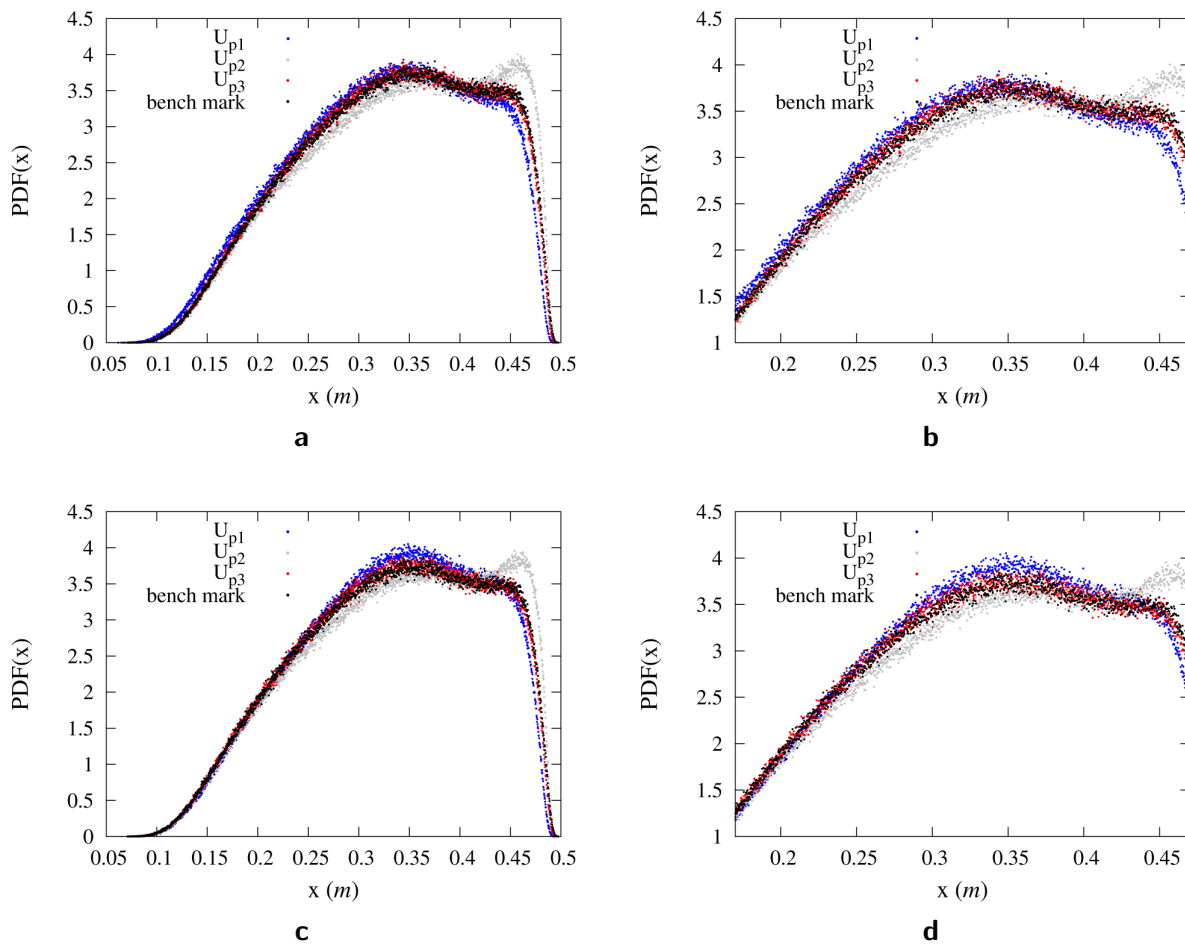


Figure 3.52: Shape of the tracer cloud in a channel flow at time $t = 40000s$. Curves for which the drift terms are calculated from the LT and the particle method are displayed on the top (a,b) and on the bottom (c,d) respectively. The left hand side shows the complete PDFs while the figures on the right are zoomed in at farther locations.

We conclude our study of tracer transport in a channel by observing that in general if the drift term U_{p3} is used in the stochastic velocity model the results obtained from the model very closely match that of the benchmark solution regardless of whether the drift term is obtained from the LT or the particle method. The conditional statistics of the du field

obtained by the LT method lack the information concerning the boundaries of the domain. When these statistics are used for finding the drift term in the stochastic velocity process, some workaround methods can be employed to alleviate the issues arising from this issue and at the same time to enforce the velocity PDF in the model. For the diffusion term, Γ_{p1} , obtained via the conditional statistics of du from the LT method however, no such strategies are used and the diffusion term in this case simply does not contain explicit information concerning the domain's boundaries. In the case of the channel however, as the boundaries only affect the smallest velocity range this does not have an observable effect on the results found using the model.

3.5 Tracer transport in a Sphere Pack

Here we will compare the results of the DNS solution of the transport ADE (equation 2.3) from MGLET (as was presented in section 2.4.3) with those obtained by our model via particle tracking. The Reynolds number of the flow is approximately $Re = 4 \times 10^{-4}$ and the molecular diffusion is set to $\Gamma = 1 \times 10^{-11} m^2/s$. The tracer is initialized on the central cross section of the domain perpendicular to the streamwise direction of the flow. DNS results for transport were obtained by solving the ADE via a finite volume method using MGLET on a domain of size $12 \times 2.4 \times 2.4 cm^3$. This domain contains 5 identical cubic sections of size $2.4 \times 2.4 \times 2.4 cm^3$ (replicated in the streamwise direction) each of which are periodic. The velocity field has been resolved via DNS simulations using MGLET on one cubic domain and has been replicated 5 times to produce the velocity field of the larger domain. When the ADE is solved on this domain the velocity field is repeated five times and the tracer as a whole inevitably re-experiences various flow structures as it moves along the different sections of the domain.

In the case of the model however, it should be noted that the geometry is not taken into account explicitly. Only in resolving the velocity field on the sphere packed domain of size $2.4 \times 2.4 \times 2.4 cm^3$ is the geometry of the porous media used. From the velocity field the du field is obtained and from that the drift and diffusion terms of the stochastic velocity model. As opposed to the DNS of the tracer transport, in the model particles evolving in time are not forced to encounter any specific flow or geometrical structures at specific spacial intervals. We however accept this discrepancy between DNS and model as the domain size at which the velocity is resolved is rather large and by the time the bulk of the tracer is transported from where it is to the same spot in the adjacent sub-domain it would have undergone enough diffusion to prevent an observable re-correlation of velocities. Another point to mention is that in the case of the sphere pack the du field is obtained via the LT method only.

3.5.1 Characteristics of the tracer cloud

Figure 3.53 shows the mean position, x , of tracer particles (centre of mass of the tracer cloud) over time in the case where U_{p1} is taken as the drift term in the stochastic velocity process. To obtain the drift and diffusion terms the conditional statistics of du were obtained using different bin size resolutions. Also included in the figure is a curve representing the centre of mass of the tracer cloud obtained via DNS solution of the transport equation. This is

done by taking the mean of the position of grid points weighted by the tracer concentration. The drift term represented by U_{p1} , for each velocity range is found by taking the average du in that velocity range (see equation 3.15). As was demonstrated in the case of the channel flow it is clear that if the du is obtained using the LT method the average du of the velocity ranges corresponding to the sphere boundaries will be underestimated as the LT method does not consider the bounce back at the wall. Therefore the heart of the cloud of particles moves slower than it should. Another interesting point about figure 3.53 is that the centre of mass of the tracer cloud shows no trend of converging towards DNS results with increasing resolution of velocity bins.

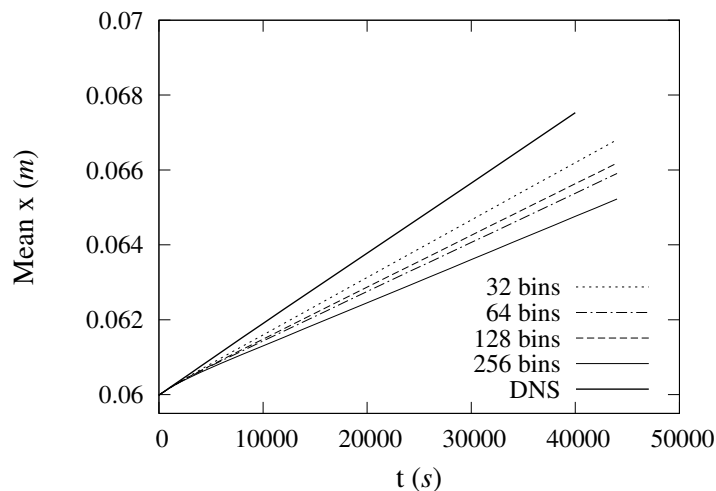


Figure 3.53: Centre of mass of the tracer cloud in a sphere pack over time obtained via different numbers of velocity bins in the case where U_{p1} is used together with the centre of mass of the cloud from DNS results.

The second method of obtaining the drift term attempts at alleviating the lack of accounting for bounce back at sphere surfaces by taking into account the velocity PDF (see equation 3.19). Figure 3.54 shows the centre of mass of the tracer cloud over time in the case where U_{p2} is taken as the drift term in the stochastic velocity process. Different curves represent the different numbers of bins used for the statistics of the du field conditioned on velocity and the benchmark solution is also included. It is quite clear that this method yields better results in terms of the centre of mass of the tracer cloud. Also it is evident that finer velocity bins (used for obtaining the conditional statistics of du) yield more accurate results.

The third method of obtaining the drift term can also overcome the bounce back issue of the LT method for the results concerning the centre of mass of the cloud. The centre of mass of the tracer cloud is plotted over time in figure 3.55 in the case where U_{p3} is used. Again various bin sizes were used for the conditional statistics of du as shown in the figure together with the benchmark solution. This method also yields better results in terms of the centre of mass of the tracer cloud as opposed to when U_{p1} is considered.

To better compare the performance of the three different methods of obtaining the drift term with regards to the advection of the centre of mass of the tracer cloud over time we

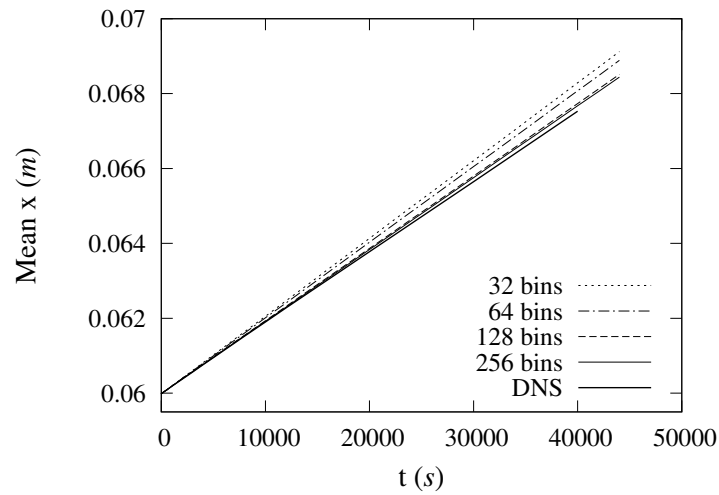


Figure 3.54: Centre of mass of the tracer cloud in a sphere pack over time obtained via different numbers of velocity bins in the case where U_{p2} is used together with the centre of mass of the cloud from DNS results.

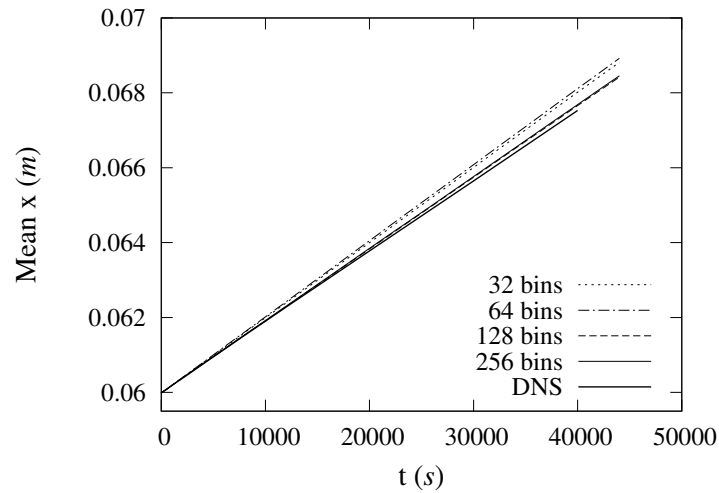


Figure 3.55: Centre of mass of the tracer cloud in a sphere pack over time obtained via different numbers of velocity bins in the case where U_{p3} is used together with the centre of mass of the cloud from DNS results.

have plotted the curves obtained using 256 velocity bins (for $du|u$) in figure 3.56. It is evident from this figure that U_{p1} as a drift term is inadequate for predicting the advection of the tracer cloud. U_{p2} and U_{p3} yield far better results in this regard with U_{p3} being slightly better than U_{p2} although this is not very clear in the figure as the difference is very small. As a side note, for every 10000 seconds the tracer cloud is displaced by a length almost equal to that of a sphere diameter ($D = 2\text{mm}$) with the average pore velocity of $\bar{u} = 1.856 \times 10^{-7}\text{m/s}$.

The evolution of the standard deviation of streamwise positions of the tracer particles is

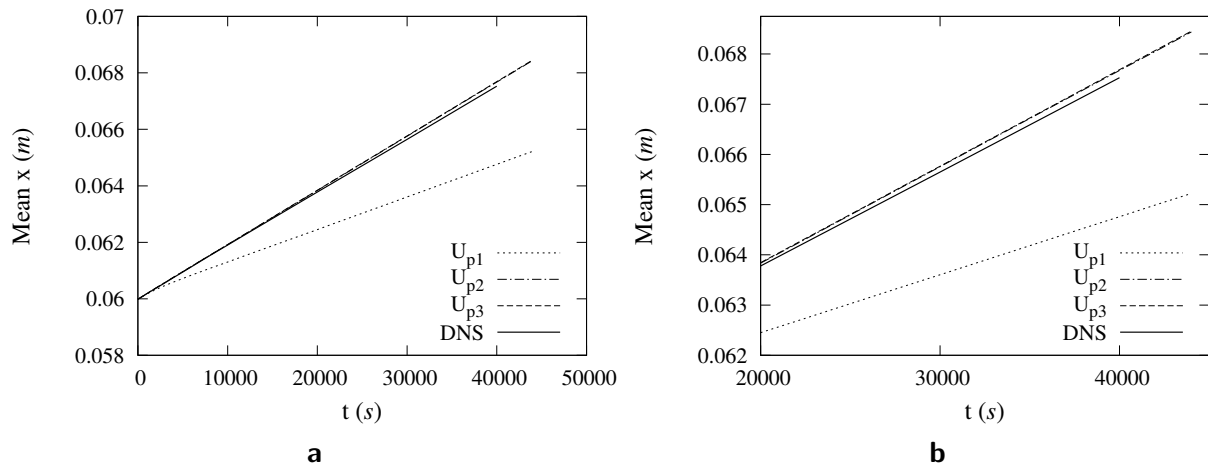


Figure 3.56: Centre of mass of the tracer cloud at various times obtained via different formulations of the drift term, using 256 velocity bins together with the centre of mass of the cloud from DNS results. Complete figure (a) and zoom at later times (b).

crucial in characterising its dispersion in a porous media. The standard deviation of the locations of tracer particles in the domain obtained via our model and the standard deviation of the locations of grid points weighted by the tracer concentration in the porous domain from DNS simulations of the transport equation are plotted in figure 3.57. These quantities represent the half width of the tracer cloud in the case of Fickian-dispersion. In this figure the results of four different configurations of the model (using different numbers of bins for the conditional statistics of du) are shown. In each case U_{p1} has been used as the drift term in the model. It is clear that the model underestimates the growth of the tracer cloud in the streamwise direction and also no improvement is evident by using finer bins for calculating conditional statistics of du and from there the drift and diffusion terms in the model.

The discrepancy between the standard deviation values predicted by the model and that obtained by DNS simulations when U_{p1} is considered as the drift term was to be expected due to the previously mentioned problems with using U_{p1} as the drift term when du is obtained via the LT method. However the issues are not improved by using U_{p2} or U_{p3} either. Figures 3.58 and 3.59 demonstrate the standard deviation of particle positions obtained via drift terms U_{p2} and U_{p3} respectively. Each figure shows the results obtained by using various numbers of velocity bins. In the case where U_{p2} is used one can see that with an increase in bin resolution the standard deviation values obtained by the model tend slightly more towards that obtained by DNS (see figure 3.58b). The same cannot be said for the case where U_{p3} is used. Nevertheless, both return similar curves and for higher bin resolutions the use of U_{p3} has no significant advantage over the use of U_{p2} .

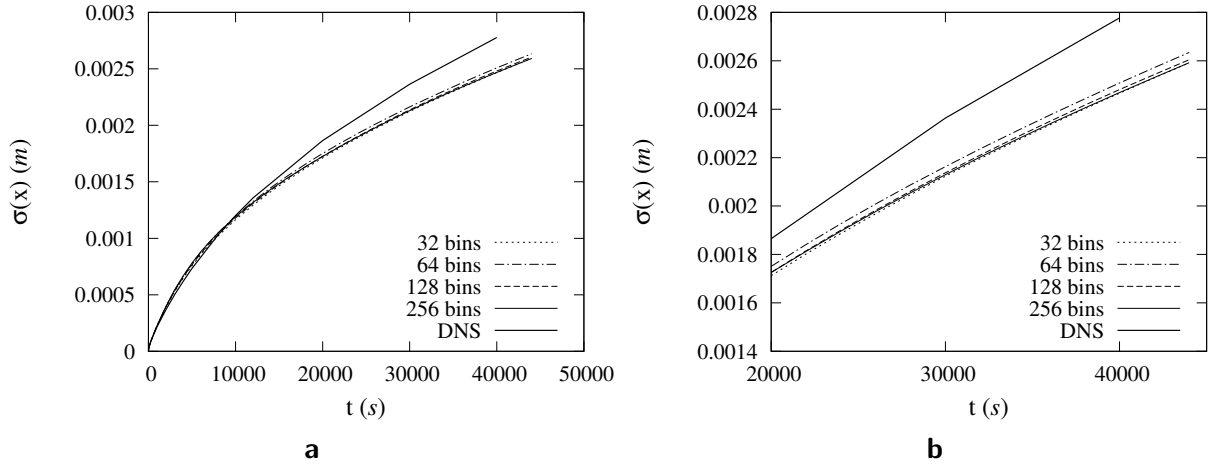


Figure 3.57: Standard deviation of particle positions at various times obtained using U_{p1} , with various numbers of velocity bins together with the centre of mass of the cloud from DNS results. Complete figure (a) and zoom at later times (b).

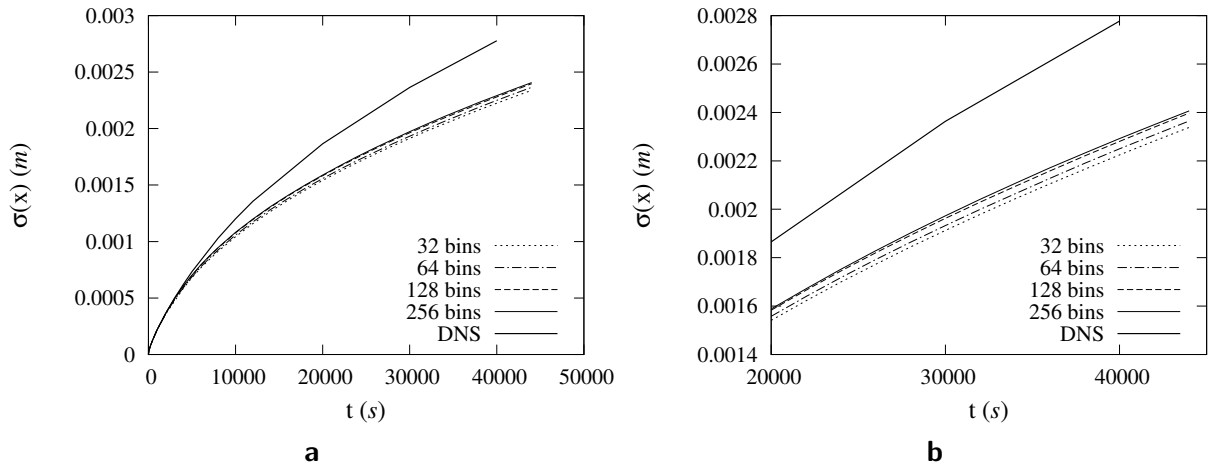


Figure 3.58: Standard deviation of the tracer cloud at various times obtained using U_{p2} , with various numbers of velocity bins together with the centre of mass of the cloud from DNS results. Complete figure (a) and zoom at later times (b).

As an overview of the performance of the three different methods of obtaining the drift term with regards to the standard deviation of particle positions over time we have plotted the curves representing the different drift terms obtained using 256 velocity bins for the conditional statistics of du in figure 3.60. Surprisingly this figure shows that when U_{p1} is used as the drift term it can predict the half width of the cloud slightly better than when U_{p2} or U_{p3} are used. However, regardless of the drift term used, the results obtained from the model significantly underestimate the growth of the tracer cloud.

Another important parameter for quantifying non-Fickian dispersion is the skewness of the

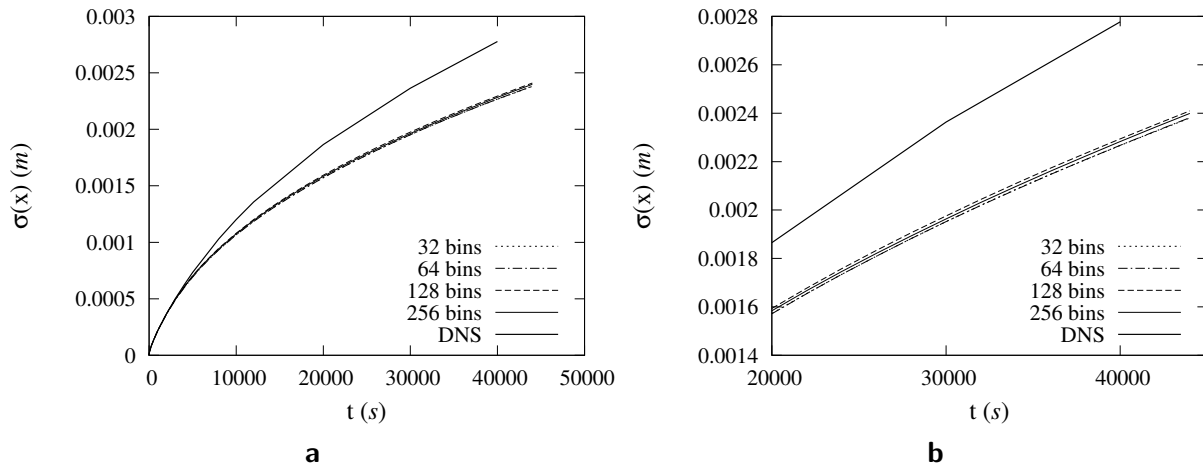


Figure 3.59: Standard deviation of the tracer cloud at various times obtained using U_{p3} , with various numbers of velocity bins together with the half width of the cloud from DNS results. Complete figure (a) and zoom at later times (b).

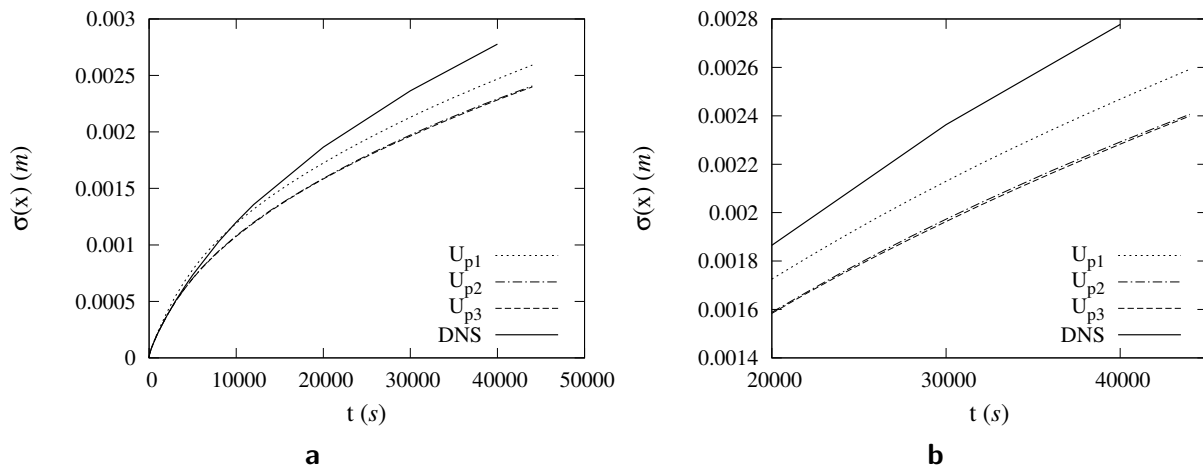


Figure 3.60: Standard deviation of the tracer cloud at various times obtained via different formulations of the drift term U_p , using 256 velocity bins together with the half width of the cloud from DNS results. Complete figure (a) and zoom at later times (b).

tracer cloud. Figure 3.61 shows the skewness of the location, x , of tracer particles over time in the case where U_{p1} is taken as the drift term in the stochastic velocity process. Drift and diffusion terms were obtained using different bin size resolutions for the conditional statistics of du . Also included in the figure is a curve representing the skewness of the tracer concentration in the case of the DNS simulation of the transport equation (equation 2.3). One can see that with an increase in the number of velocity bins used for obtaining the drift and diffusion terms the skewness increases. This is due to the increased scattering of the conditional mean and variance of du at the extremities of the velocity spectrum

where velocity bins are sparsely populated. Regardless of the number of bins the model overestimates the skewness dramatically.

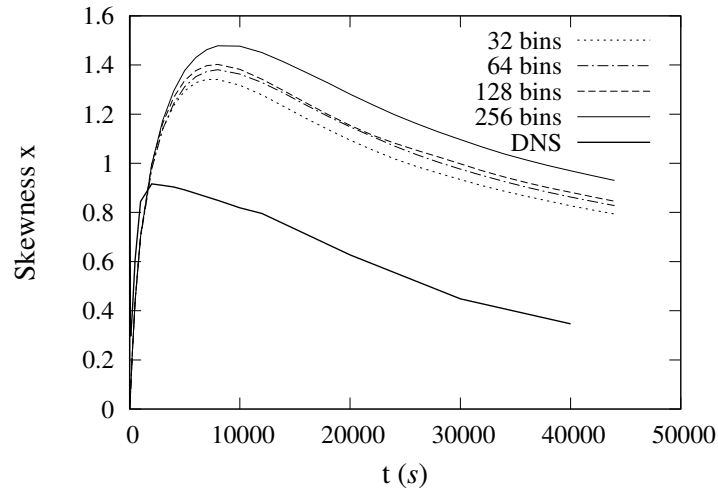


Figure 3.61: Skewness of the tracer cloud at various times obtained via different numbers of velocity bins in the case where U_{p1} is taken as the drift term together with the skewness of the cloud from DNS results.

Figures 3.62 and 3.63 show the same for the cases where U_{p2} and U_{p3} are used as drift terms in the stochastic velocity model. The overall behaviour of the skewness over time is very similar to the case where U_{p1} is used. However, it appears that the skewness is less dependent on the number of bins in these cases.

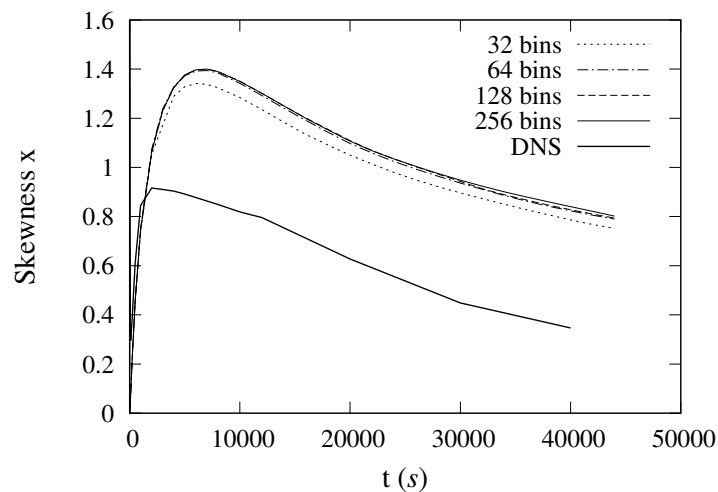


Figure 3.62: Skewness of the tracer cloud at various times obtained via different numbers of velocity bins in the case where U_{p2} is taken as the drift term together with the skewness of the cloud from DNS results.

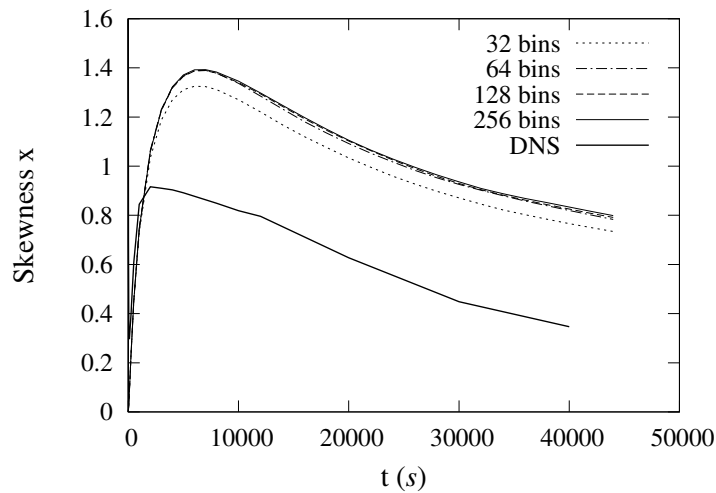


Figure 3.63: Skewness of the tracer cloud at various times obtained via different numbers of velocity bins in the case where U_{p3} is taken as the drift term together with the skewness of the cloud from DNS results.

For all three drift terms of U_{p1} , U_{p2} and U_{p3} the evolution of skewness over time looks very similar to that obtained by DNS and the difference is only in the magnitude of the skewness rather than its behaviour. To better compare the three different drift terms figure 3.64 shows the evolution of skewness for each drift term (in the case where 256 velocity bins are used for the conditional statistics of du) together with that obtained from DNS. Although all three terms greatly overestimate the skewness of the tracer cloud, the curve corresponding to U_{p3} shows the most severe overestimation. This is in contrast to what was seen in the channel flow. One must consider that the sphere pack is composed of many small and irregular channels. Any error that existed in the case of the simple channel flow would be magnified in a system that contains numerous channels.

The dispersion coefficient, Γ_D , was determined at each time, t , both from our DNS results by calculating the variance of the streamwise positions of grid points, x , weighted by the concentration and from the model by calculating the variance of particle positions. The variance was then divided by twice the time t to obtain the dispersion coefficient. Figure 3.65 shows the dispersion coefficient, Γ_D , normalized by the molecular diffusion, $\Gamma = 1 \times 10^{-11} m/s^2$, plotted against time both for DNS and for the model in the case when 256 bins are used for the conditional statistics of du and different drift terms are used in the model. For all the curves Γ_D/Γ appears to be gradually converging towards a value pointing to a gradual transition towards asymptotic dispersion. However, the model dramatically underestimates the dispersion rate.

In general we conclude that our stochastic velocity model is able to predict the centre of mass of the cloud over time reasonably well but underestimates its spreading (the standard deviation of particle positions) and overestimates its skewness. Of course to get the diffusion and drift terms of the stochastic velocity model the du field was found using the LT method which cannot account for the complicated boundaries of the sphere surfaces. To compensate we attempted to enforce the velocity PDF in the model by using U_{p2} and U_{p3} . It should be noted however that the diffusion term, Γ_p , which we did not modify or enhance is also

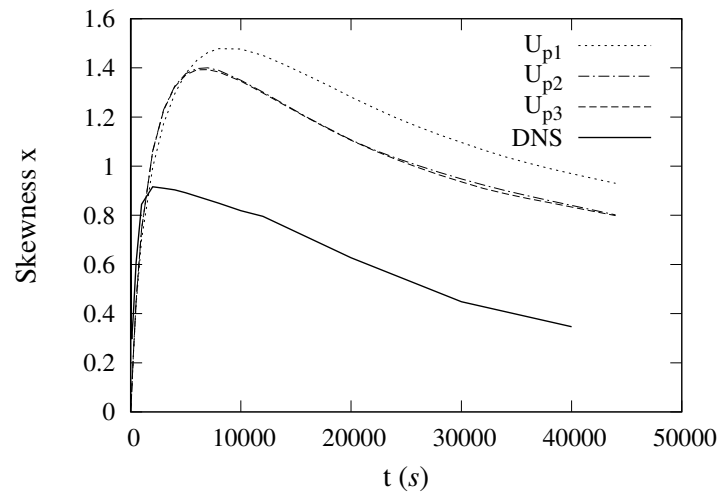


Figure 3.64: Skewness of the tracer cloud at various times obtained via 256 velocity bins in the cases where U_{p1} , U_{p2} and U_{p3} formulations are used for the drift term together with the skewness of the cloud from DNS results.

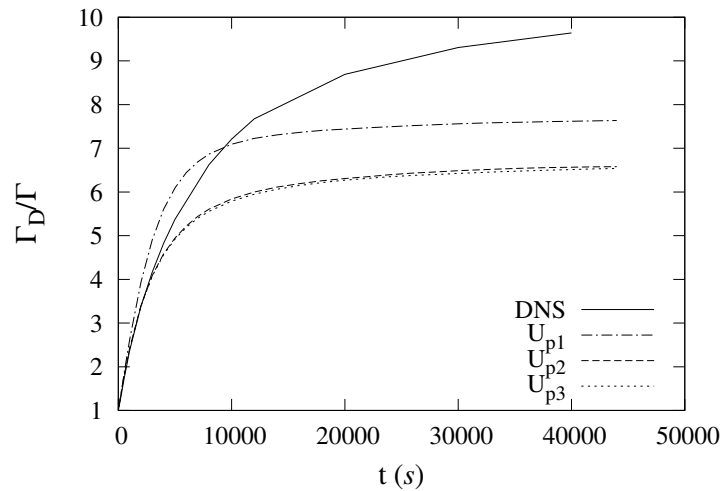


Figure 3.65: Γ_D/Γ plotted against times in a random sphere pack for $Pec = 37.11$. Results of various configurations of the model together with results from DNS

affected by not considering the boundaries as was shown in the channel flow (figure 3.9). We were also limited by the size of our velocity data base the finite size of which prohibits a better resolution for the conditional statistics of du .

3.5.2 Velocity PDFs

Here we scrutinize the accuracy of the model in predicting the velocity PDF of a tracer spreading in a sphere pack. In order to have a benchmark to compare with, at various times we take the velocity of grid points in the domain obtained by DNS, weigh them by the tracer

concentration at the grid point and calculate the velocity PDF at that time. What we obtain is equivalent to the velocity PDF of tracer particles in the domain at different times. We then compare these PDFs to the velocity PDFs of tracer particles in our stochastic velocity model.

First we demonstrate the effect of bin refinement in obtaining drift and diffusion terms on the accuracy of the velocity PDF. Figure 3.66 shows the velocity PDF obtained using different drift terms, from the conditional statistics of du via two different number of bins at time $t = 250s$. Each figure includes the PDF of the total velocity field and the velocity PDF of the tracer cloud. In figure 3.66a all PDFs are obtained using 64 bins as this is the number of bins used for the conditional statistics of du used in the model. In figure 3.66b, all PDFs are found using 256 bins for the same reason. When the drift and diffusion terms in the model are obtained by n bins the velocity PDF of the tracer obtained via the model can at best match the actual velocity PDF obtained via n bins. As was previously explained in section 2.4.3, at an early time ($t = 250s$) the velocity PDF of the tracer cloud does not exactly match that of the whole domain due to the way the tracer is initialized. The velocity PDF obtained using the model (via different drift terms) also does not match that of the whole domain but neither does it exactly match the velocity PDF of the tracer obtained via DNS. The difference however, except in the case where U_{p1} is taken as the drift term, is not very dramatic. This was to be expected as we have already established that U_{p1} does not enforce the velocity PDF in the model and that it cannot yield the correct drift in the stochastic process for velocity due to the method which was used for obtaining du .

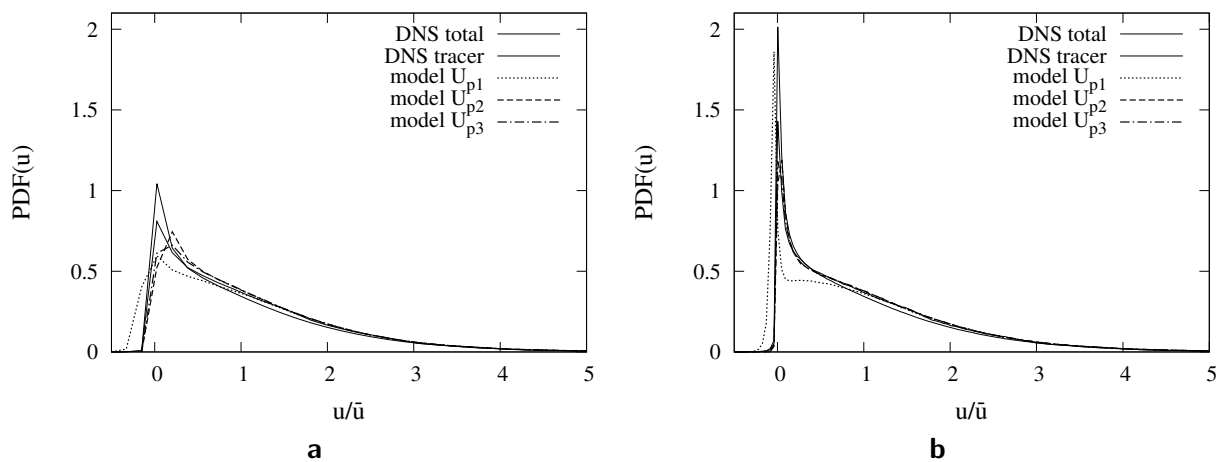


Figure 3.66: Velocity PDFs at time $t = 250s$ obtained via different formulations of the drift term. (a) 64 bins were used for finding the PDFs and for obtaining drift and diffusion terms in the model. (b) 256 bins were used for finding the PDFs and for obtaining drift and diffusion terms in the model.

It is clear that the results of the tracer transport from our model using U_{p1} cannot predict the velocity distribution of the tracer. The shift that can be seen in the velocity PDF obtained using U_{p1} is due to the fact that boundary conditions of the sphere surfaces were

accounted for. We omit the results obtained via U_{p1} in the next figure (figure 3.67) and zoom in further into more probable velocities in order to better see the effect of the bin size on the quality of the results. From this figure it appears that the more bins used for obtaining drift and diffusion terms results in a slightly better prediction of the velocity PDF by the model especially in the case where U_{p3} is taken as the drift term.

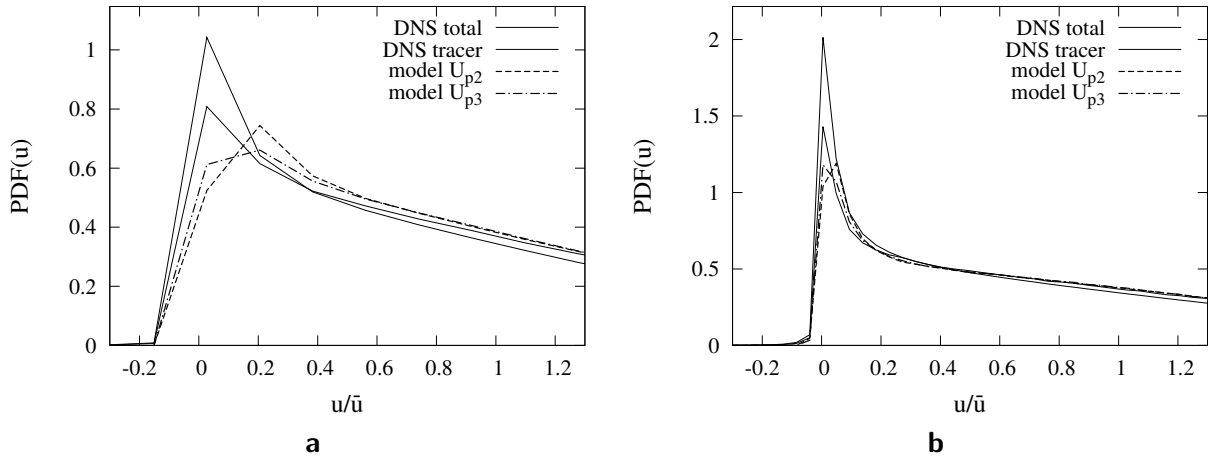


Figure 3.67: Velocity PDFs at time $t = 250s$ obtained via different drift terms zoomed in at more frequently occurring velocities. (a) 64 bins were used for finding the PDFs and for obtaining drift and diffusion terms in the model. (b) 256 bins were used for finding the PDFs and for obtaining drift and diffusion terms in the model.

Figure 3.68 shows the same but for a later time, $t = 40000s$. Please note that as was mentioned in section 2.4.3 the advective time scale for this set-up is $t_{adv} = 10776s$. At time $t = 40000s$ the velocity PDF of the whole domain matches that of the tracer cloud obtained by DNS. This is because the tracer has had time to spread over more of the domain and has experienced all of the velocities in the pore space. The velocity PDF of the tracer predicted by the model however differs from the DNS results. Although the PDFs obtained from U_{p2} and U_{p3} are slightly different it seems that both these drift terms have an equal capability for enforcing the velocity PDF in the evolution of the tracer cloud by the model. From these figures we conclude that U_{p2} and U_{p3} both have the ability to predict the particle velocity distributions quite well. However for both U_{p2} and U_{p3} the peak of the velocity PDF, which corresponds to the smallest velocities is underestimated and instead the probability of the velocities closer to \bar{u} is overestimated. Therefore the bulk of the tracer cloud, when the model is used with either of these drift terms, moves at a speed slightly higher than is observed in the DNS results as can be observed in figure 3.56. Also as by using these drift terms the velocities remain closer to the mean pore velocity, \bar{u} , the spreading of the tracer cloud is underestimated as can be seen in figure 3.60.

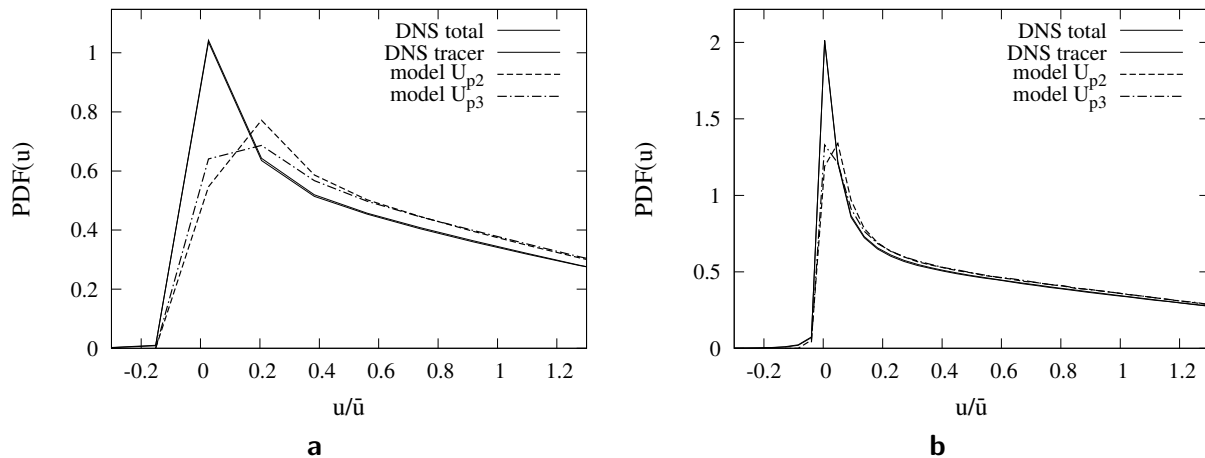


Figure 3.68: Velocity PDFs at time $t = 40000s$ obtained via different formulations of the drift term zoomed in at more frequently occurring velocities. (a) 64 bins were used for finding the PDFs and for obtaining drift and diffusion terms in the model. (b) 256 bins were used for finding the PDFs and for obtaining drift and diffusion terms in the model.

3.5.3 Tracer cloud

We will now present the actual shape of the tracer cloud in the sphere pack over time, both from the DNS of the transport equation and from the results of our model. The set-up is the same as was explained in section 2.4. To obtain the shape of the tracer cloud in the case of the DNS we calculate the probability density of the streamwise position of grid points, x , weighted by the tracer concentration and in the case of the model we simply calculate the probability density of the streamwise locations (x) of particles. The range of x is between 0 and $12cm$ and is divided into 3840 bins such that in the case of the DNS each bin contains exactly one grid point in the x direction. This PDF represents the shape of the tracer cloud. Figure 3.69 shows the shape of the tracer cloud at different times both from DNS and the model. In the case of the model we present in this figure the results obtained from using drift and diffusion terms obtained via 256 velocity bins and drift terms obtained via different methods.

It is clear that the drift term U_{p1} does not produce a good approximation of the tracer behaviour even at early times. U_{p2} and U_{p3} return very similar and slightly better results. Both however, underestimate the spreading of the tracer cloud. As was explained in the previous subsection this is due to the underestimation of the peak of the velocity PDF and overestimation of the probability of velocities in the vicinity of \bar{u} (see figure 3.68). The kinks in the velocity PDF obtained by DNS at time $t = 40000S$ (figure 3.69d) are due to the shape of the spheres and the irregular shape of the domain. This shows up because at this time the bulk of the tracer cloud has moved a distance equivalent to a few sphere diameters. The model however cannot capture these irregularities and yields a smooth PDF.

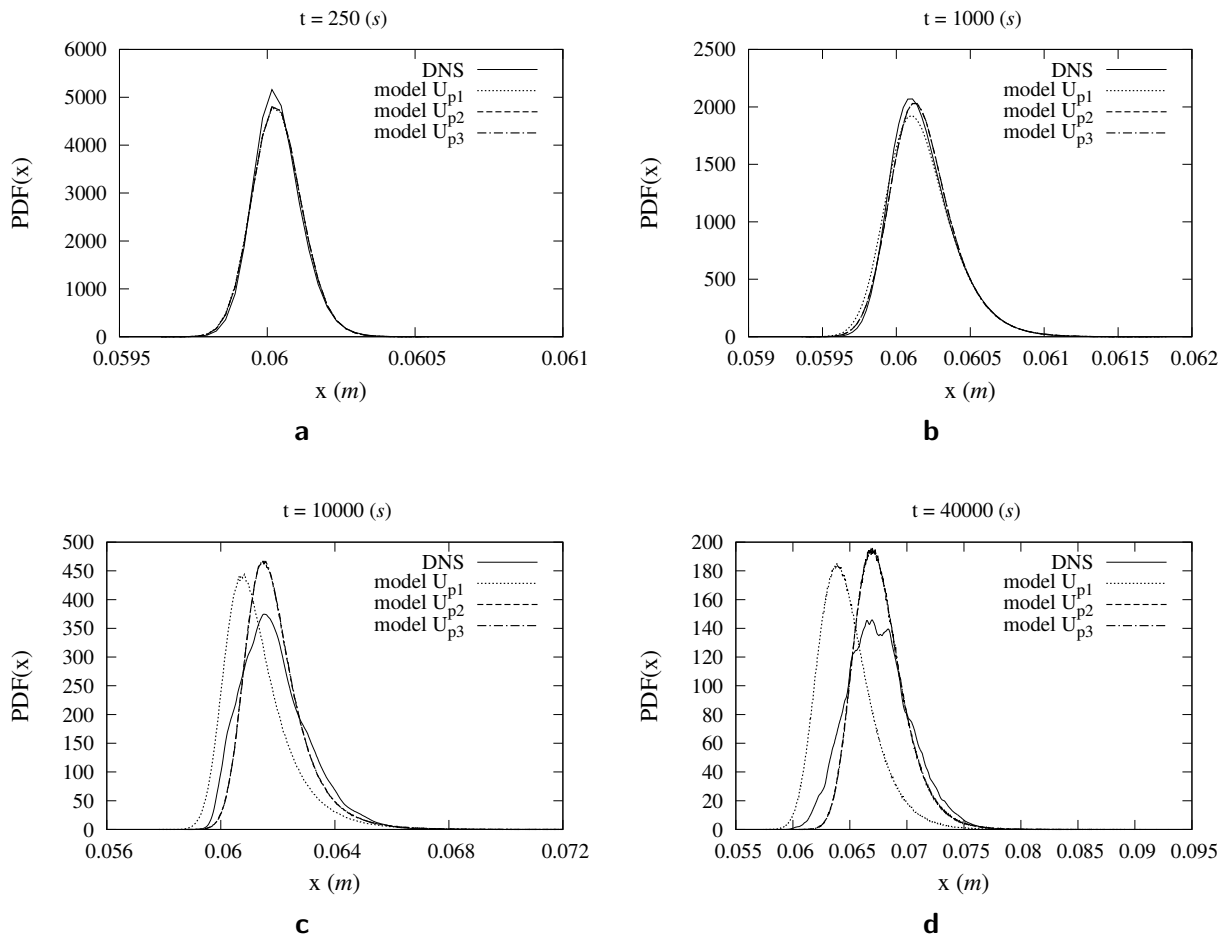


Figure 3.69: Shape of tracer in a sphere pack at various times. Different curves represent the different methods of obtaining the drift term in the model and results from DNS.

To better see the evolution of the tracer cloud figure 3.70 shows the shape of the cloud over time from the DNS results (represented by thicker lines) and from the model. In the case of the model the results are calculated via drift term, U_{p3} , obtained using 256 velocity bins. These curves are practically indistinguishable from those calculated using U_{p2} as the drift term.

The model is able to predict the motion of the centre of the tracer cloud reasonably well but the spreading of the cloud calculated from the results of the model is clearly less than that from the DNS of the tracer transport. The model is also able to demonstrate how the skewness of the cloud first increases with time and then after a certain time begins to decrease. In general the model is able to mimic the qualitative behaviour of the tracer but quantitatively the results of the model are rather inaccurate.

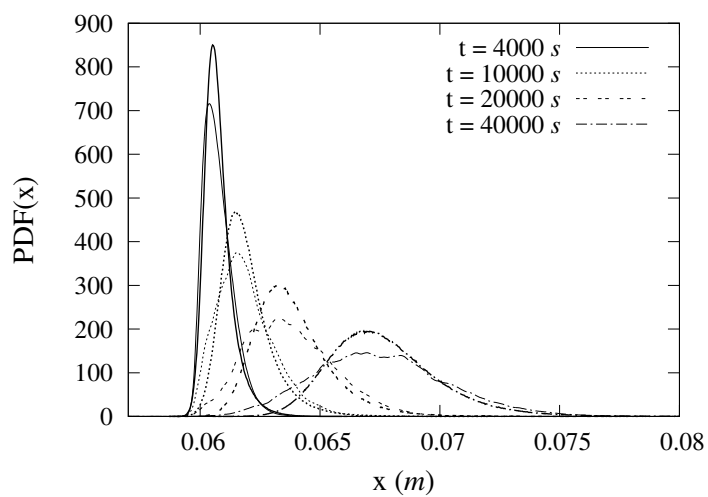


Figure 3.70: Shape of tracer in a sphere pack at various times. Curves with thicker lines represent the DNS results while those with finer lines represent the model where U_{p3} is taken as the drift term.

4 Conclusions and Outlook

In this work the statistics and PDFs of pore scale velocity components and velocity fluxes in a random sphere pack were studied in detail. Direct numerical simulations were performed to obtain the pore scale velocity field. The validity of our simulations were thoroughly evaluated by intensive grid studies and determination of the effect of the REV size on the results. The evolution of a passive tracer in the sphere pack was investigated by DNS simulations of the transport process and a model for dispersion was developed and tested both for a simple channel flow and for a sphere packed domain. The issues regarding this model were elaborated upon in detail and certain shortcomings were identified.

We observed that although our stochastic velocity model for dispersion is able to qualitatively model the dispersive behaviour, quantitatively it is not reliable. This is especially evident in predicting the higher statistical moments of the concentration distribution in space such as the skewness of the tracer cloud. Here we will point to the most important issues that contribute to the inaccuracy of our model.

In the first place our model is based on the conditional statistics of the velocity variation (du) field. The velocity variation field in the case of the sphere pack was obtained via a method which is unable to account for the boundaries of the sphere surfaces. Various strategies for overcoming this issue were employed. These strategies appeared to be very effective in the case of the channel flow but do not adequately alleviate the problems in the case of the sphere pack. Another contributing factor is that the strategies employed were all aimed at correcting the drift term in the stochastic velocity model. No attempt was made to correct the diffusion term, Γ_p , which is also affected by the boundaries as was shown in the case of the channel flow. The second contributing factor in the inaccuracy of our results is that the statistics of the velocity variation field, du , conditioned on the velocity, were found using a limited number of velocity data points. As a consequence, the conditional statistics were not well resolved. Although we obtained the velocity field on a very fine mesh the population of the pore velocity data was not sufficient for populating fine bins at the extremities of the velocity domain due to the long tails of the velocity distribution. The last factor concerning our results is the initialization of the tracer. The tracer was initialized on a cross section of the domain which was not a representative of the total domain as the domain was not large enough to be considered a real REV. However the different terms in our model were obtained via the properties of the velocity and velocity variation field of the whole domain.

The most important step that can be taken to improve the model is to make sure to obtain the velocity variation field via a Lagrangian random walk step, which we call the particle method in the text. In this way the velocity variation field will itself contain the information concerning the pore boundaries. However, as was shown for the channel flow even this method of obtaining the velocity variation field leaves room for improvement of the drift term used in the stochastic velocity method. This is mainly due to the resolution of the

conditional statistics of the velocity variation field. In order to obtain a better resolution a very large velocity data base or the use of adaptive bin sizes is required. Discretization of the domain into finer bins or even the use of a larger domain is an important step toward the improvement of the method. Using a domain large enough to be considered an appropriate REV has the added benefit of providing cross sections large enough to be representatives of the whole domain. Therefore, initializing the tracer on just a cross section rather than on the whole domain will pose no problem in using a model based on the statistics of the whole domain.

Bibliography

- [1] R. C. Acharya, A. J. Valocchi, C. J. Werth, and T. W. Willingham. Pore-scale simulation of dispersion and reaction along a transverse mixing zone in two-dimensional porous media. *Water Resour. Res.*, 43, 2007.
- [2] J. Bear. *Dynamics of Fluids in Porous Media*. American Elsevier Pub. Co., 1972.
- [3] B. Berkowitz, A. Cortis, M. Dentz, and H. Scher. Modeling non-fickian transport in geological formations as a continuous time random walk. *Rev. Geophys.*, 44, May 2006.
- [4] F. C. Blake. The resistance of packing to fluid flow. *Trans. Am. Inst. Chem. Eng.*, 14:415–421, 1922.
- [5] E. A. Borges da Silva, d. P. Souza, A. A. Ulson de Souza, and S. M. A. Guelli U. de Souza. Prediction of effective diffusivity tensors for bulk diffusion with chemical reactions in porous media. *Braz. J. Chem. Eng.*, 24:47–60, 2007.
- [6] M. Breuer, N. Peller, Ch. Rapp, and M. Manhart. Flow over periodic hills - numerical and experimental study over a wide range of reynolds numbers. *Computers and Fluids*, 38(2):433–457, February 2009.
- [7] J.H. Conway and N.J.A. Sloane. *Sphere Packings, Lattices and Groups*. Springer-Verlag New York, 2 edition, 1993.
- [8] G. Garmeh, R. T. Johns, and L. W. Lake. Pore-scale simulation of dispersion in porous media. *Society of Petroleum Engineers*, 14:559–567, December 2009.
- [9] L.W. Gelhar, A.L. Gutjahr, and R.L. Naff. Stochastic analysis of macrodispersion in a stratified aquifer. *Water Resour. Res.*, 15(6):1387–1397, 1979.
- [10] L.W. Gelhar, C. Welty, and K.R. Rehfeldt. A critical review of data on field-scale dispersion in aquifers. *Water Resour. Res.*, 28(7):1955–1974, July 1992.
- [11] F. H. Harlow and J. E. Welsh. Numerical calculation of time-dependent viscous incompressible flow with free surface. *Phys, Fluids*, 8:2182–2189, 1965.
- [12] S.M. Hassanizadeh. On the transient non-fickian dispersion theory. *Transport in Porous Media*, 23:107–124, 1996.
- [13] C. hlavaáěk and M Kubíček. Modeling of chemical reactors£xx heat and mass transfer in porous catalyst the particle in a non-uniform external field. *Chemical Engineering Science*, 25:1527–1536, 1970.
- [14] A. Hokpunna and M. Manhart. Compact fourth-order finite volume method for numerical solutions of Navier-Stokes equations on staggered grids. *Journal of Computational Physics*, 229:7545–7570, 2010.

- [15] M.E. Kainourgiakis, E.S. Kikkinides, A.N. Galani, G.Ch. Charalambopoulou, and A.K. Stubod. Digitally reconstructed porous media: Transport and sorption properties. *Transport in Porous Media*, 58, 2005.
- [16] W. Kinzelbach and G. Uffink. *The Random Walk Method and Extensions in Ground-water Modelling*, pages 761–787. Kluwer Academic, Norwell, Mass., 1991.
- [17] P.K. Kitanidis. Particle-tracking equations for the solution of the advection-dispersion equation with variable coefficients. *Water Resource Research*, 30(11):3225–3227, November 1994.
- [18] J. Kozeny. Ueber kapillare leitung des wassers im boden. *Sitzungsber Akad. Wiss.*, 136(2a):271–306, 1927.
- [19] E.M. Labolle, G. E. Fogg, and A. F. B. Tompson. Random-walk simulation of transport in heterogeneous porous media: Local mass-conservation problem and implementation methods. *Water Resour. Res.*, 32(3):583–593, 1996.
- [20] T. Le Borgne, M. Dentz, and J. Carrera. Lagrangian statistical model for transport in highly heterogeneous velocity fields. *Phys. Rev. Lett.*, 101(9):090601, 2008.
- [21] T. Le Borgne, M. Dentz, and J. Carrera. Spatial markov processes for modeling Lagrangian particle dynamics in heterogeneous porous media. *Phys. Rev. E*, 78(2):026308, 2008.
- [22] P. Lehmann, M. Berchtold, B. Ahrenholz, J. Tölke, A. Kaestner, M. Krafczyk, H Flühler, and H. R. Kunsch. Impact of geometrical properties on permeability and fluid phase distribution in porous media. *Advances in Water Resources*, 31:1188–1204, 2008.
- [23] M. Levy and B. Berkowitz. Measurement and analysis of non-fickian dispersion in heterogeneous porous media. *J. Contaminant Hydrology*, 64:203–226, July 2003.
- [24] M. Lieb, T. Neckel, H.-J. Bungartz, and S. Sun. Towards a Navier Stokes - Darcy upscaling based permeability tensor computation. *Procedia Computer Science*, 9:717–726, 2012.
- [25] C.P. Lowe and D. Frenkel. Do hydrodynamic dispersion coefficients exist? *Physical Review Letters*, 77(22):4552–4555, 1996.
- [26] B.D. Lubachevsky and F. Stillinger. Geometric properties of random disk packings. *Journal of statistical physics*, 60(5,6):561–583, 1990.
- [27] M. J. MacDonald, C.-F. Chu, P. P. Guilloit, and K. M. Ng. A generalized blake-kozeny equation for multisized spherical particles. *AIChE J.*, 37(10):1583–1588, 1991.
- [28] R.S. Maier, D.M. Kroll, R.S. Bernard, S.E. Howington, J.F Peters, and H.T. Davis. Pore-scale simulation of dispersion. *Phys. Fluids*, 12(8):2065–2079, 2000.
- [29] R.S. Maier, D.M. Kroll, Y.E. Kutsovsky, H.T. Davis, and R.S. Bernard. Simulation of flow through bead packs using the lattice boltzmann method. *Phys. Fluids*, 10(1):60–74, 1998.

- [30] M. Manhart. A zonal grid algorithm for DNS of turbulent boundary layers. *Computers and Fluids*, 33(3):435–461, March 2004.
- [31] N. S. Martys. Numerical simulation of hydrodynamic dispersion in random porous media. *J. Chromatography*, A(707):35–43, 1995.
- [32] D.W. Meyer, P. Jenny, and H.A. Tchelepi. A joint velocity-concentration pdf method for tracer flow in heterogeneous porous media. *Water Resour. Res.*, 46, 2010.
- [33] D.W. Meyer and H.A. Tchelepi. Particle-based transport model with markovian velocity processes for tracer dispersion in highly heterogeneous porous media. *Water Resour. Res.*, 46, 2010.
- [34] A. F. Morais, H. Seybold, H. J. Herrmann, and J. S. Andrade Jr. Non-newtonian fluid flow through three-dimensional disordered porous media. *Physical Review Letters*, 103(19), 2009.
- [35] K.B. Neeves. *Convection-enhanced drug delivery: porous media models and microfluidic devices*. PhD thesis, Cornell University, 2006.
- [36] W. Nowak, R.L. Schwede, O.A. Cirpka, and I. Neuweiler. Probability density functions of hydraulic head and velocity in three-dimensional heterogeneous porous media. *Water Resource Research*, 44, 2008.
- [37] S. Ovaysi and M. Piri. Direct pore-level modeling of incompressible fluid flow in porous media. *J. Computational Physics*, 229(19):7456–7476, September 2010.
- [38] S. Ovaysi and M. Piri. Pore-scale modeling of dispersion in disordered porous media. *J. Contaminant Hydrology*, 124:68–81, 2011.
- [39] N. Peller. *Numerische Simulation turbulenter Strömungen mit Immersed Boundaries*. PhD thesis, Technische Universität München, 2010.
- [40] N. Peller, A. Le Duc, F. Tremblay, and M. Manhart. High-order stable interpolations for immersed boundary methods. *International Journal for Numerical Methods in Fluids*, 52:1175–1193, 2006.
- [41] M. Rashidi, L. Peurrung, A. Tompson, and T. Kulp. Experimental analysis of pore-scale flow and transport in porous media. *Advances in Water Resources*, 19(3):163–180, 1996.
- [42] J. Salles, J.-F. Thovert, R. Delannay, L. Prevors, J.£L. Auriault, and P. M. Adler. Taylor dispersion in porous media. determination of the dispersion tensor. *Physics of Fluids A*, 5(10):2348–2376, 1993.
- [43] A.E. Scheidegger. *The Physics of Flow through Porous Media*. University of Toronto Press, Toronto, 1960.
- [44] U.M. Scheven and P.N. Sen. Spatial and temporal coarse graining for dispersion in randomly packed spheres. *Phys. Rev. Lett.*, 89(25), December 2002.
- [45] S.E. Silliman and E.S. Simpson. Laboratory evidence of the scale effect in dispersion of solutes in porous media. *Water Resour. Res.*, 23:1667–1673, August 1987.

- [46] C.S. Slichter. Field measurements of the rate of movement of underground waters. U.S. Geol. Survey, Water Supply Paper No. 140, 1905.
- [47] H. Steinhaus. *Mathematical Snapshots*. Dover Publications, New York, 3 edition, 1999.
- [48] O.D.L. Strack. A mathematical model for dispersion with a moving front in groundwater. *Water Resour. Res.*, 24:1939–1947, 1992.
- [49] N. Suciu, F. A. Radu, A. Prechtel, and P. Knabner. Coupled finite element - global random walk simulation of transport in porous media with random hydraulic conductivity. In *Proc. Fifth ACOMEN International Conference*, Liege, Belgium, November 2011.
- [50] G.I. Taylor. Diffusion by continuous movement. *Proc. London Math. Soc.*, 20:196–211, 1921.
- [51] A.F. Tompson, E.G. Vomvoris, and L.W. Gelhar. Numerical simulation of solute transport in randomly heterogeneous porous media: Motivation, model development, and application. Report Number 316, Ralph M. Parsons Lab., Massachusetts Institute of Technology, Cambridge, MA, 1988.
- [52] A.F.B. Tompson. On a new functional form for the dispersive flux in porous media. *Water Resour. Res.*, 24:1939–1947, 1988.
- [53] R. Verstappen and A. Veldman. Symmetry-preserving discretization of turbulent flow. *J. of Comp. Phys.*, 187:343–368, 2003.
- [54] D. Wells. *The Penguin Dictionary of Curious and Interesting Geometry*. Penguin, London, 1991.
- [55] J. H. Williamson. Low-storage Runge-Kutta schemes. *J. Comput. Physics*, 35(48), 1980.
- [56] D. Zhang. *Stochastic Methods for Flow in Porous Media: Coping with Uncertainties*. Academic Press, San Diego, Calif., 2002.
- [57] D. Zhang, R. Zhang, S. Chen, and W. E. Soll. Pore scale study of flow in porous media: Scale dependency, rev, and statistical rev. *Geophysical Research Letters*, 27(8):1195–1198, April 2000.
- [58] T. Zhu, C. Waluga, B. Wohlmuth, and M. Manhart. A study of the time constant in unsteady porous media flow using direct numerical simulation. *Transp Porous Med*, 104(1):161–179, 2014.